THE UNIVERSITY OF MICHIGAN

INDUSTRY PROGRAM OF THE COLLEGE OF ENGINEERING

SPRAYS FORMED BY FLASHING LIQUID JETS

Ralph Brown

A dissertation submitted in partial fulfillment
of the requirements for the degree of
Doctor of Philosophy in the
University of Michigan
1960

July, 1960

IP-448

engin

UMP8542

Doctoral Committee:

Professor J. Louis York, Chairman
Doctor R. Stephen Berry
Professor Jay A. Bolt
Assistant Professor M. Rasin Tek
Professor Brymer Williams

ACKNOWLEDGEMENTS

First and foremost, the author wishes to express his sincere thanks to Professor J. Louis York for his able guidance, encouragement, and friendship during all phases of this work.

Sincere thanks are also due Professors Brymer Williams, J. A. Bolt, M. R. Tek, and Dr. R. S. Berry, the remaining members of the doctoral committee, for their helpful advice and suggestions.

Many thanks also go to Gordon Ringrose, for his invaluable assistance in preparation and calibration of the electrical circuits.

The author would also like to express his sincere appreciation to the Delavan Manufacturing Company, Des Moines, Iowa for their financial assistance and research grants that helped support this research.

The assistance of the Industry Program of the College of Engineering, in the final preparation and reproduction of the manuscript is greatly appreciated.

TABLE OF CONTENTS

LIST OF TABLES

LIST OF FIGURES

LIST OF FIGURES (Continued)

LIST OF APPENDICES

NOMENCLATURE

Alphabetic

A	area	$ft.^2$
C	bubble-growth-rate constant in superheated liquid	$ft./hr.^{\frac{1}{2}}$
C'	bubble-growth-rate constant in supersaturated liquid	$ft./hr.^{\frac{1}{2}}$
C_i	initial gas concentration	weight fraction
C_f	final gas concentration	weight fraction
C_1	heat capacity of vapor	b.t.u./lb.-°F
C_2	heat capacity of liquid	b.t.u./lb.-°F
D	drop diameter	microns
$\overline{D_{mn}}$	mean drop diameter, subscripts referring to which mean, see Chapter V. Equation (1)	microns
D_{vmd}	volume median drop diameter	microns
d	jet diameter	inches
$f(D)$	probability distribution function	
$F(D)$	cumulative distribution function	
g_c	conversion factor, lb. and lb. force	$ft.-lb./lb.force-sec.^2$
h_i	enthalpy in initial state	b.t.u./lb.
h_f	enthalpy in final state	b.t.u./lb.
k	thermal conductivity	$b.t.u.-ft./hr.-ft.^2-°F$
k_g	mass transfer coefficient	$mol./hr.-ft.^2-m.f.$
L	latent heat of vaporization	b.t.u./lb.
ΔN	percentage of drops in any given size range	

NOMENCLATURE

Alphabetic (Continued)

p_v	vapor pressure	lb./ft.^{2}
Δp	difference in pressure inside and at great distance from bubble	lb./ft.^{2}
P_o	external pressure on liquid	lb./ft.^{2}
ΔP	injection pressure	psig
R	gas constant	$\frac{(\text{lb./ft.}^2)(\text{ft.}^3)}{(\text{lb.mole})(^\circ\text{R})}$
T	temperature	°F
T_o	liquid temperature	°F
t	time	microseconds
r	bubble radius	microns
r_o	minimum initial radius for bubble growth	microns
r_1	initial bubble radius	microns
V	relative velocity between liquid jet or drop and surrounding vapor	ft./sec.
v_1	specific volume of vapor	ft.^{3}/lb.
v_2	specific volume of liquid	ft.^{3}/lb.
X	weight fraction flashing	
y	mole fraction of gas being transferred in surrounding gas	
y_i	mole fraction of gas at liquid-vapor interface	

Greek

δ	delta, uniformity parameter for logarithmic-normal distribution

NOMENCLATURE

Greek (Continued)

ϵ	epsilon, surface roughness - arithmetic average	
λ	lambda, disturbance wavelength	inches
μ	mu, viscosity	centipoises
π	pi, a constant	
ρ_1	vapor density	lb./ft.^{3}
ρ_2	liquid density	lb./ft.^{3}
ρ_g	density of surrounding vapor	lb./ft.^{3}
σ	sigma, interfacial tension	dyne/cm.
$\Delta\tau$	tau, superheat	°F

Dimensionless Groups

N_{We}	Weber number, =	$\frac{\rho_g V^2 d}{2g_c\sigma}$
R	Reynold's number, =	$\frac{V\rho_2 d}{\mu}$
W	Weber constant, =	$V\sqrt{\rho_2 d/g_c\sigma}$

Subscripts

1	refers to vapor
2	refers to liquid
i	refers to initial state
f	refers to final state

CHAPTER I

INTRODUCTION

Spraying is the process of breaking a mass of liquid into a zone of drops. Sprays are most often produced by the injection of a liquid under pressure through a device which forms an unstable jet or sheet or by the passage of a high velocity air stream over a liquid jet. In both these methods, the liquid is broken into drops by the action of the stresses at the liquid-vapor interface. The object of this investigation is a study of the characteristics of the sprays formed by flashing liquid jets. In a flashing liquid, the spray is formed partly by the internal gas evolution which rapidly expands the jet. The specific objectives can be divided into two major categories: 1) determination of the break-up mechanism and the controlling physical variables, and 2) finding the effects of operating variables on spray characteristics such as drop-sizes, drop-size distributions, drop-velocities, spray patterns and vaporization rates.

Flashing, defined as spontaneous vapor evolution, can occur if liquid is injected at a temperature above the saturation temperature of the liquid at the pressure of the receiving medium. In this case, the liquid is "superheated" with respect to the receiving pressure. The liquid must attain its saturation temperature in order to reach a condition of thermodynamic equilibrium. The sensible heat available from the liquid by this temperature reduction provides the latent heat for the

spontaneous vaporization of a portion of it. Flashing may also occur if gas is dissolved in the liquid at a concentration greater than the solubility of the gas in the liquid at the pressure of the receiving medium. Here, the liquid is "supersaturated" with respect to the receiving pressure. In this case, a portion of the dissolved gas must come out of solution in order to reduce the concentration to its equilibrium value.

The most common application of flashing for the formation of sprays are the household "aerosol bombs" for the spraying of insecticides, perfumes, and deodorants. The material to be sprayed is stored in a pressure vessel with a portion of propellant. The propellant is commonly an inert, non-toxic compound which is gaseous at room temperature. Typical propellants are Freon-12 or nitric oxide. When the mixture of the material and propellant is injected into the atmosphere, a fine spray results.

Although flashing for the formation of sprays is not widely employed in other applications, there are several areas where it might be advantageous. In fuel combustion, the fuel can be preheated before injection into the combustion chamber. Fine fuel sprays could be formed at low injection pressures if they are injected at a high enough temperature. Another possible application is spray drying. Injecting a superheated material has two advantages in this case. The spray is at a high temperature so that the liquid portion of the material sprayed vaporizes rapidly, and the spray zone is contained in a relatively small volume, reducing the necessity of very wide spray towers.

This method of spray formation produces sprays having certain characteristics. Whether this method or another of the various available methods of spray formation is desirable in a given application depends upon the requirements of that particular application. A small drop-size is not always the most important factor. The applications suggested here utilize various spray characteristics peculiar to this method of spray formation. A purpose of this research is to present the characteristics of the sprays from flashing liquids so that the information might be of value in considering it as a method of spray formation for any particular application.

This investigation is restricted to the break-up of cylindrical liquid jets. The break-up of a cylindrical liquid jet is probably considered the most fundamental means of making a spray and has wide application. The break-up of these jets has been both theoretically and experimentally studied by several investigators. Therefore, the results obtained with flashing can be compared with the information available concerning ordinary jet disintegration. To date, there has been no investigation reported in the literature of the sprays formed by flashing liquids.

Another reason for studying cylindrical jets is that the nozzle design for producing them is very simple--a circular orifice. Simplicity of nozzle design is important in any break-up study as the nozzle design often has a profound effect on the break-up mechanism. With an orifice nozzle, the design parameters which affect the break-up are easily controlled.

The break-up mechanism is studied by taking high-speed silhouette photographs of the flashing jet to "stop" the break-up action. The photographs are taken of water jets under various injection conditions. The important variables are injection temperature and design of the orifice. Photographs are taken of both superheated and supersaturated water jets.

A quantitative measure of the liquid break-up is made by drop-size analyses. There are several methods of obtaining drop-size data but the only one feasible in this case is a photographic technique in which high-speed photographs are taken across the spray zone. This is necessary because of the high vaporization rates and velocities of the drops in the spray which do not permit physical sampling. Drop size analyses are made for sprays from water and Freon-11 jets. The analyses are made for sprays formed over a wide range of operating variables including orifice diameter, orifice roughness, injection pressure, and injection temperature.

CHAPTER II

SURVEY OF LIQUID JET BREAK-UP

This chapter will review some of the experimental and theoretical information available in the literature on the break-up of cylindrical liquid jets. This will enable us to compare the effectiveness of injecting a flashing jet to form a spray with injecting a thermodynamically stable liquid jet.

The manner in which a liquid jet disintegrates into droplets varies considerably depending on the relative values of certain physical variables. To describe the various physical processes of the disintegration, we can refer to a study by Lee and Spencer[17]* that presents high-speed photographs of liquid jets injected under various conditions. Assume that liquid is flowing through a given size orifice into stagnant gas in the direction of the gravitational force and the velocity is slowly increased. At the lowest jet velocities, the jet breaks up as a result of the pinching effect of surface tension. The jet first deforms in a symmetric, varicose manner and then breaks into droplets as shown in Figure 1a. The jet velocity is increased so that the aerodynamic effects caused by the vapor flowing over the liquid become important. This produces faster disintegration as a result of vapor flow causing a decrease in pressure over the bumps in the jet and an increase in the wells as schematically presented in Figure 1b. With further increase

* Superscript numbers refer to literature citations in Appendix D.

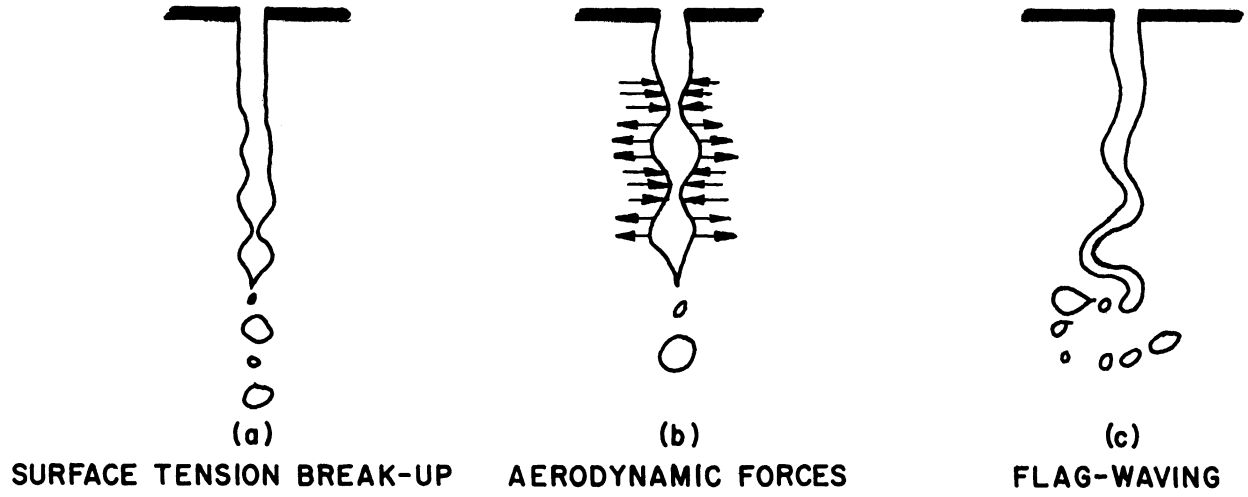

Figure 1. Break-Up of a Cylindrical Liquid Jet.

in velocity, the aerodynamic forces cause the jet to deform in an unsymmetrical, "flag-waving" manner illustrated in Figure 1c. The whipping action at the end of the jet causes it to break into drops. At still higher velocities, the almost immediate, chaotic mass disintegration of the jet can be observed. High-speed photographs have shown that the liquid is actually caught up and drawn out by the vapor. The liquid is pulled into fine ligaments which further disintegrate by the surface-tension mechanism. The larger drops formed from the initial break-up of the jet may further be shattered. This final disintegration process is called "atomization."

In all the theoretical analyses of the break-up of liquid jets developed to describe the above processes, certain assumptions had to be made to solve the equations of fluid flow. The analyses are based upon the assumption that small random microdisturbances exist on the liquid surface. These may be caused by a number of factors including roughness on the orifice surface, impurities in the liquid or vapor, or turbulence. There are forces acting upon these disturbances causing them either to diminish or grow. An expression is obtained for the growth rate of these disturbances. The disturbances which are shown to have the maximum growth rate are assumed to ultimately lead to the jet break-up. This type of analysis leads to two useful results. First, the size of the disturbance is generally characterized by its length in comparison to the jet diameter. The length of the disturbance that has the maximum growth rate gives the volume fraction of the liquid contained in that disturbance.

This gives an estimate of the size of drop that will result from the disturbance. Second, the growth rate of the disturbance gives a measure of the break-up length of the liquid jet. This method of approach is valid if the disturbances are small compared to the size of the jet and randomly imposed. If imperfect machining of an orifice produces a situation where a large disturbance is imposed in a non-random fashion, this analysis may not be of value.

The first mathematical treatment of the instability of cylindrical liquid jets was made by Rayleigh[27] in 1878. He treated both the problem of injecting a jet of heavy liquid into a vapor, and injecting a gas into another gas. In his treatment of the liquid jet he assumed that the capillary force, or surface-tension force, was of major importance. A sinusoidal disturbance for the surface of the jet was assumed. Expressions for the potential and kinetic energies of the deformed jet were found, and from these the growth rate of the disturbance was found as a function of the jet diameter, surface tension, and disturbance wavelength. From this analysis the disturbance on an inviscid liquid jet having the maximum growth rate was found to be dependent only on the jet diameter and is given by

$$\lambda = 4.508\, d \qquad (1)$$

where λ = disturbance wavelength, and
d = jet diameter.

This solution is important in that it accurately predicts the drop-size from the size of the disturbance by assuming the drop is formed from the cylindrical portion of the jet having a length given by Eq. (1).

This is only valid for the break-up of a low-velocity jet as shown in Figure 1a, as it neglects the aerodynamic forces that become important at the higher velocities. Experimental measurements of the wave-length by Tyler[28] agree very well with Eq. (1).

In a subsequent paper, Rayleigh[26] extended his analysis of liquid jets to include liquids of high viscosity. This showed that as the viscosity was raised, the wavelength of the disturbance having the maximum growth rate was increased.

A second theoretical study of jet break-up was made by Weber[30] in 1931. Weber first considered the same hydrodynamical equations and assumptions as did Rayleigh in solving the disturbance growth rate for low and high-viscosity jets. By making certain mathematical assumptions, he obtained an explicit relation for the wavelength of the disturbance of maximum growth rate as a function of liquid properties.

$$\lambda = \pi d \sqrt{2\left(\frac{3\mu}{\sqrt{\rho_2 d \sigma}} + 1\right)} \qquad (2)$$

where μ = liquid viscosity,
ρ_2 = liquid density, and
σ = interfacial tension.

This equation shows that for inviscid liquids ($\mu = 0$), the solution agrees very well with that found by Rayleigh.

$$\lambda = 4.44\, d \qquad (3)$$

Weber's analysis goes further than that of Rayleigh in that he then considers the effect of aerodynamic forces on the jet disintegration. He first considers the effect of symmetrically-imposed forces as shown in Figure 1b. This analysis shows that the disturbance growth rates increase with jet velocity. This results in the fact that the break-up time (time = 0 at the orifice) decreases with jet velocity. The length of the disturbance with the maximum growth rate again increases with jet viscosity. Weber then considers the case where the jet is distorted in a sinuous manner which occurs at the higher velocities. In this case, the cross section of the jet is assumed constant, and the sinuous jet is considered as an elastic beam, subject to thrust and bending. The jet is assumed to be sinusoidally distorted and an attempt is made to obtain the size of the distortion with the highest growth rate. The size of the disturbance is found to decrease with a dimensionless constant, now referred to as the Weber number.

$$N_{we} = \frac{\rho_g V^2 d}{2 g_c \sigma} \tag{4}$$

where ρ_g = the density of the surrounding gas,
V = the velocity of the jet, and
g_c = conversion factor, absolute to engineering units.

High viscosity again has the effect of increasing the length of the disturbance with the highest growth rate and increasing the break-up time.

The models of jet formation employed by Weber in his analyses were based on an experimental study of the break-up made by Haenlein[9]. The results predicted by Weber agree in character with the experimental

results of Haenlein. The results of the previously mentioned photographic study of Lee and Spencer[17] also agree with Weber's theoretical results.

Several investigators, particularly Castleman[4,5], point out that Weber's analyses do not apply to very high values of jet velocity where the jet disintegrates very close to the orifice. Photographic studies have indicated that many drops are created by the formation of ligaments on the surface of the jet. No mathematical analyses have been attempted for this regime of atomization as a result of its random nature. However, there are certain characteristics of the spray that may be predicted.

A large drop in a high velocity air stream is unstable and is subject to further disintegration. This shattering of drops that have been broken off the liquid jets is referred to as "secondary atomization." The importance of this concept is that knowing the maximum size of a stable drop as a function of the relative velocity between drop and vapor, we can predict the maximum drop-size in a spray from a jet injected at a given velocity. The mechanism of secondary atomization has been studied by Baron[2], Littaye[18], and Lane[16]. The most useful result of these studies has been the criterion for the onset of secondary atomization developed by Littaye[18].

$$N_{we} = \text{constant} \tag{5}$$

This says that if the Weber number is a higher value than a constant, the drop is unstable and will be shattered.

Several empirical and semi-empirical relations have been presented to give the maximum drop-size for a liquid jet spray and its break-up length. A good correlation for maximum drop size is Holroyd's[13]

$$D/d = W^{-2/3} f(R) \tag{6}$$

where D = maximum drop diameter,
$W = V\sqrt{\rho_2 d/g_c \sigma}$ and
R = Reynold's number $= V\rho_2 d/\mu$.

It should be pointed out here that some confusion exists in the literature as to the definition of the Weber number. Some investigators define it as in Eq. (4) and others call W, in Eq. (6), the Weber number. In this study, any reference to the Weber number will mean that defined by Eq. (4). This definition seems preferable since it is the ratio of the impact stress of the gas at the gas-liquid interface, $\rho_g V^2/2g_c$; and the normal stress on any cross section caused by surface tension, σ/d. This is a ratio of a stress tending to distort the jet to a stress tending to restore it to its original configuration and in this sense, is a measure of the jet stability. There is a direct relation between the two definitions of Weber number and it is given by

$$N_{we} = \frac{\rho_g}{2\rho_2} W^2 \tag{7}$$

Holroyd[13] says that the function of Reynold's number, f(R), in Eq. (6) should be obtained empirically for any particular application. Miesse[19] has correlated the maximum drop-size data for the break-up of water and liquid nitrogen jets and applied Holroyd's equation to obtain

the equation:

$$D/d = W^{-2/3}(23.5 + 0.000395\ R). \qquad (8)$$

Both Eq. (6) and Eq. (8) are for jet velocities where secondary atomization does not occur. In cases where secondary atomization does take place, the maximum drop-size may be reduced considerably.

Baron[2] suggests the function of dimensionless groups to correlate break-up length data be given by

$$L/d = Wf_1(R) \qquad (9)$$

where L = the break-up length.

Miesse[19] applied his data to this relation to obtain the correlation

$$L/d = 1.7\ W\ (0.0001\ R)^{-5/8} \qquad (10)$$

This brief survey has been intended to point out the present state of the knowledge of liquid jet break-up, and is not intended as a complete literature survey. A complete literature survey of this subject is available[24]. The main purposes of this survey are: 1) to provide a basis for the choice of range and magnitudes of operating variables for the flashing study, and 2) to provide a basis for the comparison of the break-up of cold liquid jets and the break-up of flashing liquid jets. The choice of operating variables for the flashing study is in a range where the atomization of ordinary liquid jets to a spray is poor, that is, where the drop-sizes are the same order of magnitude as the jet diameter. The purpose of employing flashing would therefore be to obtain a fine atomization from cylindrical liquid jets at pressures where more complicated devices than orifices must be used to obtain fine sprays.

The atomization of the jets is poor in the regimes of the jet deformation and break-up shown in Figure 1. The onset of these various regimes of deformation can be characterized by the same criterion that is applied to the stability of droplets in a high-velocity vapor stream[11,16]. The regimes are characterized by the Weber number. The Weber numbers for the various break-up processes for low viscosity jets are tabulated in Table I.

TABLE I. BREAK-UP CONDITIONS FOR A LOW VISCOSITY CYLINDRICAL LIQUID JET

pinching break-up when $N_{we} < 0.2$	Figure 1a
sinuous break-up when $0.2 < N_{we} < 8$	Figure 1c
atomization when $N_{we} > 8$	

"Atomization" in Table I refers to the point where ligament formation is induced on the jet surface and the original jet drops are subject to secondary atomization. Note that this begins where the impact stress on the jet surface is about an order of magnitude greater than the surface normal stress. It should be emphasized that the values given in Table I are very approximate as the transition between the regimes of jet deformation is very gradual and does not take place at a sharply critical Weber number. The experiments with flashing are designed to cover a range of Weber numbers that cross the "critical" for the onset of atomization. This would determine whether the break-up of flashing

jets is also subject to a change at the critical Weber number. The Weber numbers in Table I are given for low viscosity liquid jets. The effect of high-viscosity is to raise the value of the "critical" Weber number for the onset of atomization. Increased viscosity therefore has the effect of increasing the stability of a liquid jet or drop. The critical Weber numbers for the onset of atomization of drops and jets as a function of viscosity are given by Hinze[11].

CHAPTER III

EXPERIMENTAL APPARATUS AND PROCEDURES

The Injection System

A diagram of the liquid injection system is presented in Figure 2. Injection is by gas pressure over the liquid in the storage tank. This prevents pressure fluctuations which are inherent with injection by reciprocal or rotary pumps. The system is designed so that liquid may be injected under the following conditions:

1) Hot water--The vented storage tank is filled with water and steam is bubbled through until the temperature is 212°F. Steam is passed through the water for a few minutes to remove any air in the tank and the tank is then sealed. The steam can then be injected until the tank pressure reaches 135 psig corresponding to a saturation temperature of 358°F. This hot water passes through the heat exchanger where it can be cooled to the desired temperature by varying the cold water flow in the outer jacket. The injection pressure across the nozzle may be regulated either by the steam pressure in the tank or the gate valve downstream of the heat exchanger.

2) Hot or cold liquids--Any liquid can be put in the tank and injected under air or gas pressure through the heat exchanger where it is heated to the desired temperature by passing steam or hot water through the outer jacket.

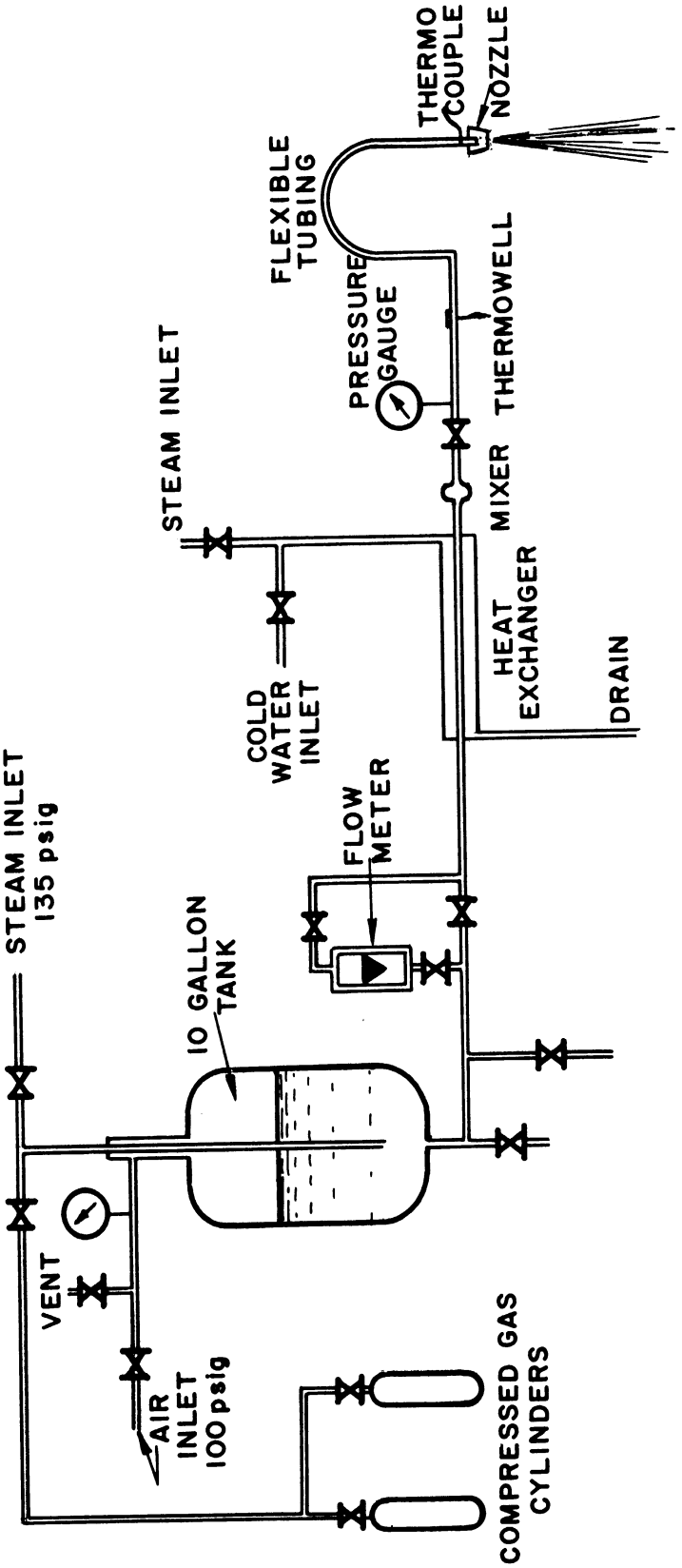

Figure 2. Liquid Injection System.

3) Liquid with dissolved gas--Gas from cylinders may be bubbled through liquid in the tank in the same manner that steam is bubbled through the water. Gas is bubbled through the vented tank for 20 minutes to assure it is dissolved to saturation and all the air is vented from the tank. The tank is then sealed and gas injected until the desired pressure is attained.

In summary, the injection system will inject cold, superheated, and supersaturated liquids into the atmosphere at pressures up to 300 psig. Provision is made for metering the flow with a Fischer-Porter variable-area flowmeter capable of measuring flow rates from 0.026 gal./min. to 0.211 gal./min. with an accuracy to the nearest 0.002 gal./min. An iron-constantan thermocouple measures the temperature of the pipe just upstream of the nozzle. The pipe and thermocouple are heavily insulated and the temperature can be measured to the nearest 0.5°F. Injection pressures are measured by a calibrated Jas. P. Marsh Corp. Mastergauge Type 103 which measures pressures to the nearest 1 psig. The calibrations are discussed in detail in Appendix A.

High-Speed Photography

Several methods of analyzing sprays are available. Most of these, however, depend on the physical sampling of the spray or on the scattering of light by the spray. Physical sampling is usually accomplished by having drops impinge on cups or microscope slides or by sucking them out of the spray by a tube. Any physical sampling technique has the disadvantage that the impingement process discriminates against capturing the smaller drops

and the larger drops are shattered. This is particularly aggravated in the case of the sprays from the superheated jets. The drops are at their saturation temperature as soon as they are formed and so vaporize at a very high rate. They must therefore be sampled near the orifice where their velocities are the highest. The higher velocities increase the tendency to shatter the large drops when making the sample. The light scattering techniques have the disadvantage that the data is extremely difficult to analyze unless the drops are in a very narrow range of sizes. Neither physical sampling or light scattering techniques yield any information concerning drop velocities.

In the photographic technique of spray analysis, a photographic sample of the spray can be taken without disturbing the flow pattern. In general, photographic techniques rely on taking high-speed photographs in various locations of the spray. The photographic method employed here is that described by York and Stubbs[32] which uses double exposures to obtain drop velocities. This method provides drop-size distributions and drop velocities for various locations in a spray and for the whole spray.

High-speed photographic techniques are employed for another type of measurement. That is the photographic study of the break-up of the flashing jets. The equipment and techniques for taking the photographs for the break-up studies and the spray analyses are almost identical, the major difference being the location of the field of the spray photographed with respect to the orifice.

The camera arrangement for the high-speed photographs is shown in Figure 3. The camera lens is an Argus with a variable aperture setting from f-3.5 to f-16 and a focal length of 50 mm. The geometry of the camera provides for a magnification of 10X of the image on the film. This photographs a sample of the volume of the spray with a face 0.4-in. x 0.5-in. parallel to the face of the lens and a depth of field depending upon the aperture setting (about 2 mm, at f-3.5). In a spray analysis, the aperture setting must remain constant in order to maintain a constant depth of field. Mylar filters are therefore used to control the intensity of illumination from the photolights. Lighting is provided by two General Electric Photolights Cat. No. 9364688G1, which give a high-intensity flash for approximately 1 microsecond. The lights can be positioned at right angles with a half-silvered mirror between them as in Figure 3 and discharged with a definite time delay governed by the time-delay circuit. This produces a double exposure of the drops with a known time delay for velocity measurements. The lights may also be employed singly for single-flash photographs. The light beam is directed at the lens, producing a shadow photograph of the drops. Photographs are taken with Kodak Contrast Process Ortho film because it has high contrast and good resolution.

In the spray analyses, the nozzle is placed on a movable stand so that the samples can be photographed at various locations in the spray. The nozzle is connected to the injection system by means of insulated flexible metal tubing. The positions of the numbered sample locations for all the spray analyses are shown in Figure 4.

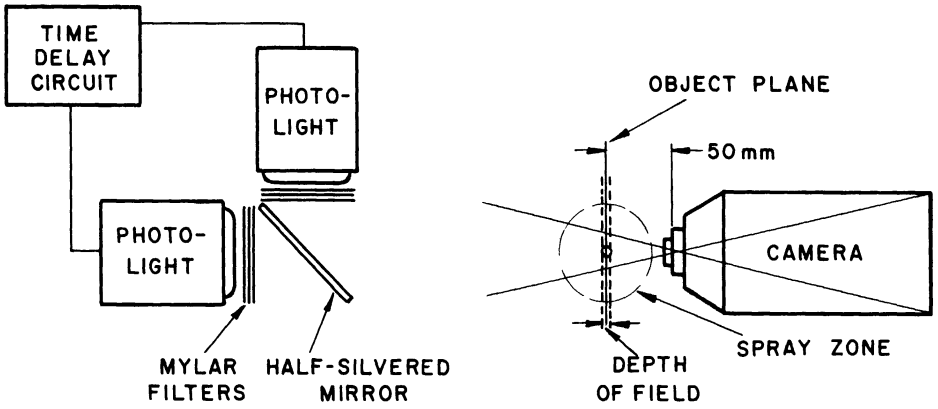

Figure 3. Camera Arrangement for High-Speed Photographs.

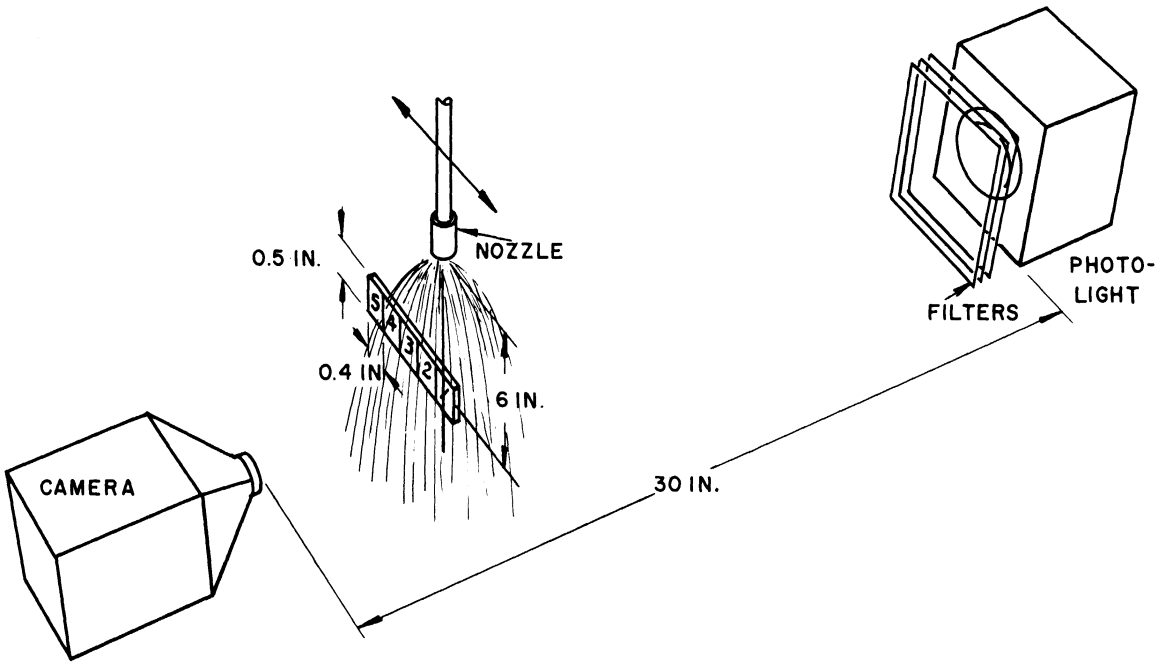

Figure 4. Sample Locations.

In a typical spray analysis, single-flash photographs are taken in a number of the sample locations depending on the width of the spray zone. Some double-flash photographs are also taken for velocity measurements. The double-flash photographs are not used to obtain drop-size distributions because the double exposure reduces the resolution of the smaller drops. After the photographs are developed, the drops are measured on an optical comparator which projects a 10X magnification of the negative. This provides a 100X magnification of the original drops. Since photographs of the spray show both drops in sharp focus and blurred drops, as in Figure 5, a standard technique has to be employed to determine which of the drops should be considered as part of the sample. This is done by taking several photographs of drops of various size suspended on glass fibers. The lens is advanced a known distance before taking each picture to obtain photographs of the drops at known distances from the point of focus. One of these photographs is established as the limit of focus and any drops as sharp or sharper than these are accepted. Drops are counted and measured by adding the number of drops in a photograph found to lie within given size ranges. This analysis gives the percentage of drops in each sample that lies within each size range. This gives a spatial drop-size distribution in a sample. The distribution desired, however, is that in a given period of time or temporal distribution. This is found from the spatial distribution by multiplying it by the velocities of the drops in each size range which have been measured from the double-flash

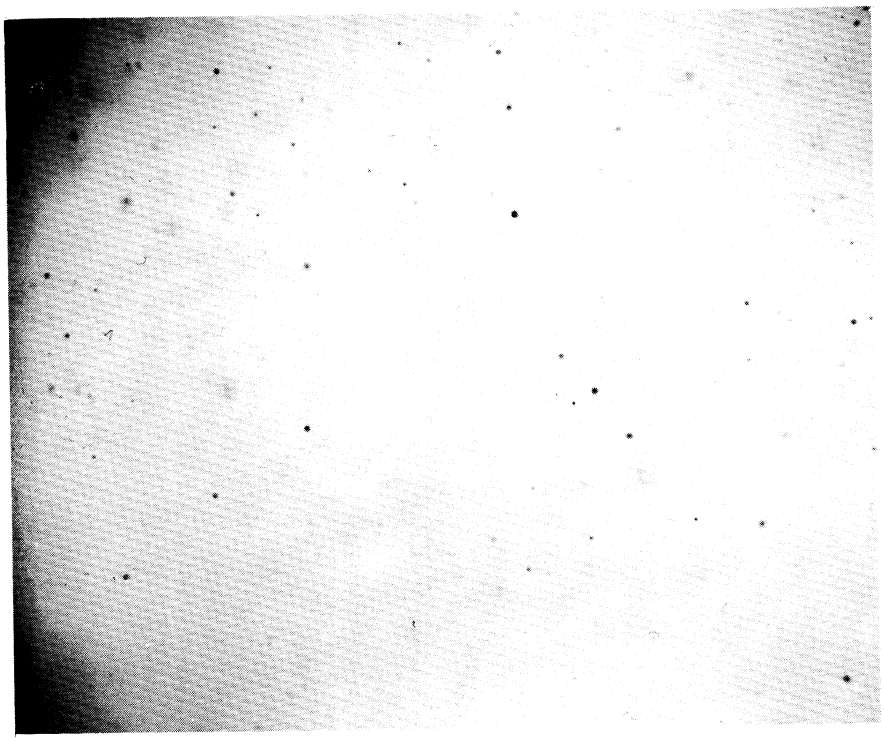

Figure 5. Typical Drop-Size Photograph, 10X.

photographs. The drop-size distribution for the entire spray is calculated from the distributions in each location. The mean drop diameters may be calculated from these distributions. A sample calculation for a spray is presented in Appendix C.

The break-up photographs are taken with the same equipment as the spray analyses except that the photograph is usually taken at the orifice exit. No filters are used to reduce the light intensity but the aperture is reduced to f-5. Both single and double-flash photographs of the jets are taken.

Orifice Nozzles

Although the design of an orifice nozzle is rather simple, there are still a number of design variables that may be considered. The obvious ones are the geometric variables of orifice diameter and orifice length. Others are orifice shape and metal surface roughness. Experiments are made over a range of orifice diameters that are given in Table II. The orifice length must be small enough so that vapor evolution is not initiated inside the orifice as this causes a severe reduction in mass flow rate at high injection temperatures or concentrations. The results of preliminary experiments (see Appendix A) indicate that orifices with L/D (length to diameter) ratios of 1 are sufficiently short to prevent vapor evolution in the orifices for the conditions of these experiments.

The three main types of nozzles are illustrated in Figure 6. Nozzles of type A are sharp-edged orifices which produce extremely smooth, undisturbed liquid jets. The nozzles of type B are tap-drilled and the edges rounded. The surface roughnesses are measured with a Micrometrical Manufacturing Co. Profilometer with a type QC Amplimeter and a type AE Pilotor. These nozzles produce jets whose surface is slightly disturbed by the metal surface. A nozzle of this type with a sharp downstream edge was tried but the dribbling greatly increased the mean drop-sizes.

The nozzle of type C was designed to provide an extremely rough surface. This was made by cementing 170/200 mesh glass beads on the inside surface of a 0.060-in.-diameter nozzle with epoxy resin. The surface roughness is estimated from a photograph of the nozzle shown in Figure 7. This roughness is severe enough to tear portions of the liquid jet off at the orifice.

TABLE II

DESCRIPTION OF NOZZLES

Type	Diameter (inches)	Length (inches)	L/D	Roughness (microinches ARS)	ϵ/D
A	0.030	0.030	1	-	-
A	0.040	0.040	1	-	-
A	0.080	0.080	1	-	-
B	0.020	0.020	1	-	0.0004 (est.)
B	0.031	0.025	0.8	-	0.0004 (est.)
B	0.040	0.035	0.9	14 ± 1	0.00035
B	0.060	0.054	0.9	25 ± 1	0.00042
C	0.020	0.057	3	3000	0.12

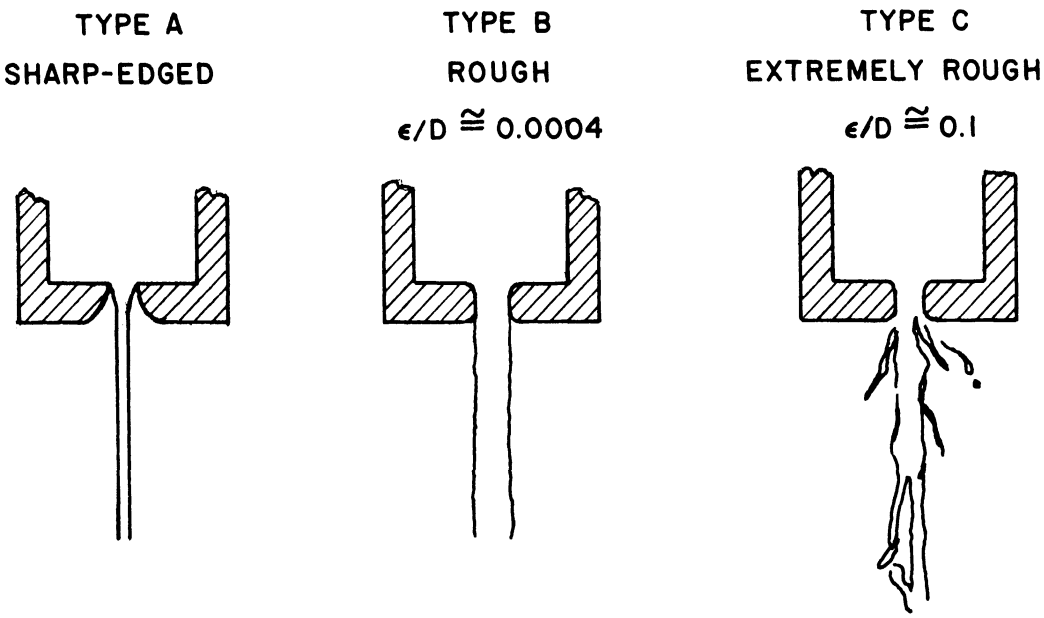

Figure 6. Experimental Nozzle Types.

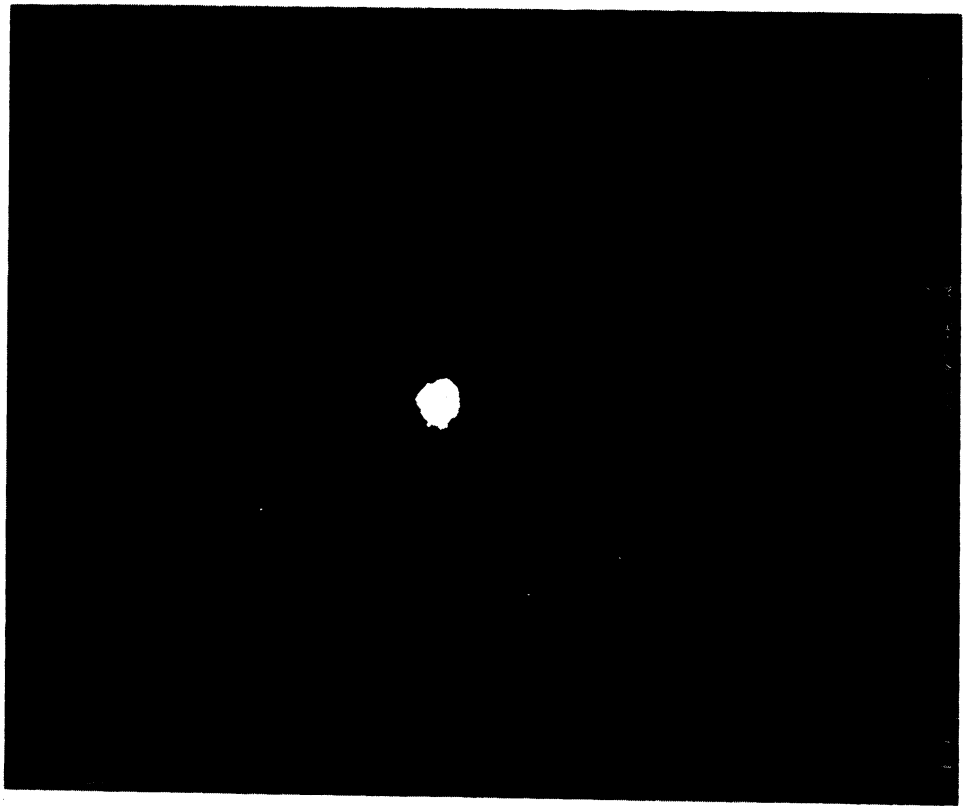

Figure 7. Orifice of Nozzle Type C with Sand, 10X.

Range of Experimental Variables

The liquids that are injected are water and Freon-11. Cold water saturated with carbon dioxide at 90 psig is also injected. Injection pressures for the water and Freon-11 range from 60 psig to 130 psig. Water jets are injected with temperatures up to 300°F corresponding to 9.2 wt. percent flashing when the liquid is reduced to 212°F. The Freon-11 is injected with temperatures to 152°F. corresponding to 21.0 wt. percent flashing when the liquid is reduced to 74.8°F., its saturation temperature at one atmosphere. With the range of injection pressures and orifice diameters employed, the variation in volumetric flow rate went from 0.925 cubic feet/hour to 11.70 cubic feet/hour.

Freon-11 was chosen because of its convenient boiling point, non-flammability, and difference in physical properties as compared to water. The liquid density of Freon-11 is about 50 percent greater than that of water and the gas density is about 10 times that of water vapor. Furthermore, the surface tension of Freon-11 is about 1/3 the surface tension of water.

CHAPTER IV

THE BREAK-UP MECHANISM

Photographic Study of the Break-Up

To investigate the method of flashing, injection temperature, orifice diameter, and orifice roughness on the break-up mechanism, about 130 high-speed photographs were taken of water jets. Some of these photographs, representing the important results, are presented here. In most cases, the lens was positioned so that the photographs show a 10X magnification of a 0.5-in. portion of the jet starting at the orifice.

Figures 8-10 are a series of photographs of jets from the 0.031-in.-diameter, rough-surface (type B) nozzle over a range of temperature. At 251°F. the superheating has essentially no effect on the jet. Only one small bubble can be seen on the surface. At 268°F. the superheating does partially disintegrate the jet, but the spray still contains a core of large drops. Several bubbles can be observed on the surface of the jet and the jet is expanding slightly. At 295°F. the jet is completely disintegrated into a spray of fine droplets. This disintegration can easily be noted in the photograph by the rapidly expanding jet a short distance from the nozzle. Visual observation of the spray has indicated that the temperature difference from the value where the jet disintegrates to a spray with a core of large drops to the value where the jet completely disintegrates to a fine spray is amall, about 5°F. Figure 11 shows a jet at 304°F. from a nozzle similar to a 0.031-in.-diameter, type B nozzle except with a sharp

downstream edge. Dribbling on the edge causes relatively large drops to form. Rounding the outer edge prevents most of this dribbling. The best temperatures for observation of the bubbles growing on the jets are in the 265°-270°F. range for this nozzle. There are few bubbles below that range and above it the rapid disintegration clouds any that may be there. Figure 12 is a double-exposure of the jet at 268°F. One can observe the expansion of the bubbles on the surface of the jet from the first exposure to the second.

Figure 13 shows a jet from the 0.020-in.-diameter, type B nozzle at 284°F. Bubbles can be observed on the surface of the jet. The jet also appears less turbulent than those of the larger diameter as would be expected in view of the lower Reynold's number. The important difference between this nozzle and the larger one is that, at this temperature, a jet from the larger orifice would be completely disintegrated. The appearance of the bubbles in this jet is similar to those in the larger diameter jet at about 268°F. The jet is only partially disintegrated by bubble growth, the final spray containing a core of large drops.

The photographs of the jets from the sharp-edged orifice nozzles show some outstanding differences from those of the rough-orifice nozzles. Photographs of jets from the 0.040-in.-diameter orifices do not indicate any effect of the flashing until the temperature reaches about 275°F. Figures 14 and 15 show jets at 286°F. The jets at this temperature all break up completely but in different ways. About 20 photographs of jets

from this nozzle at this temperature and injection pressure were taken and each one is entirely different. Observations from the photographs indicate that the jet disintegrates anywhere from 1/8-1/2 in. from the orifice. Often a delicate network of bubbles appear on the surface and often the jet just seems to explode suddenly. An extremely loud noise is associated with this break-up above about 275°F. Visual observation of the jets suggest that the break-up point oscillates and the density of the spray formed by the jet fluctuates at any given point. A Strobotac, which is a variable-frequency flash unit, was directed on the jets but the point of break-up could not be made stationary indicating that this point did not oscillate at a regular frequency. The intact portion of the jets appeared smooth, which is indicated by the photographs. Note that the jets from the 0.031-in., type B nozzle and the 0.040-in., type A nozzle are about the same diameter. This results from the fact that a jet formed from a sharp-edged orifice contracts more than one from a round-edged, rough orifice.

When injecting water at 130 psig through a 0.030-in. diameter sharp-edged orifice at 287°F., the jet was to all appearances completely disintegrated to fine spray. Photographs at the orifice, however, showed smooth and undisturbed jets. Therefore, several photographs were taken of the jet at various distances from the orifice. Figure 16, which is taken 1-in. from the orifice shows that the break-up does take place in this case, but further from the orifice. Apparently, bubbles are nucleated inside the body of the jet and grow until they break the jet. In this

photograph the bubble that has broken has cut the jet, leaving intact portions on either side of the bubble. The bubble following the one that has broken is about to repeat this same action. The intact portions of the jet will be further atomized by aerodynamic forces. A crackling noise is associated with this break-up, not quite as loud and intense as with the larger sharp-edged orifices.

Photographs of water jets that had dissolved carbon dioxide in them appeared identical to pure water jets at the same temperature. The water was saturated with the gas at 90 psig which would cause about 1 wt. percent of the liquid to flash when the liquid is injected into the atmosphere. These jets were also produced by a long orifice nozzle (L/D = 6) that had been used in preliminary experiments. The dissolved gas still had no effect upon the jet break-up. The important point of comparison here is that when a superheated water jet was injected through this same nozzle at a temperature such that 1 wt. percent flashed, vapor evolution was initiated inside the orifice throat and the jet was broken up.

Analysis of the Break-Up Mechanism

The mechanism by which flashing causes the break-up of superheated liquid jets is bubble formation. This is apparent by the observation of the bubbles on the surfaces and inside of the superheated jets in the photographic study. The expanding bubbles tear apart and break the

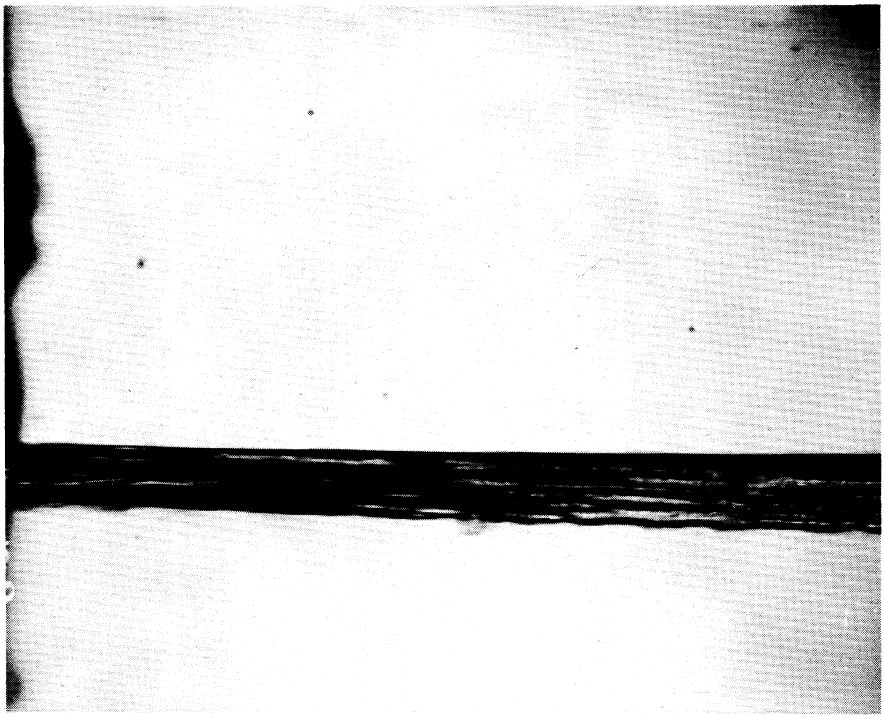

Figure 8. Flashing Jet 10X. Type B, D = 0.031-in., P = 120 psig, T = 251°F.

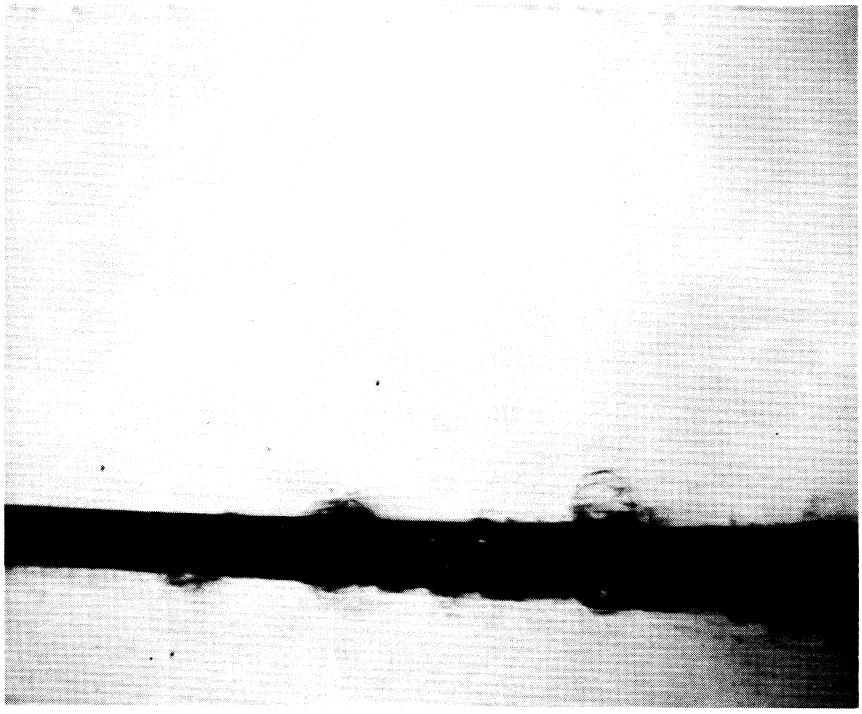

Figure 9. Flashing Jet 10X. Type B, D, = 0.031-in., P = 120 psig, T = 268°F.

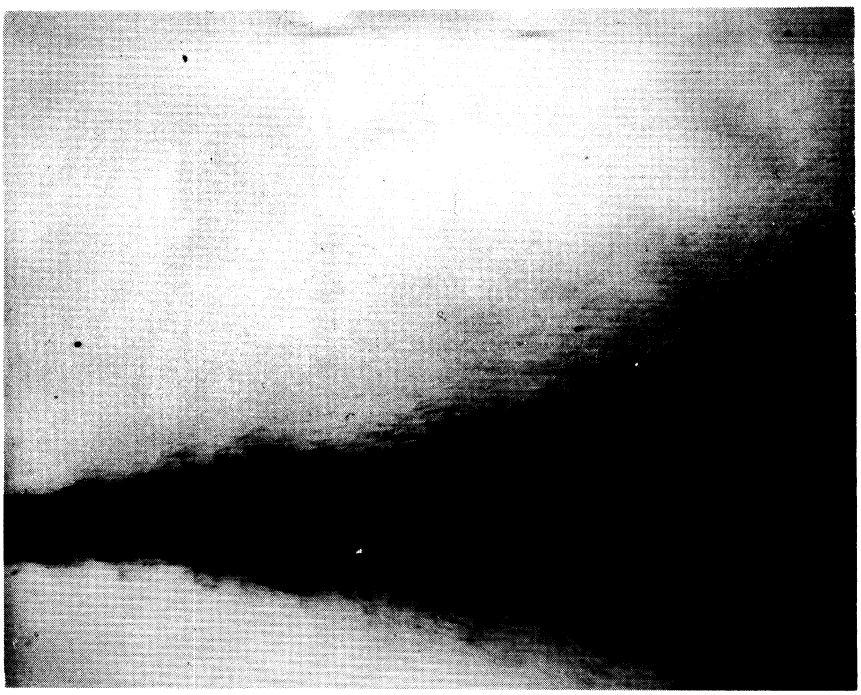

Figure 10. Flashing Jet 10X. Type B, D = 0.031-in., P = 120 psig, T = 295°F.

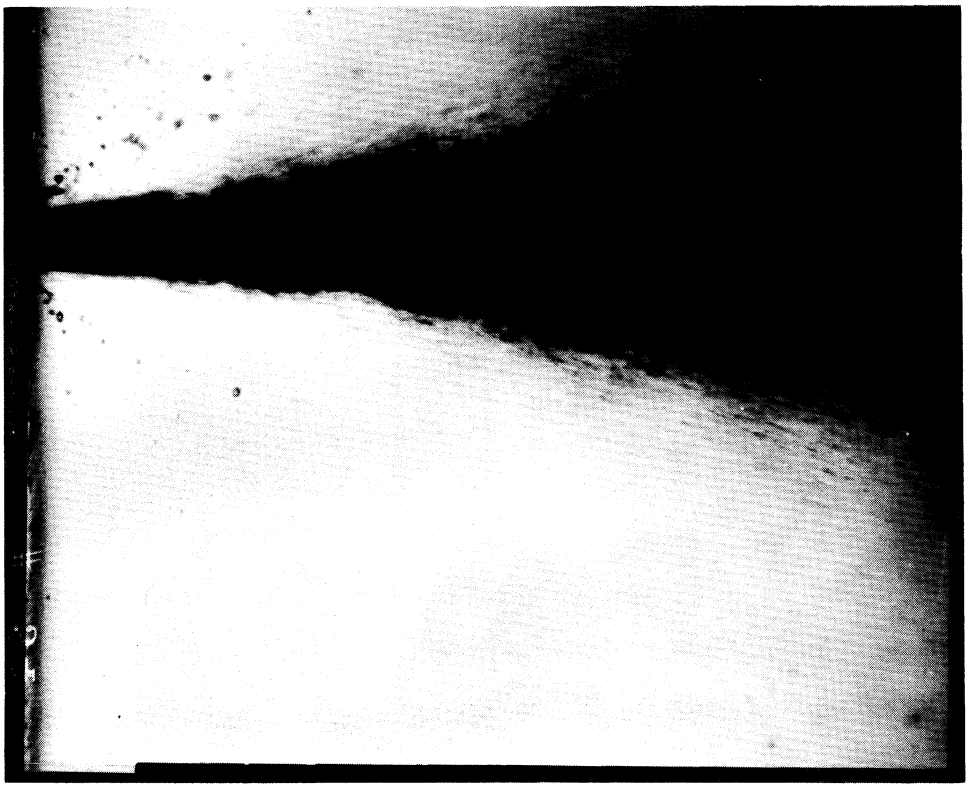

Figure 11. Flashing Jet 10X. Type B with Sharp Downstream Edge, D = 0.031-in., P = 120 psig, T = 304°F.

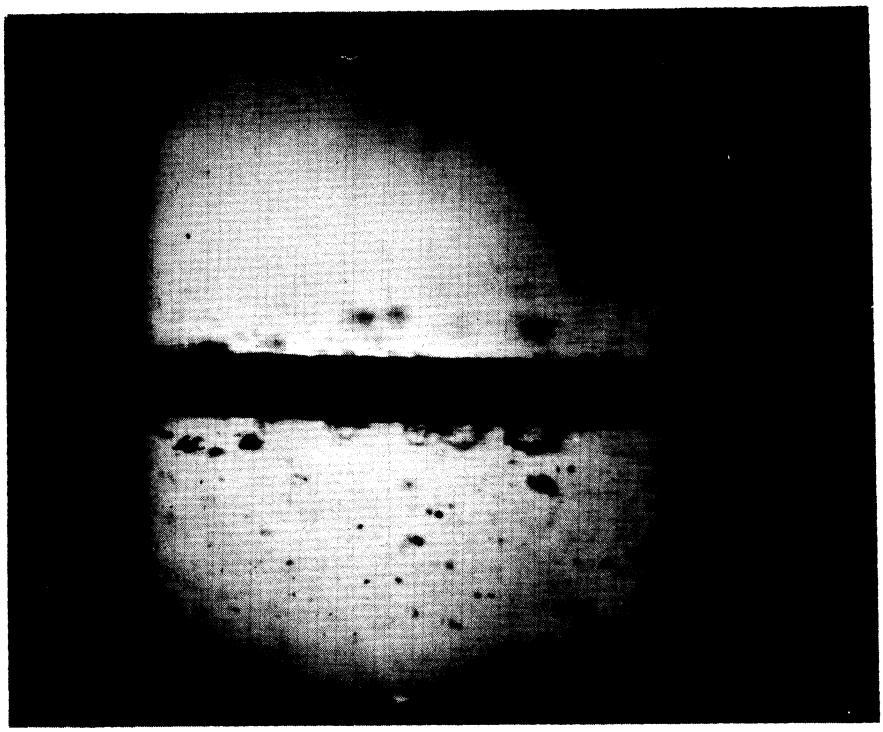

Figure 12. Flashing Jet 10X. Type B, D = 0.031-in., P = 120 psig, T = 268°F, Double Exposure (14 Microsecond Delay)

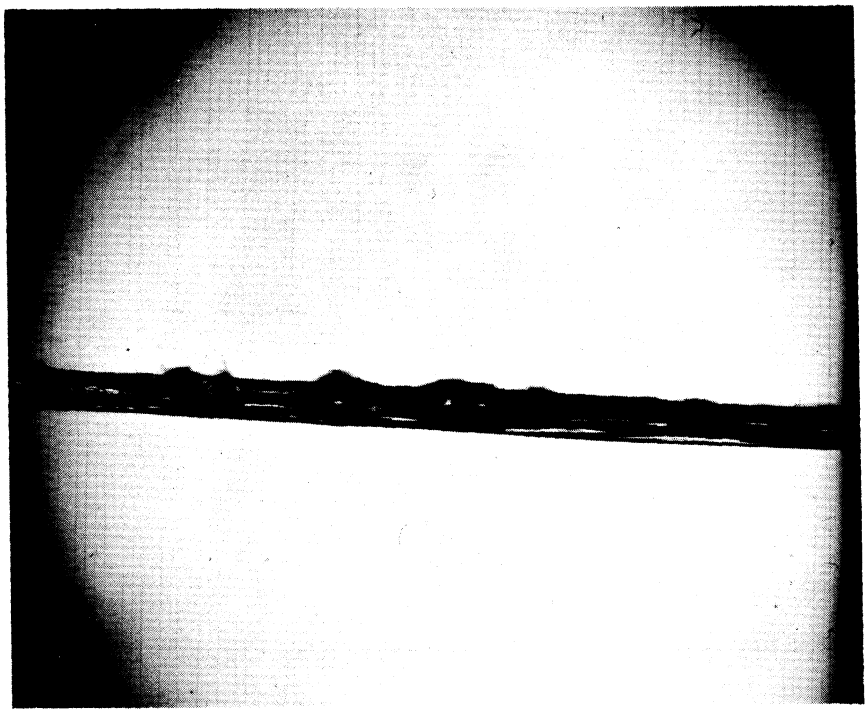

Figure 13. Flashing Jet 10X. Type B, D = 0.020-in., P = 120 psig, T = 284°F.

Figure 14. Flashing Jet 10X. Type A, D = 0.040-in., P = 120 psig, T = 286°F.

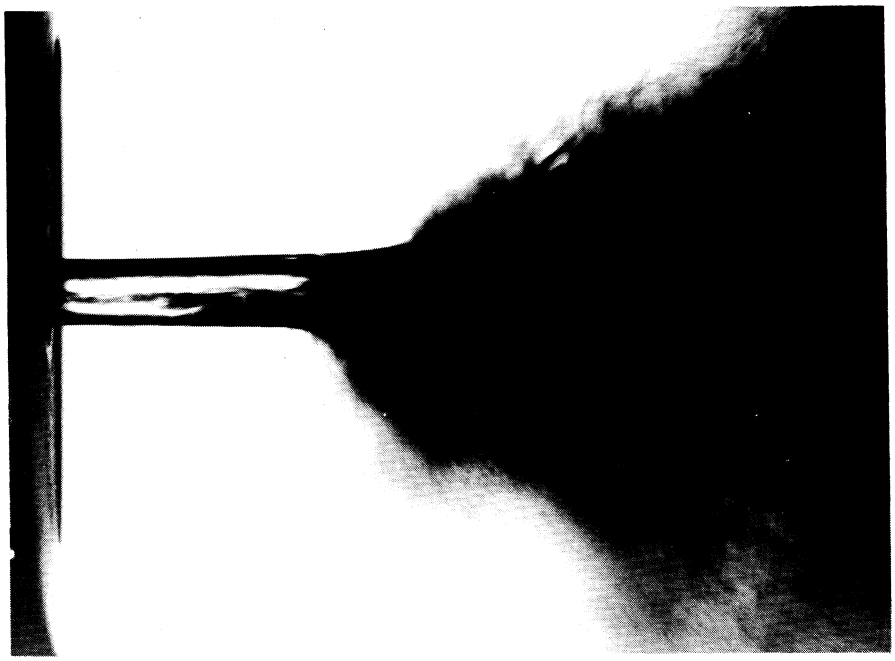

Figure 15. Flashing Jet 10X. Type A, D = 0.040-in., P = 120 psig, T = 286°F.

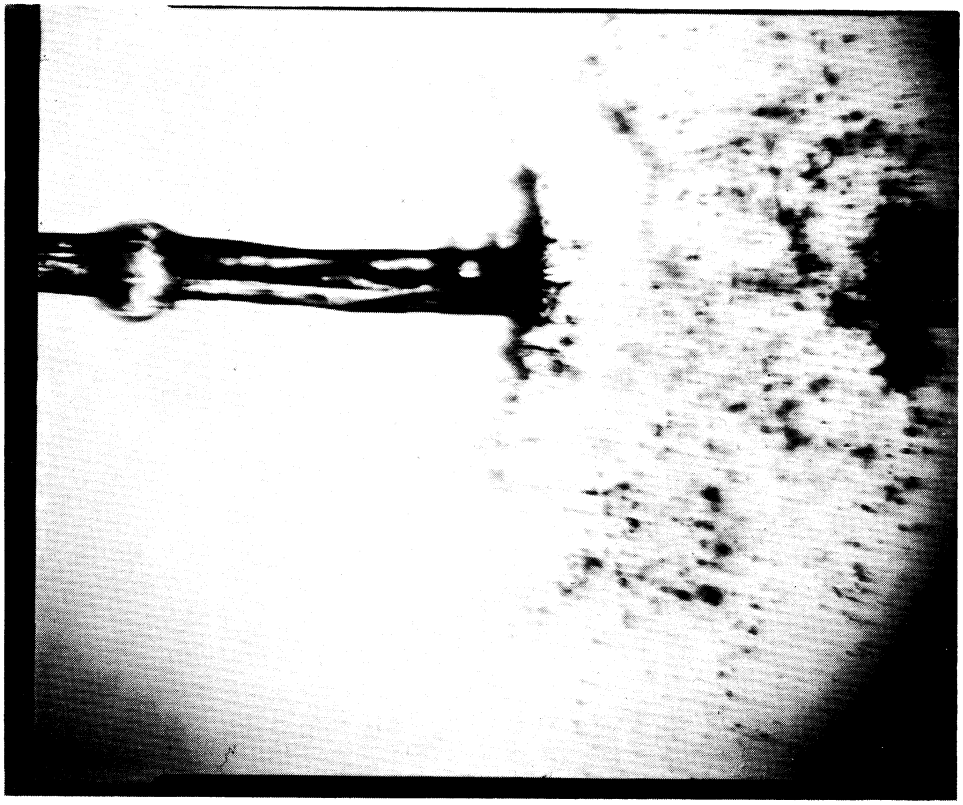

Figure 16. Flashing Jet 10X. Type A, D = 0.030-in., P = 131 psig, T = 287°F. One inch from Orifice.

jets. Some explanation must be made, however, for the striking differences between the photographs of the break-up of the jets from the rough-surface orifices and the sharp-edged orifices. The rough-orifice jets, when injected at a sufficiently high temperature, simply expand a short distance from the orifice to form a fine spray. The superheated jets from the sharp-edged orifices, however, disintegrate in a random, explosive manner. The situation here is analogous to boiling a liquid in a test tube. If some porous stones are in the tube, small bubbles will nucleate on the surface of these stones and the liquid will vaporize into these bubbles, causing them to grow and rise. If only pure liquid is in the test tube, vaporization will take place by a series of small explosions referred to as "bumping." The reason for the two different vaporization mechanisms is the same in the case of the water jets and the heated test tube; vapor bubbles will not grow in a superheated liquid unless bubble nuclei are already present.

The surface tension of a liquid exerts a pressure on a spherical bubble in the liquid of a magnitude given by the following expression:

$$P = \frac{2\sigma}{r} \qquad (1)$$

where P = pressure inside minus pressure outside the bubble,
σ = surface tension of the liquid, and
r = radius of the bubble.

Considering the limiting case for water, if a bubble is the mean diameter of a water molecule, $r = 1.9$ Å, the excess pressure inside the bubble would be 7500 atmospheres assuming surface tension is constant down to

atomic dimensions. For a bubble to grow in a superheated liquid, the vapor pressure of the liquid minus the pressure on the liquid must be greater than the pressure exerted on the bubble given by Eq. (1). A minimum initial radius for bubble growth can be found by equating these two pressures.

$$\frac{2\sigma}{r_o} = p_v(T_o) - P_o$$

$$r_o = \frac{2\sigma}{p_v(T_o) - P_o} \qquad (2)$$

where r_o = the minimum initial radius for bubble growth,
p_v = the vapor pressure of the liquid which is a function of its temperature, T_o, and
P_o = the pressure on the liquid.

Several values of this initial radius for water are given in Table III.

TABLE III

MINIMUM INITIAL RADIUS FOR BUBBLE GROWTH IN WATER UNDER ONE ATMOSPHERE

r_o	(microns)	5.90	0.605	0.470	0.378	0.300	0.245	0.201
T_o	(°F.)	220	266	275	284	293	302	311

There are a number of different means by which small nuclei for bubble formation may be provided to a superheated liquid. These nuclei may be initiated by vapor spaces in the small cavities of boiling stones, free vortex motion in a highly turbulent situation, or by small gas bubbles held in the liquid. Whatever the means, bubble formation in a continuous phase of superheated liquid cannot take place without some original bubble nuclei.

In the case of the rough orifice, the nuclei are probably provided by low pressure eddies behind the sharp micro-roughnesses on the orifice surface. These first produce bubbles on the surface of the jet. When the temperature is high enough, these bubbles are also produced throughout the body of the jet and lead to its eventual break-up. With the sharp-edged orifice, the superheated liquid passes by the orifice undisturbed into the atmosphere. There is no provision for the continuous nucleation of the bubbles on the orifice surface. Rather, the spontaneous nucleation of bubbles in these jets is initiated by some random disturbance. Such a disturbance might be an aerodynamic distortion of the jet or a small vibration of the nozzle. The reason for the differences in the photographs can therefore be summarized by saying that surface roughness provides for bubble nucleation in a stable continuous manner, but without roughness, bubble nucleation is subject to random effects.

Consider a superheated jet being injected into the atmosphere. The temperature of the jet right near the orifice is its injection temperature. Traveling away from the orifice, the jet cools down to well below its saturation temperature by vaporization and convection from the surface. If a bubble is nucleated at the orifice, it will grow until it reaches the point in the jet where the temperature is below the saturation temperature. Then it will start to collapse. This growth-collapse phenomenom is commonly observed in surface boiling systems and is mathematically described by Bankoff and Mikesell[1]. Figure 17 is a diagram of what a multiple exposure photograph of such a bubble might look like.

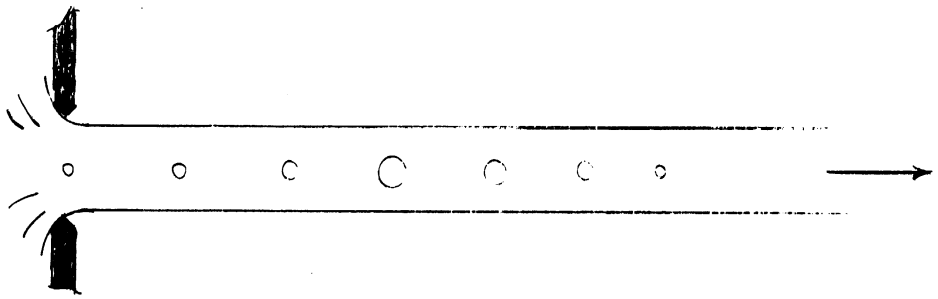

Figure 17. The Growth and Collapse of a Bubble in a Superheated Jet.

If the bubble does not grow to a large size, it will not affect the jet. If it does grow large enough, however, it can either break the jet or shatter it before it has an opportunity to collapse. From this model, we can see that the growth rate of the bubble is a critical factor. Since the break-up takes place near the orifice, it is the growth rate at the injection temperature that is of interest. Means are available to predict the growth rate of a bubble in a superheated or supersaturated liquid given some of its physical and thermodynamic properities.

Solutions for the problem of the growth of a vapor bubble in a superheated liquid have been presented by Plesset and Zwick[23], and by Forster and Zuber[7]. These solutions take the Rayleigh equation[15] for the motion of a bubble in a nonviscous, incompressible liquid,

$$r \frac{d^2r}{dt^2} + \frac{3}{2}\left(\frac{dr}{dt}\right)^2 = \Delta p \frac{1}{\rho_2} \qquad (3)$$

where r = the bubble radius,
t = the time,
Δp = the pressure difference inside and at great distance from the bubble, and
ρ_2 = the liquid density

and extend it to include the pressure on the bubble by the surface tension.

$$r \frac{d^2r}{dt^2} + \frac{3}{2} \left(\frac{dr}{dt}\right)^2 = \left(\Delta p - \frac{2\sigma}{r}\right) \frac{1}{\rho_2} \tag{4}$$

The pressure difference, Δp, can be connected to the temperature difference, ΔT, between the saturation temperature inside and at great distance from the bubble by the Clausius-Clapyron equation.

$$\Delta p = \frac{L}{T(v_1 - v_2)} \Delta T \tag{5}$$

where L = the latent heat of vaporization of the liquid,
T = an average value of the temperature between the initial liquid temperature and the saturation temperature at the external pressure, and
v_1, v_2 = the specific volumes of the vapor and liquid, respectively.

The value of the temperature inside the bubble is assumed to be the temperature of the bubble wall, which is a good assumption since the temperature gradients within the bubbles are negligible in view of the small bubble sizes and the high thermal diffusivity of the vapor. The temperature at the bubble wall must be determined by the solution of the heat conduction problem across a spherical moving boundary where vaporization is taking place. The Forster and Zuber solution assumes the bubble wall constitutes a spherically-distributed heat sink and uses the Green's function for the domain[3] integrated over the space that the vaporization takes place. The Plesset and Zwick solution uses an approximate solution to the heat conduction problem across a spherical

moving boundary that assumes the thickness of the layer of the liquid in which the temperature reduction takes place is small compared to the radius of the bubble at any time[22]. Both solutions proceed from these assumptions and employ different mathematical techniques to find an approximate solution to the integro-differential equation involved. The mathematical details are omitted here as they are available in the references. Both solutions arrive at the same results.

The solutions indicate that there are two regions of bubble growth. In the first region, the bubble radius is of the same order of magnitude as its original radius, r_o. Here the growth rate is quite rapid because the increasing radius is relaxing the surface-tension pressure on the bubble. There also has not been enough vaporization to cool the liquid on the bubble surface and severely reduce the vapor pressure. This rapid expansion rate is shortly slowed down by the cooling of the liquid around the bubble and the subsequent reduction of the vapor pressure inside it. The rate is then governed by the balance between heat transfer and vaporization and is approximately given by:

$$r \cong r_1 + C\, t^{\frac{1}{2}} \qquad (6)$$

where C = a constant dependent on the physical properties of the system, and
r_1 = the initial bubble radius ($r_1 \geq r_o$).

This growth-rate relation describes the bubble as soon as the radius is about 10 times the minimum initial radius, which is the case within a few microseconds. This secondary-growth-rate function agrees very

well with data obtained by Deragabedian[6] for growth rates of bubbles in superheated water.

The importance of this solution as applied to the study of the jet break-up is that Forster and Zuber give the growth-rate constant, C, in terms of the physical properties of the liquid and its thermodynamic condition.

$$C = \left(\frac{\Delta\tau c_2}{L}\right)\left(\frac{\rho_2}{\rho_1}\right)\left(\pi D_{th}\right)^{\frac{1}{2}} \tag{7}$$

where $\Delta\tau$ = the superheat,
D_{th} = thermal diffusivity of the liquid,
ρ_1 = density of the vapor at the external pressure and the saturation temperature,
ρ_2 = density of the liquid
c_2 = specific heat of the liquid, and
L = latent heat of vaporization of the liquid.

The same solution can be applied to the formation of gas bubbles in a supersaturated liquid. The difference is that mass is being transferred through the liquid rather than heat.

$$C' = \left(\frac{c_i - c_f}{1 - c_f}\right)\left(\frac{\rho_2}{\rho_1}\right)\left(\pi D_m\right)^{\frac{1}{2}} \tag{8}$$

where c_i = the initial gas concentration,
c_f = the gas solubility at the external pressure, and
D_m = molecular diffusivity of the gas through the liquid.

The expressions for the growth-rate constants given in Eqs. (7) and (8) are grouped in three terms. The first is the weight-fraction flashing when the liquid pressure is reduced and the temperature drops to the saturation temperature at the lower pressure. The second term is the

liquid to gas density ratio which is equivalent to the gas to liquid specific volume ratio. The product of the first two terms therefore are proportional to the volume increase of the material in the flashing process. The third term is a measure of the rate at which heat or molecules are transferred from the body of the superheated or supersaturated liquid into the bubbles.

The importance of these growth-rate constants as applied to a flashing jet is that we can compare the growth rates of bubbles in various superheated and supersaturated systems to estimate the relative effectiveness of flashing in shattering a liquid jet. This growth-rate constant is calculated at various superheats for a few pure liquids and plotted in Figure 18. In all cases the external pressure is atmospheric. The constant is also calculated for some supersaturated systems and plotted in Figure 19. In this case the constants are plotted versus injection pressure, and calculated assuming the liquid is saturated with the gas at the injection pressure. These calculations show that the growth-rate constants for the dissolved gas systems are considerably lower than for the superheated systems. This explains why injecting carbon dioxide in water had no effect on the jet break-up. The main reason for these low growth-rate constants is that the values of thermal diffusivities in liquids are about 100 times those for the molecular diffusivities of a dissolved gas in a liquid. The values of the corresponding growth rates for superheated and supersaturated systems differ by a factor which is

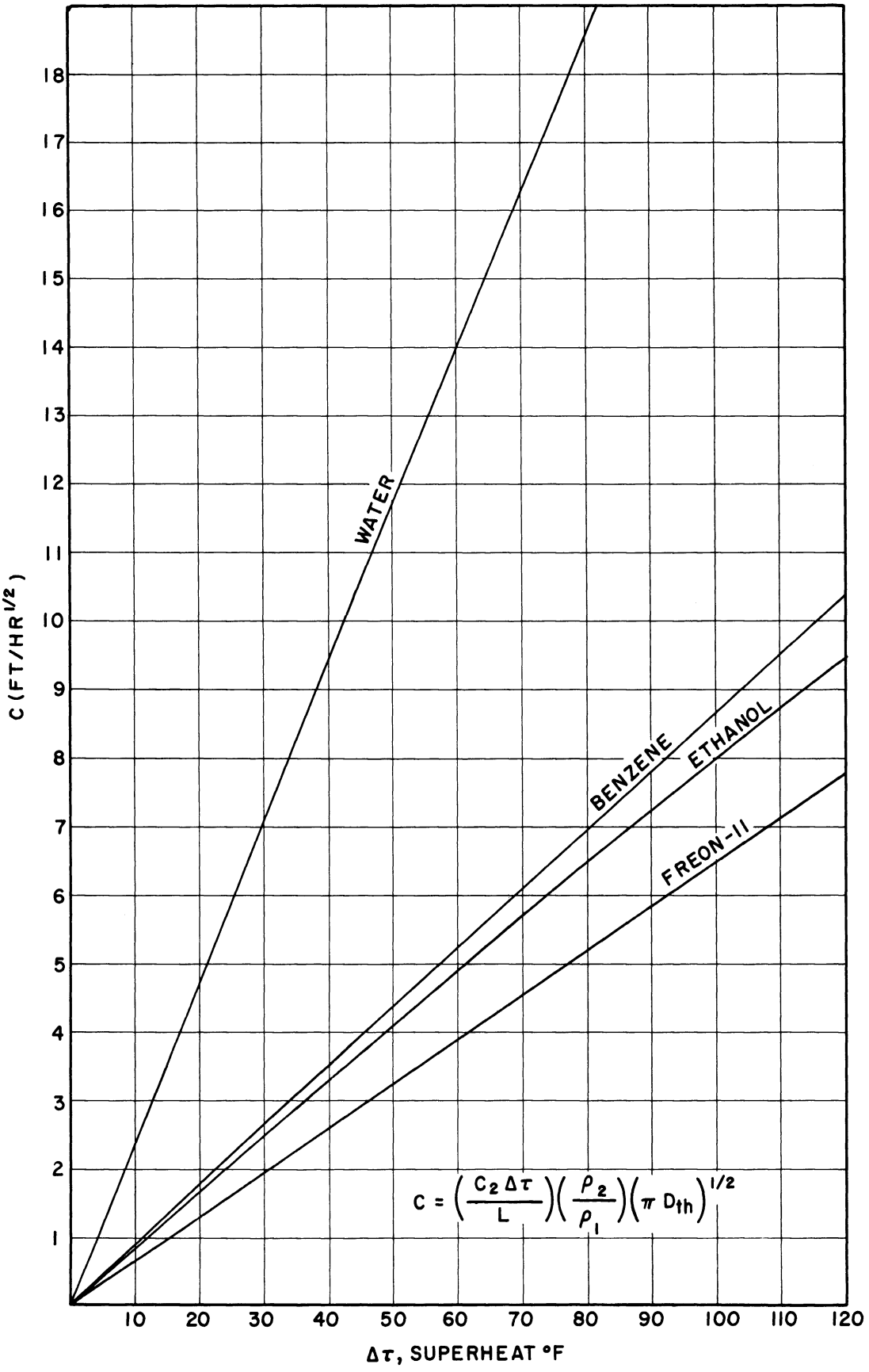

Figure 18. Bubble-Growth-Rate Constants for Superheated Systems at One Atmosphere.

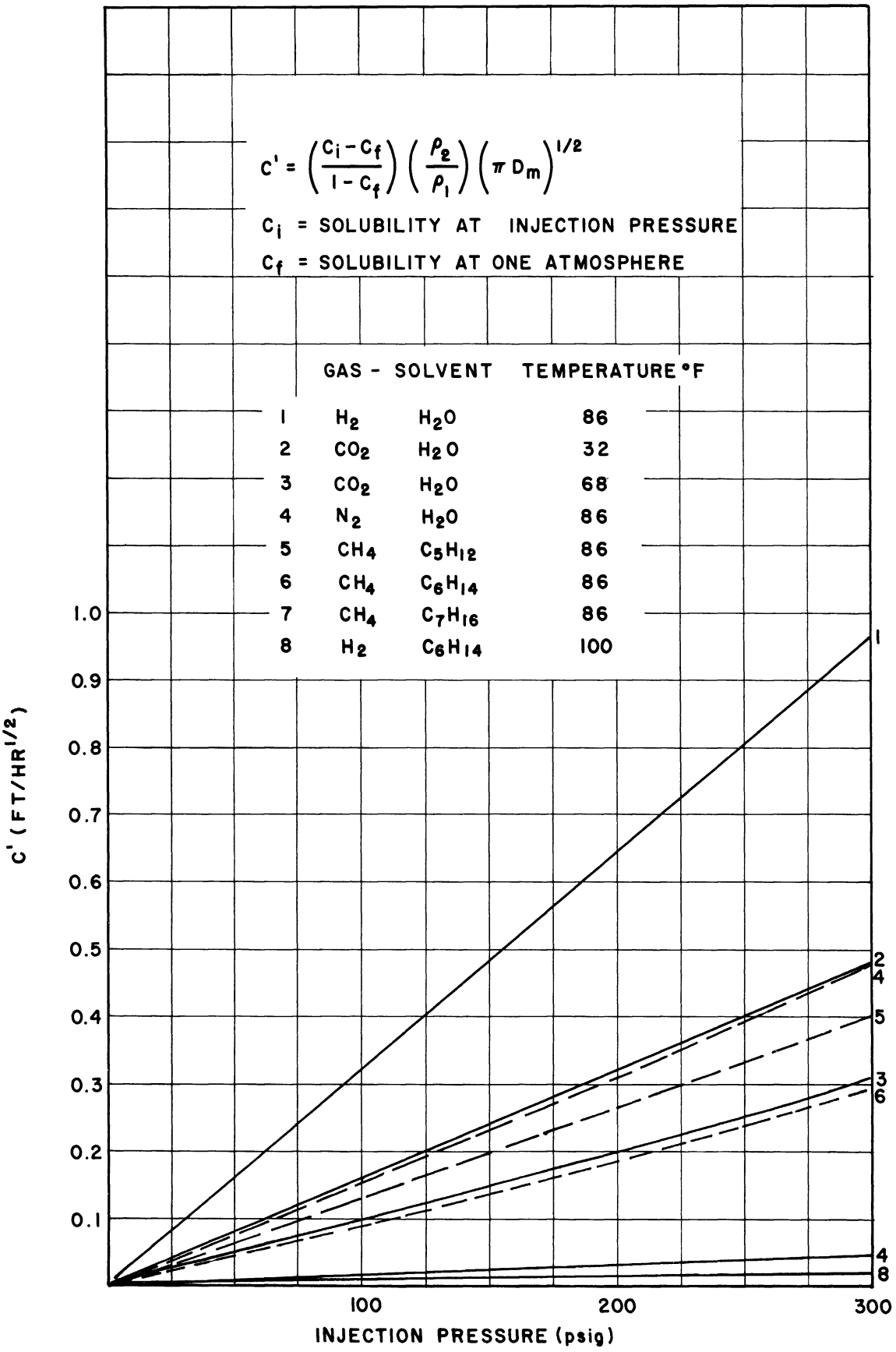

Figure 19. Bubble-Growth-Rate Constants for Supersaturated Systems at One Atmosphere.

the square root of this, or aprroximately 10. The growth-rate constants for supersaturated systems could be increased by increasing the initial solubilities, but this would require raising the injection pressures. This would defeat the purpose of employing flashing, however, which is to promote effective break-up at low injection pressures. Minimum injection pressures are required to inject jets in the superheated condition but these are relatively low. For example, all the superheats in Figure 18 may be attained with injection pressures no greater than 60 psig.

It should be pointed out that this predicted growth-rate constant refers to bubbles submerged in large extents of liquid at a uniform temperature. The bubble-growth rates required in the liquid jets are for bubbles near the orifice and within the body of the jet. These are the bubbles that contribute to the break-up. The liquid jet is at a fairly uniform temperature near the orifice. The growth-rate relation given in Eq. (6) does not refer to bubbles on the surface of the jets. This is of no matter as these surface bubbles do not greatly contribute to the break-up. The bubbles that are observed on the jets in Figures 9 and 12 have been formed at a temperature below that where the jet is effectively shattered. Several photographs were taken of the jet from the 0.031-in.-diameter rough-surface nozzle when water at 120 psig and 268°F. was injected through it. The sizes and distances from the orifice of a total of 18 bubbles from 10 photographs were measured. There was a distribution of bubble sizes, and only the largest ones were

measured. The sizes are plotted versus time (time = 0 at the orifice) in Figure 20. Note that the surface bubbles do not grow as large as predicted for a submerged bubble, and appear to grow linearly with time, rather than proportional to the square root of time. This result may be predicted by considering the simplified case of a hemispherical bubble on a flat liquid surface. Neglecting surface tension forces and assuming a constant liquid surface temperature, the liquid evaporates into the bubble at a rate proportional to the area covered by the bubble.

$$Vol = Ak't \tag{9}$$

where Vol = volume of the bubble,
k' = a constant, and
A = area covered by the bubble.

Substituting the expressions for volume and area as a function of diameter into Eq. (9), the diameter is shown to be directly proportional to time.

$$D = 3k't \tag{10}$$

The surface bubbles appear to be caused by the roughness of the orifice and are not to be confused with the bubbles that grow inside the body of the jets and shatter them.

The Effect of Physical and Dynamic Properties on the Break-Up

The bubble-growth rate, although important, is not the only criterion for shattering a jet. Some properties of the jet are also involved. The photographs of the water jets clearly demonstrate this. Figures 14, 15 and 16 are of water jets injected through sharp-edged

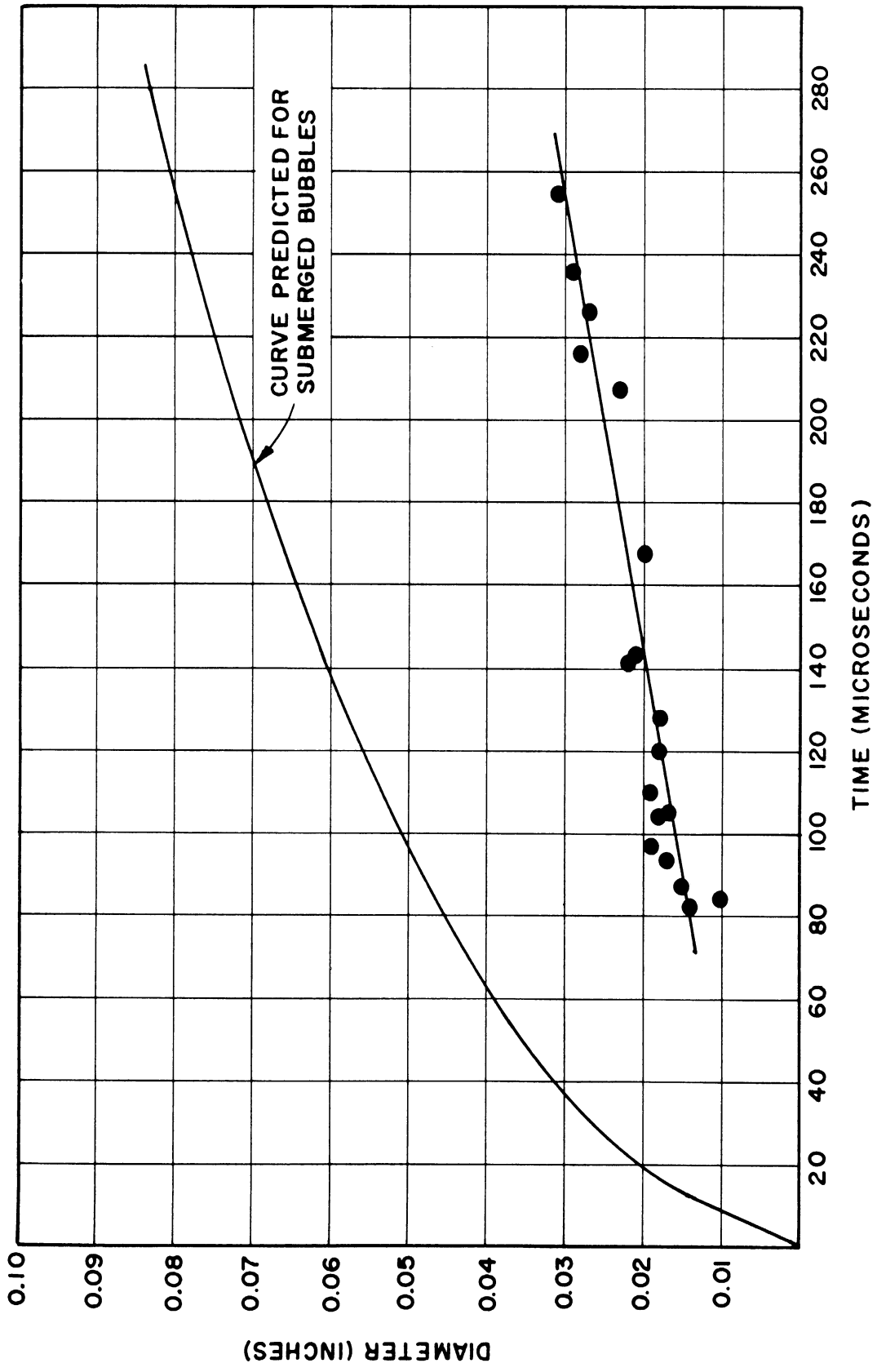

Figure 20. Experimental Surface Bubble-Growth Rates for Bubbles on 0.03-in.-diameter Water Jet Injected at 268°F.

orifices at about the same injection temperatures and pressures. The bubble-growth rates are the same in all the jets because of the equal temperatures. The larger jets (Figures 14 and 15) are completely shattered by the gas evolution. The smaller jet, however, is only broken up as a result of the bubbles cutting it into sections. Cylindrical portions of the jet are still intact after the bubbles have burst. This same type of difference was noted in the discussion of Figure 13, which pointed out that a jet injected under the same conditions from a 0.031-in.-diameter rough orifice would have been shattered while this smaller one was not. These photographs indicate that the degree to which the growing bubbles affect the jet are influenced by some properties of the jet. The fact that at a given bubble-growth rate, one jet is shattered and another is cut into intact portions, suggest that the jet stability is probably an important factor. As we have seen in Chapter II, the Weber number is a measure of this jet stability.

To measure the effect of Weber number on the shattering temperature, water was injected through the experimental nozzles at pressures ranging from 60-130 psig and temperatures ranging from room to 300°F. In a typical run, water was injected through a nozzle at a constant pressure and the temperature was allowed to rise slowly. As the temperature was raised, a fine spray could sometimes be observed around the jet starting between one and two inches from the orifice. This spray was more prominent with the rough-surface orifices. The jets, as has already been mentioned, were completely shattered within about a 5°F. temperature range. These shattering

temperatures are plotted versus Weber number in Figure 21. The Weber numbers are based upon the jet diameters obtained from photographs of the jet, not the orifice diameters. The velocities are calculated from the injection pressures and liquid density. A sample calculation is presented in Appendix C. Shattering temperatures could not be obtained for the jets from the orifices with sand ($\epsilon \cong 0.1$) because the roughness was severe enough to disintegrate the jets within 1-inch from the orifice with cold water.

The shattering temperature is very definitely a function of Weber number, the jet disintegrating at lower temperatures for the higher Weber numbers. There appears to be a break in the function of temperature versus Weber number at $N_{We} = 12.5$. The shattering temperatures are considerably lower at Weber numbers above this. This coincides with the existence of a "critical" Weber number for cold jets given for the point where the jet starts to become atomized. The accuracy of the shattering temperature is less at the Weber numbers above 12.5 because the cold jets break fairly close to the orifice. It is therefore difficult to estimate at what point the flashing is making the major contribution to the jet disintegration. The shattering temperatures appear to be independent of which of the two types of nozzles formed the jets.

If we hypothesize that at a given Weber number, a liquid jet must have a minimum bubble-growth rate to be shattered by vapor evolution; a shattering temperature - Weber number relation may be predicted for any liquid. The bubble-growth rate in a liquid corresponds to its temperature

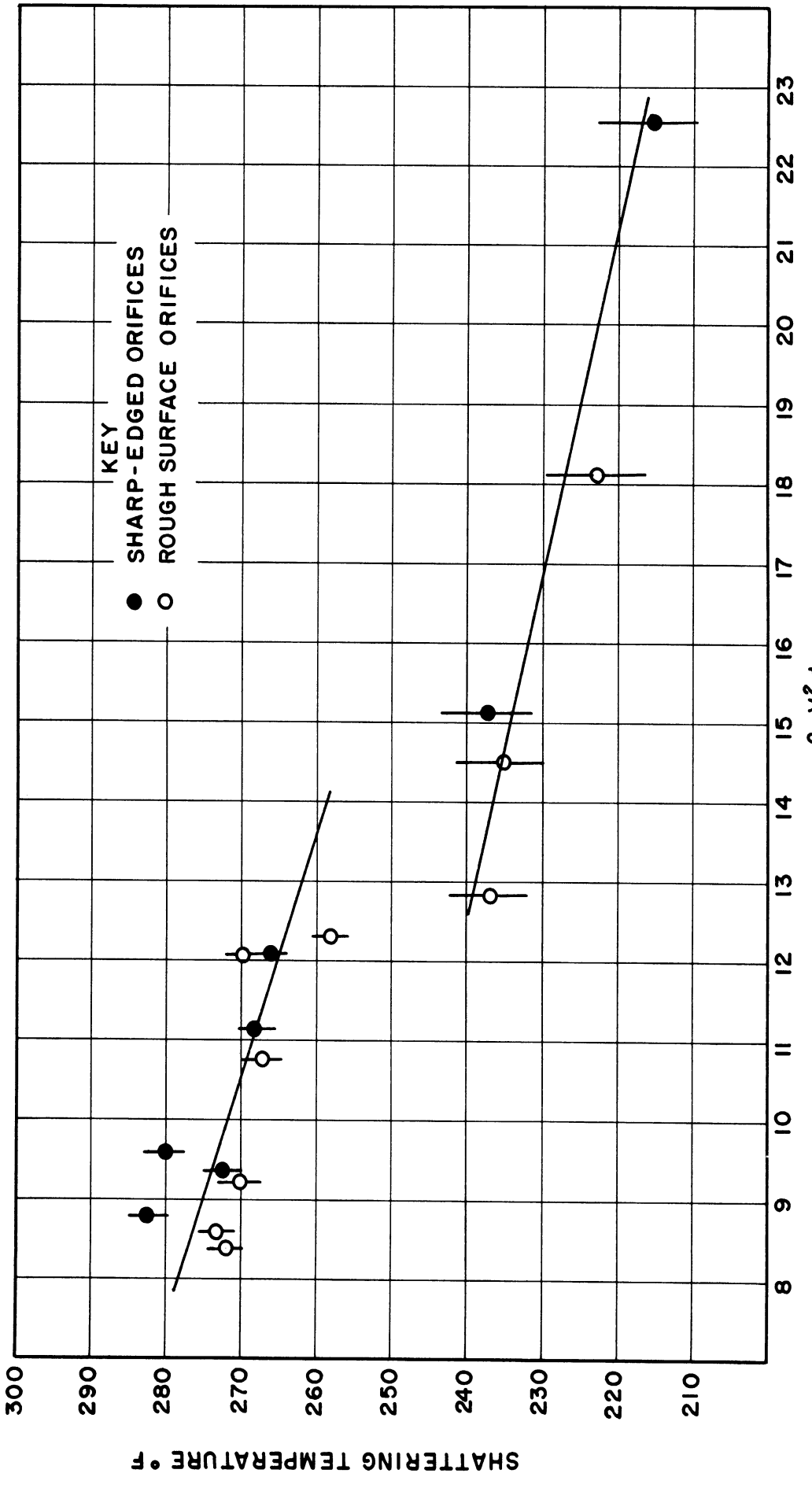

Figure 21. Effect of Weber Number on Water Jet Break-Up.

or gas concentration as given by Eqs. (7) and (8). This hypothesis may be tested by plotting the bubble-growth-rate constant at the shattering temperatures of water and Freon-11 versus the Weber number. This plot is presented in Figure 22 and shows that the points for the two liquids follow the same functional relation. A least-squares correlation for the bubble-growth rate at the shattering temperature was made and is given by

$$\begin{aligned} C &= 19.7 - 0.581\, N_{we} \qquad \text{for } N_{we} < 12.5 \\ C &= 11.5 - 0.419\, N_{we} \qquad \text{for } N_{we} > 12.5 \end{aligned} \tag{11}$$

Although this test is experimentally made with only two liquids, it covers a wide range of physical variables. For example, consider injecting water and Freon-11 through a 0.04-in.-diameter sharp-edged orifice at 100 psig. The break-up temperature for the water jet is 272°F. and for the Freon-11 jet is 118°F. These break-up temperatures correspond to bubble-growth-rate constants of 14 ft./hr.$^{\frac{1}{2}}$ for water and 2.8 ft./hr.$^{\frac{1}{2}}$ for Freon-11. The reason the bubble-growth rate for the Freon-11 is so much smaller than that for water is that Freon-11 has such a high vapor density. The Weber number for the Freon-11 jet is much greater than that for the water jet even though they are the same diameter and nearly the same velocity. This is because the interfacial tension of Freon-11 is so much lower than that of water, being 19 dyne/cm. compared to 59 dyne/cm. for water. The water and Freon-11 jets have Weber numbers of 9.3 and 24, respectively.

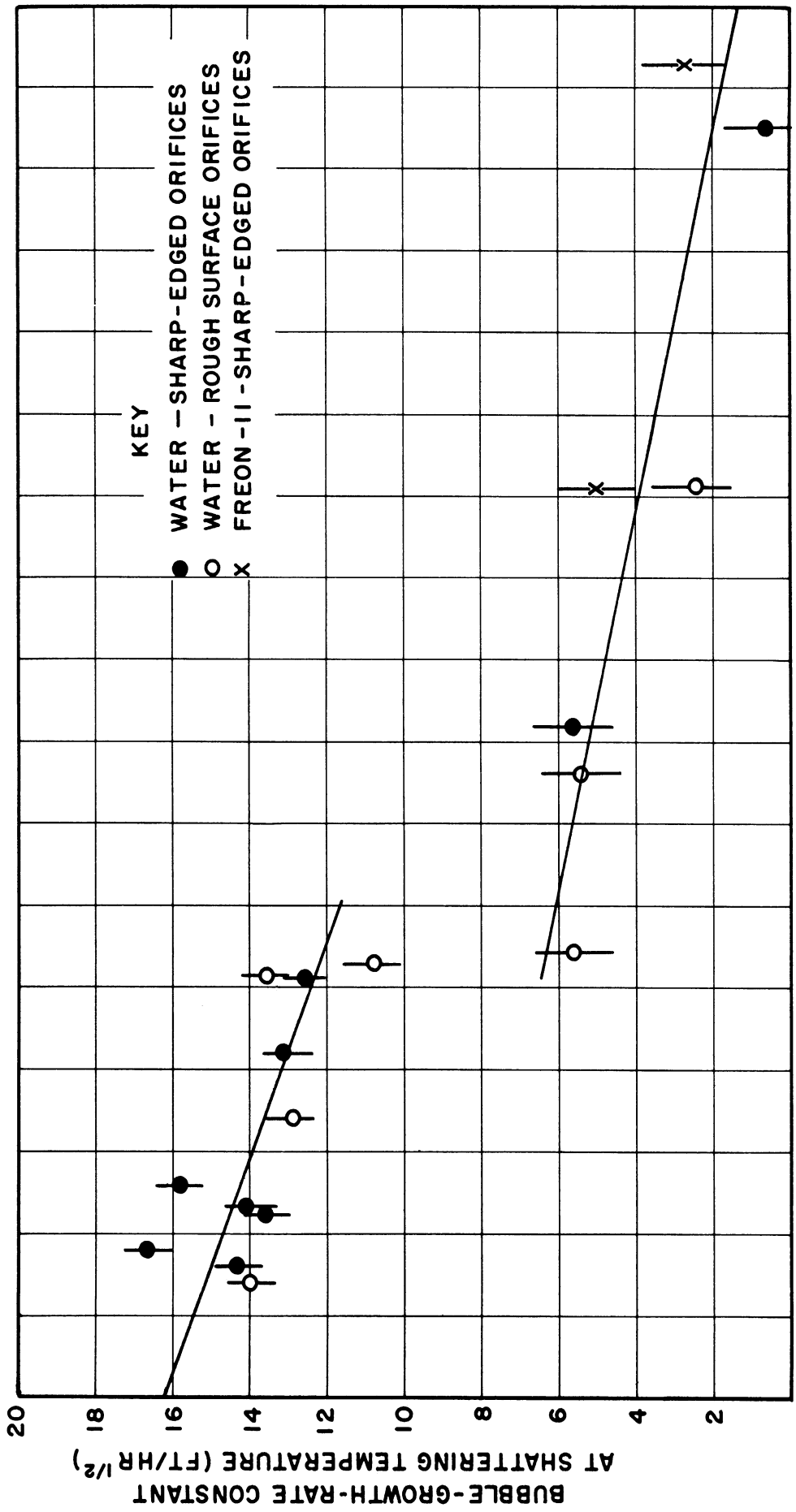

Figure 22. Effect of Weber Number on Water and Freon-11 Jet Break-Up.

One of the assumptions applied in the formulation of the bubble-growth-rate problem was that the liquid was low viscosity. This is true for the liquids injected in these experiments. Also, the literature on cold jet break-up has not indicated that a strong effect of viscosity on jet stability exists with the range of viscosities covered in these experiments. We should therefore not expect viscosity to affect the jet break-up for this study. A plot of the bubble-growth-rate constant at the shattering temperature versus Reynolds number given in Figure 23 shows that no correlation can be made. Some of the water points seem to follow a trend, but this is because the Reynold's number, like the Weber number are relations involving jet velocity and diameter. At several points where the water temperatures are similar, and thus the viscosities approximately the same value, we should expect a function bearing a certain relation to the Weber number to act similarly when plotted versus the Reynold's number. This breaks down, however, when widely different injection temperatures are involved and the viscosity varies considerably. The water and Freon-11 points do not coincide at all when plotted versus Reynold's number.

Another possible influence of turbulence is on the bubble-growth rate. The bubble-growth-rate relations are solved by obtaining the bubble wall temperature through a solution of the heat conduction problem and ignoring convection from the bubble wall. When bubbles shatter a jet, they do so within a 1-in. section. The characteristic diffusion length $(2D_{th}t)^{\frac{1}{2}}$ for heat diffusion in a 1-in. section of a jet traveling 100 ft./sec. is

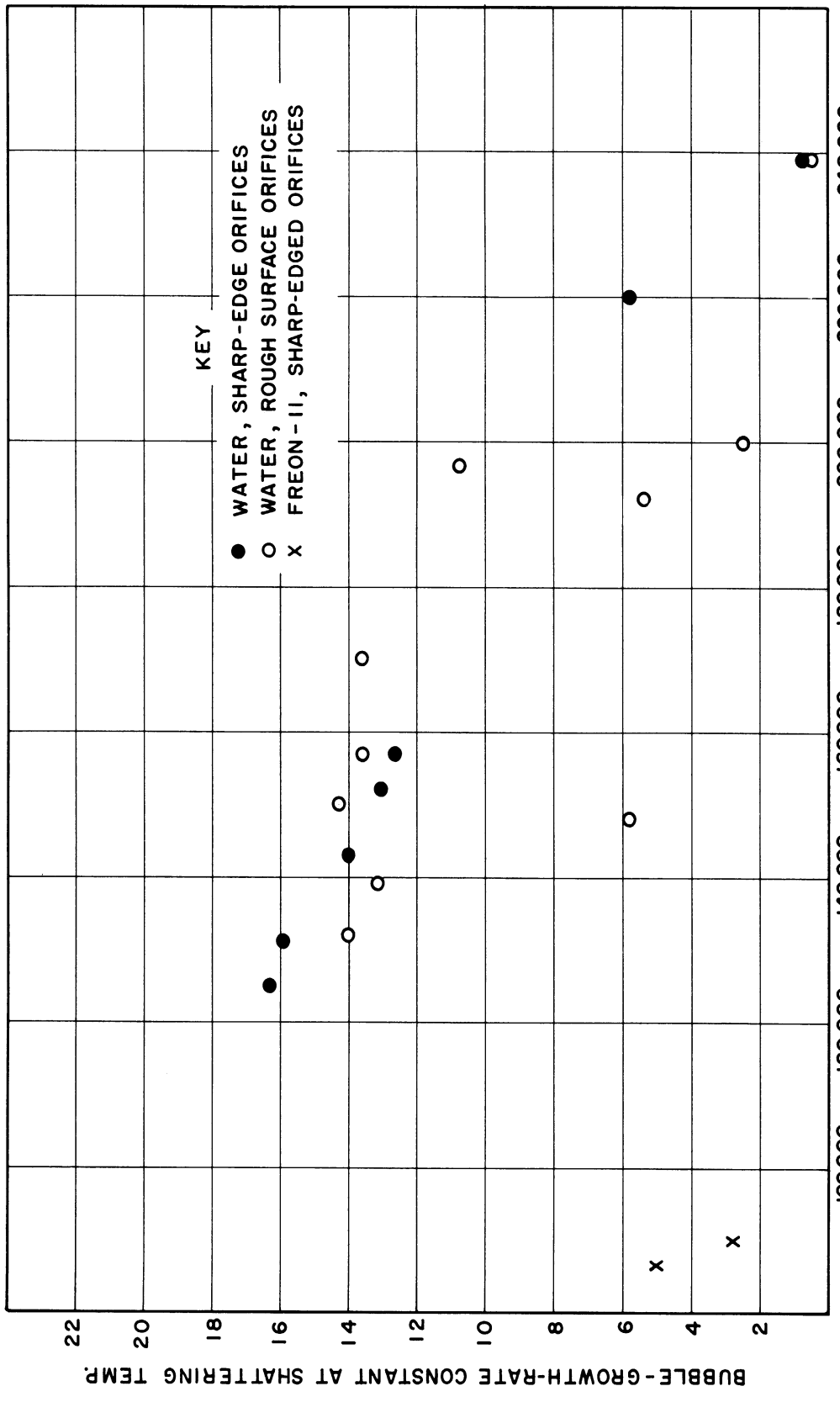

Figure 23. Effect of Reynold's Number on Water and Freon-11 Jet Break-Up.

about 0.0005-in. This is about 1/100 of the film thickness for heat transfer at these levels of turbulence. The thickness of the liquid layer around the bubble wall where the significant temperature reduction takes place is therefore well within the laminar region around the bubble wall. The exclusive consideration of the heat conduction problem is valid in this case and turbulence should have no effect.

The difficulty in injecting superheated liquids into the atmosphere over a wide range of viscosity is that pure liquids have approximately the same viscosity at their boiling points. The viscosity data for a number of liquids, including straight chain hydrocarbons, esters, alcohols, aromatics, and halogen-substituted hydrocarbons were investigated and this seems to apply to all liquids. Mixtures must therefore be injected in order to obtain a wide range of viscosity. This complicates the problem because not only will high viscosities affect the jet stability, the bubble-growth-rate relations may not apply. There may be a large variation in the viscosity at the bubble wall and in the body of the jet because of the temperature differences. In view of the large scope of the problem required to find the effect of high viscosity on the break-up of flashing jets, it is not included as part of this study.

CHAPTER V

THE SPRAYS FROM FLASHING JETS

Drop-Size Distributions

Drop-size analyses were made for the sprays from water and Freon-11 jets over a wide range of injection conditions. The conditions and mean drop-size results are presented in Table IV. About 35,000 drops were counted and measured to make the 18 analyses, between 1500 and 2000 drops per analysis. The details of photographing the sprays, analyzing the data, and accuracy of the analyses are presented in Chapter III and Appendix A. In all but three cases, the analyses were made at injection temperatures above the value where the jet was shattered by flashing. Cold jets were usually not completely broken up at the sample location (6 inches from the orifice), just sinously deformed. The only cold jets which were disintegrated sufficiently to make an analysis were from the largest diameter nozzle and the nozzle with with sand on the orifice surface.

A drop-size analysis is designed to give an estimate to the probability distribution function, $f(D)$, which is defined in such a way that $f(D)dD$ is the percent of the total number of drops that have diameters between D and $D + dD$. The results of an actual analysis give the percentages, ΔN, of the drops found to lie within each of the experimental size ranges, ΔD. These percentages can be divided by the magnitude of the size intervals to provide the average percentage of drops per unit size over

TABLE IV

MEAN DROP-SIZES

Run No.	Nozzles			Jet Conditions					Mean Drop-Sizes (microns)				
	Type	D in.	Jet D in.	T°F	ΔP	N_{we}	C $ft/hr^{\frac{1}{2}}$	Liquid	δ	D_{10}	D_{20}	D_{30}	D_{32}
1	A	0.040	0.032	287	120	11.3	17.9	H_2O	1.39	34.7	43.2	48.9	62.9
2	B*	0.031	0.031	287	120	11.0	17.9	H_2O	1.39	54.4	59.8	64.3	74.5
3	A	0.080	0.066	204	80	14.9		H_2O	0.88	142	186	227	336
4	A	0.080	0.066	236	80	15.2	5.0	H_2O	1.22	43.0	50.9	59.6	82.2
5	A	0.080	0.066	236	120	22.7	5.0	H_2O	1.43	33.9	39.4	44.9	58.3
6	A	0.030	0.025	287	130	9.57	17.9	H_2O	1.49	35.7	45.6	62.6	85.1
7	B	0.031	0.031	287	90	8.21	17.9	H_2O	1.71	34.3	40.0	48.7	71.9
8	B	0.040	0.035	270	130	13.3	13.6	H_2O	1.77	30.7	34.9	39.4	50.0
9	B	0.040	0.035	287	90	9.27	17.9	H_2O	1.62	35.0	38.4	41.9	49.6
10	B	0.040	0.035	287	130	13.4	17.9	H_2O	1.69	29.8	33.9	35.7	39.4
11	B	0.060	0.053	254	120	18.4	9.9	H_2O	1.21	35.6	42.9	52.0	76.3
12	B	0.060	0.053	270	80	12.4	13.6	H_2O	1.67	32.7	37.4	44.1	61.2
13	B	0.060	0.053	270	120	18.5	13.6	H_2O	1.53	29.6	33.6	38.0	48.5
14	C	0.020	0.020	80	94	5.14		H_2O	0.73	82.3	118	197	280
15	C	0.020	0.020	270	130	7.56	13.6	H_2O	1.95	25.1	27.4	30.4	38.9
16	C	0.020	0.020	278	120	7.03	15.4	H_2O	1.60	24.2	27.1	30.0	36.6
17	A	0.030	0.025	152	94	18.1	5.0	F-11	1.66	28.5	32.4	36.0	44.4
18	C	0.020	0.020	125	95	14.1	3.2	F-11	1.16	36.1	43.4	55.0	84.5

each experimental size range. This average percentage of drops per unit size range for each size range can be plotted versus the drop size, giving the experimental distribution function. This is defined in the same way as the probability distribution function, except that average values of f(D) are given between the finite intervals D + ΔD, rather than point values at each D. The probability distribution function can be estimated from the experimental distribution function. An example of an experimental distribution function and its corresponding estimated probability function is shown in Figure 24.

The mean diameters for a drop-size probability distribution are given by

$$\overline{D_{mn}} = \left[\frac{\int_0^\infty D^m f(D)dD}{\int_0^\infty D^n f(D)dD} \right]^{\frac{1}{m-n}} \qquad (1)$$

These may be estimated from the experimental distributions by

$$\overline{D_{mn}} \simeq \left[\frac{\sum D_{AV}^m \Delta N}{\sum D_{AV}^n \Delta N} \right]^{\frac{1}{m-n}} \qquad (2)$$

The mean diameters that were calculated for these analyses were the linear mean diameter, $\overline{D_{10}}$; surface mean diameter, $\overline{D_{20}}$; volume mean diameter, $\overline{D_{30}}$, and volume-surface mean diameter, $\overline{D_{32}}$. These are given in Table IV.

One notable observation of the drop-size results is that although water was injected at temperatures such that between 2.50 wt. percent and 7.85 wt. percent flashed, and the experimental Weber numbers ranged from

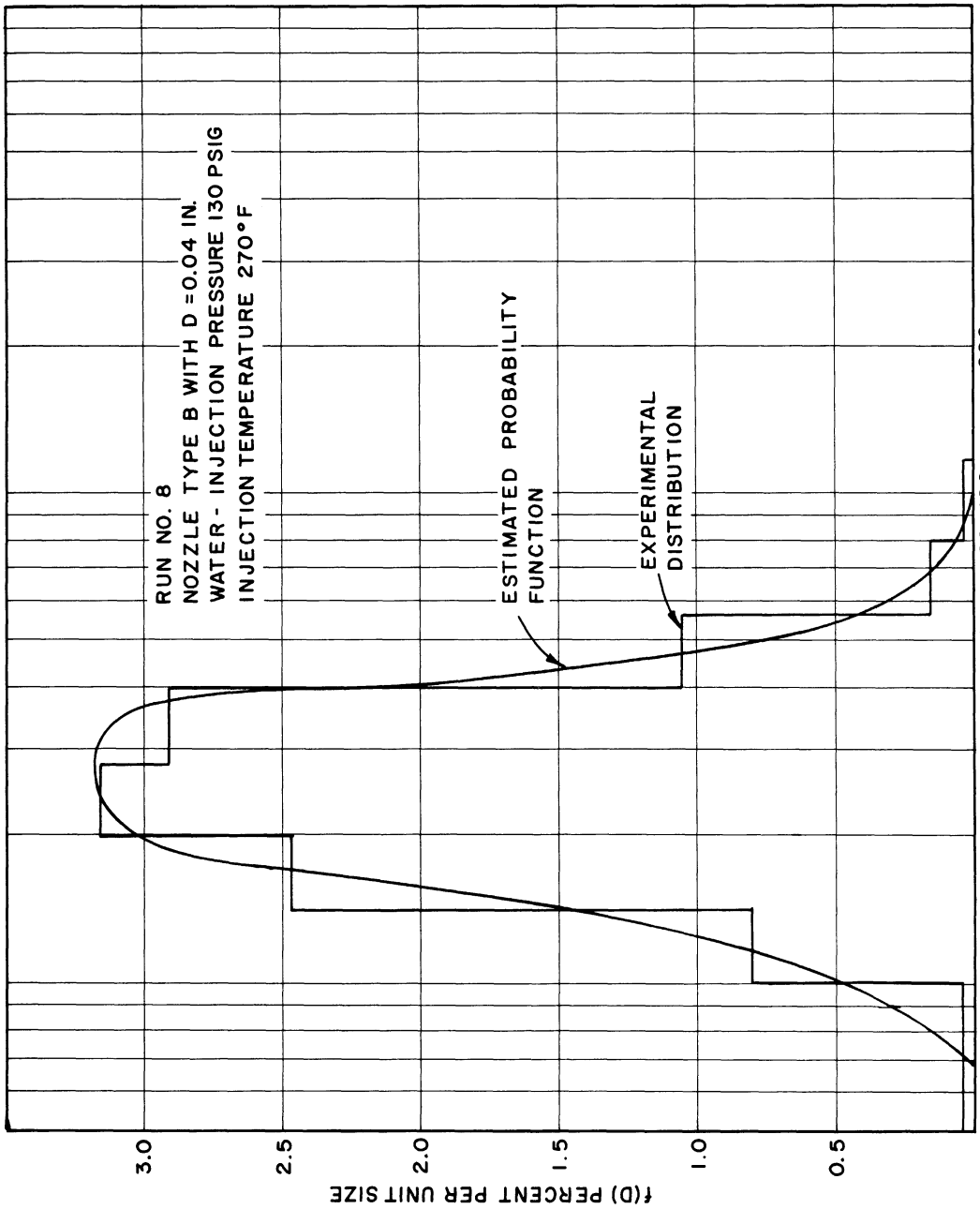

Figure 24. Typical Drop-Size Distribution

7.0 to 22.7, the range in the linear mean diameters of the sprays from the flashing jets was only from 24.2 microns to 43.0 microns. Apparently, once the Weber number and bubble-growth rate are high enough to shatter the jet, more intense conditions do not have a great effect on the drop-size.

Observation of the data for the flashing water jets seemed to indicate that at a given injection temperature, the drop-sizes decrease with increasing Weber number. This may be seen in Figure 25 which presents three distribution functions for sprays from jets injected at 270°F., where C is 13.6 ft./hr$^{\frac{1}{2}}$. The drop-sizes also appeared to decrease at similar Weber numbers when the injection temperature was increased. Figure 26 shows three of the distribution curves for water injected at Weber numbers between 12.4 and 15.2 at temperatures such that the bubble-growth-rate constants were 5.0, 13.6, and 17.9 ft./hr$^{\frac{1}{2}}$.

The best correlation that could be made for the drop-sizes of the sprays from the flashing water jets took the form

$$\overline{D_{10}} = \frac{1840 - 5.18\ T\ (°F)}{N_{we}} \quad \text{(microns)} \qquad (3)$$

This correlation is made from the jets from the type A and B nozzles. The standard deviation is 6.1 percent. The correlation is shown graphically in Figure 27 which is a plot of $(\overline{D_{10}})(N_{we})$ versus C. This can also be plotted against the injection temperature as the bubble-growth rate is essentially directly proportional to the temperature for water. The correlation shows the fact that the orifice may be sharp-edged or have a rough surface has no

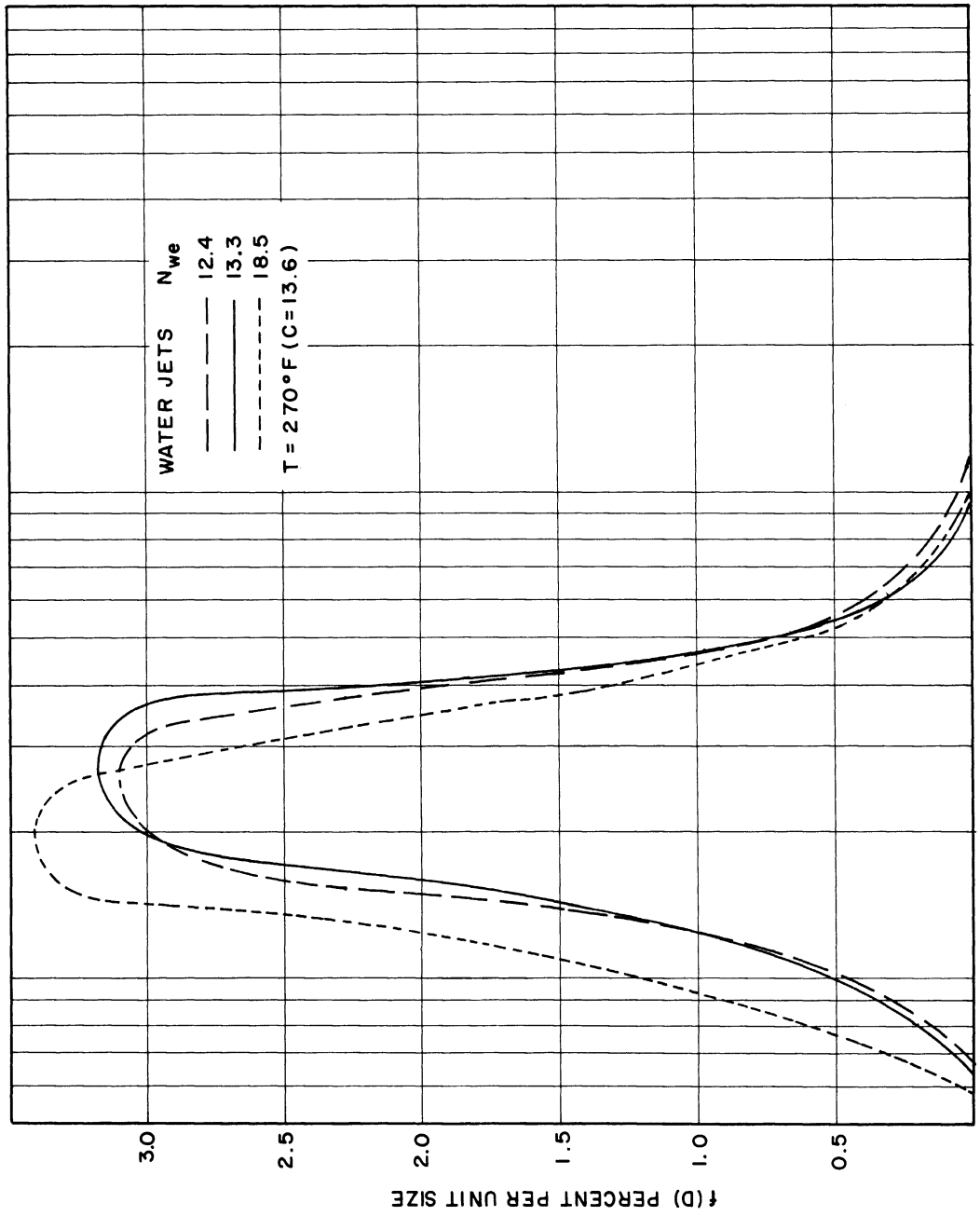

Figure 25. Effect of Weber Number on Drop-Size Distributions at Constant Injection Temperature.

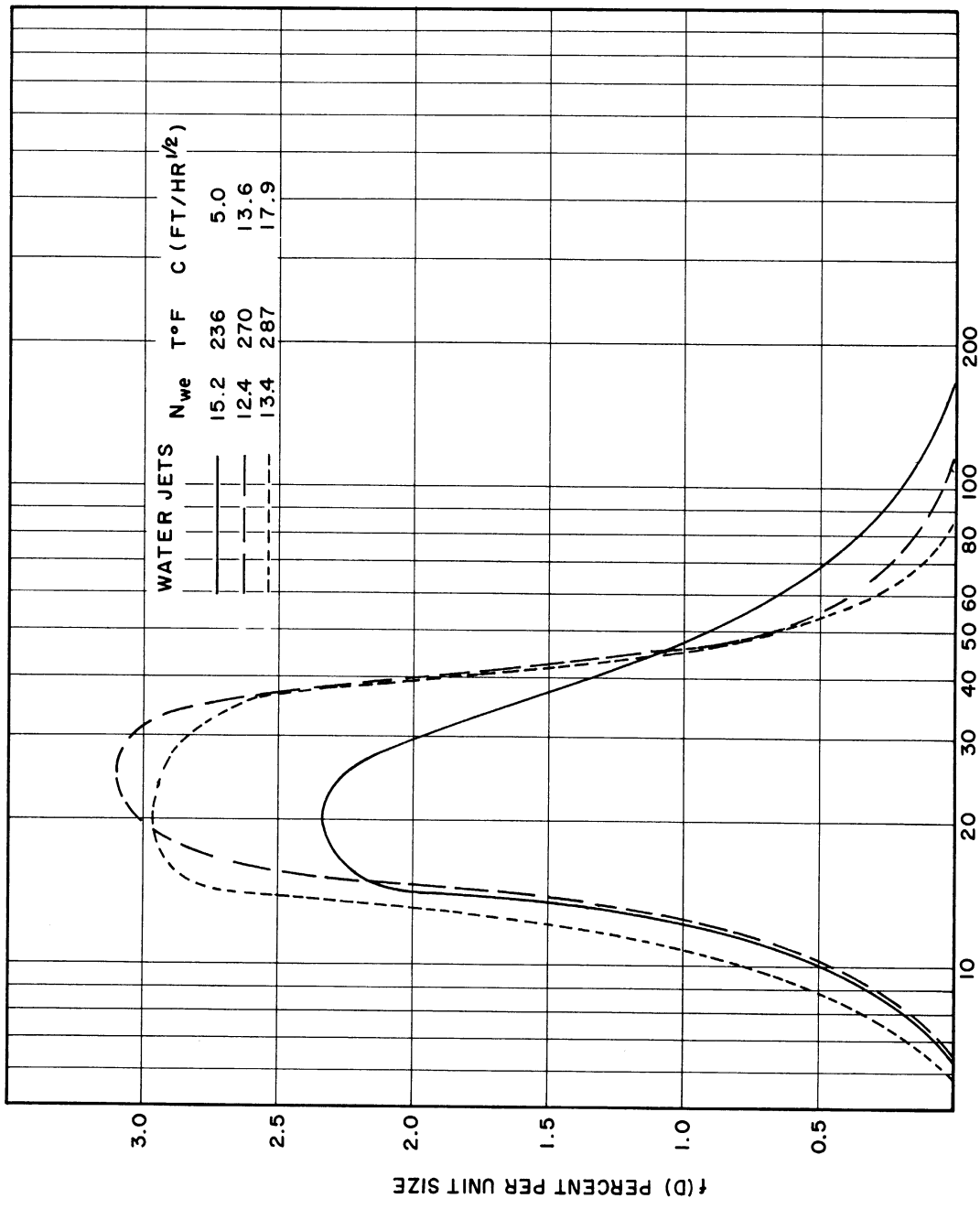

Figure 26. Effect of Injection Temperature on Drop-Size Distributions at Similar Weber Number.

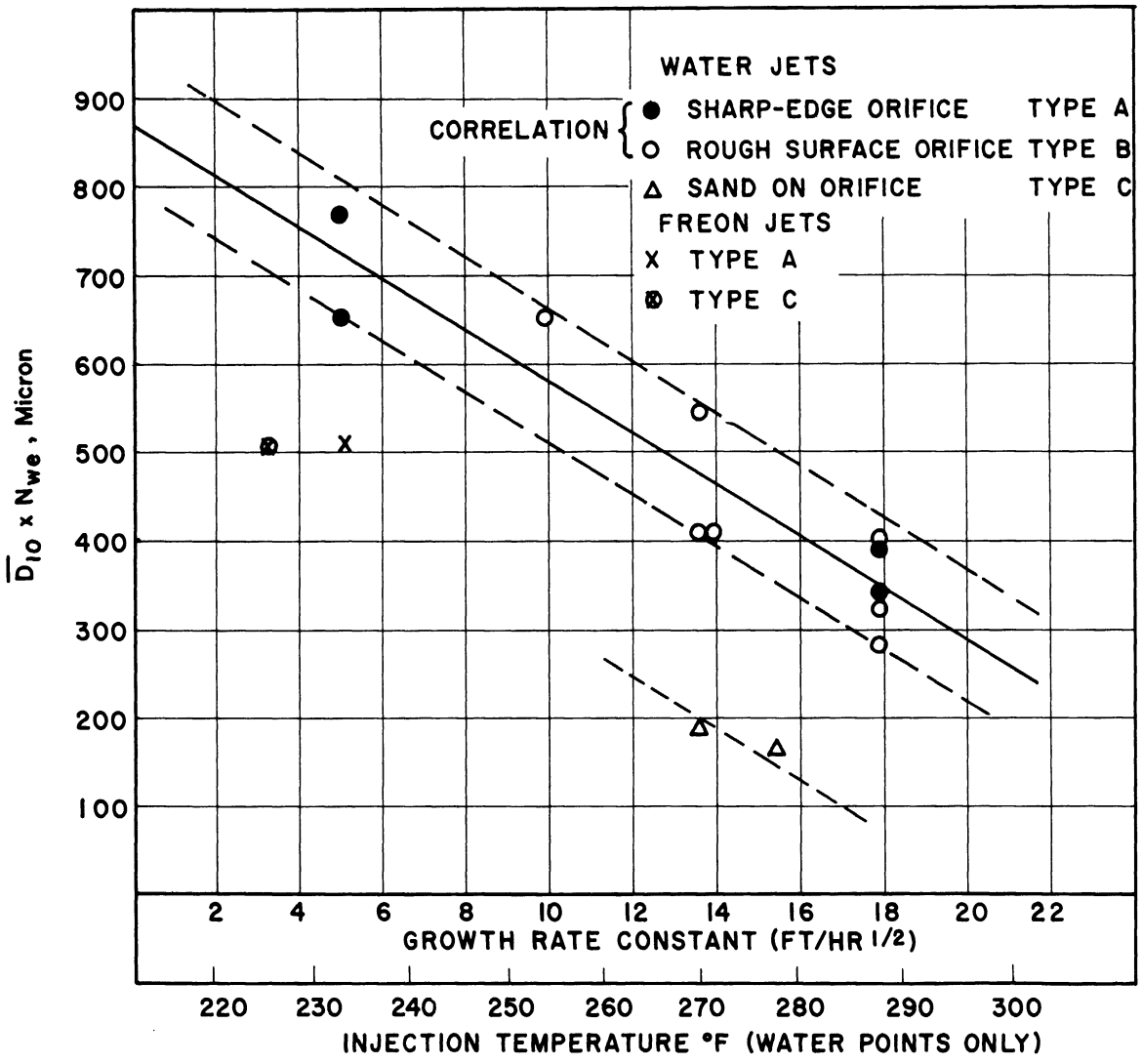

Figure 27. Effect of Bubble-Growth Rate and Weber Number on Drop-Sizes.

effect on the drop-size. The drop-sizes are affected by very rough surfaces ($\epsilon \gtrsim 0.1$). This is because the pieces of sand are large enough to tear ligaments off the jets and decrease the mean drop-size. It was pointed out before that only a small range of mean drop-sizes was recorded for the study of the flashing water jets, but if the very rough orifices are not included, the average drop-size range is further reduced, the linear mean varying only from 29.6 microns to 43.0 microns.

The drop-sizes for the Freon-11 sprays are smaller than for the water sprays as one can see by the points in Figure 27. These smaller drop-sizes for Freon-11 are probably a result of the lower surface tension. A lower surface tension allows for the transient existence of smaller liquid ligaments and thinner liquid films during the jet shattering process, which disintegrate to smaller drops. The surface tension also affects the size of the larger drops because a large drop is more readily shattered if it has a low surface tension.

The drop-sizes for the sprays from the cold water jets were considerably higher than those from the flashing jets. The linear mean diameters of the two cold jet sprays were 82 microns and 142 microns, compared to the 24-43 microns linear mean diameters for the flashing sprays.

An attempt was made to fit the drop-size distributions to an empirical distribution function so that the uniformity of the various sprays could be directly compared. The empirical distribution chosen for this was the logarithmic-normal-probability distribution function[20].

This form appeared to be suitable because the distribution curves plotted versus the logarithm of drop diameter in Figures 24, 25, and 26 looked symmetrical. This distribution function is given by

$$f(D) = \frac{\delta}{\sqrt{\pi}} e^{\left[-\left(\delta \ln\left(\frac{D}{D_{vmd}}\right) + \frac{3}{2\delta}\right)^2\right]} \frac{1}{D} \qquad (4)$$

where δ = characterizing parameter which is measure of the size uniformity, and
D_{vmd} = the volume median diameter.

An experimental distribution which follows this empirical function should yield a straight line when the cumulative number distribution,

$$f(D) = \int_o^D f(D)dD \cong \sum_o^D \Delta N \qquad (5)$$

is plotted on the probability scale versus the logarithm of drop diameter. An example of such a plot is given in Figure 28 for the distribution for run No. 9. This gives a very good straight line except at the highest drop percentages. This is not too serious as the highest percentages are those where one would expect the least accuracy. Plots for most of the analyses also produced straight lines, with occasional discrepancies at cumulative percentages above 98. Values of the uniformity parameter, δ, are readily obtained from the log-probability plots by the slope of the lines.

$$\delta = 0.394 \; / \; \log_{10}(D_{90}/D_{50}) \qquad (6)$$

where D_{90}, D_{50} = are the diameters for the cumulative percentages of 90 and 50, respectively.

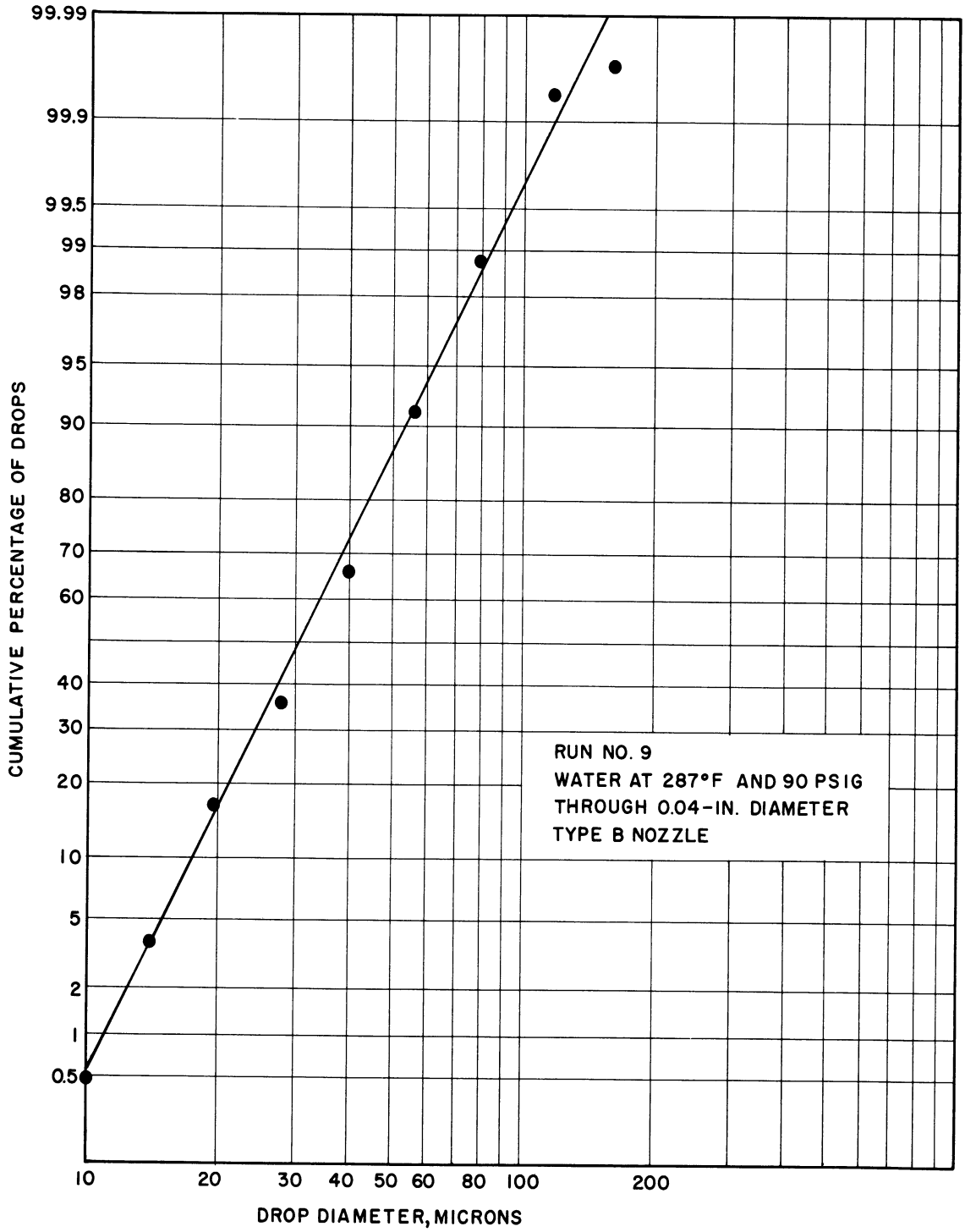

Figure 28. Typical Cumulative Distribution Function (Log-Probability Scales).

The magnitude of this parameter is a measure of the uniformity of the distribution, the higher values signifying the more uniform distributions. The values of δ are given in Table IV. Attempts to correlate the uniformity parameter with the operating variables were not too successful. This is not too suprising, as the range of δ is small, $1.21 < \delta < 1.95$. The average value of δ for the 14 analyses of the sprays from flashing water jets was 1.55. This may be compared to the average value for the sprays from the cold-water jets which was 0.80. The uniformity parameters for the sprays from the water jets are plotted in Figure 29 versus the bubble-growth-rate constant. Although it is not conclusive, the uniformity appears to increase with bubble-growth rate. The major difference is the difference in δ between the sprays from the flashing jets and the cold jets (C=0). The values of δ for the spray from the flashing Freon-11 jet formed by the nozzle of type A lies within the range for the flashing water sprays. It is not valid to compare δ for the Freon-11 spray from the nozzle of type C, because although the jet is superheated, it would not have shattered if a very rough surface had not been employed.

Ranz[25] has given typical values of δ for sprays from various types of atomizers.

TABLE V. TYPICAL UNIFORMITY PARAMETERS FOR ATOMIZERS

Atomizer	δ
Gas Atomizer	0.93
Spill-Controlled Swirl Nozzle	1.29
Vaned-Disk Sprayer	1.54

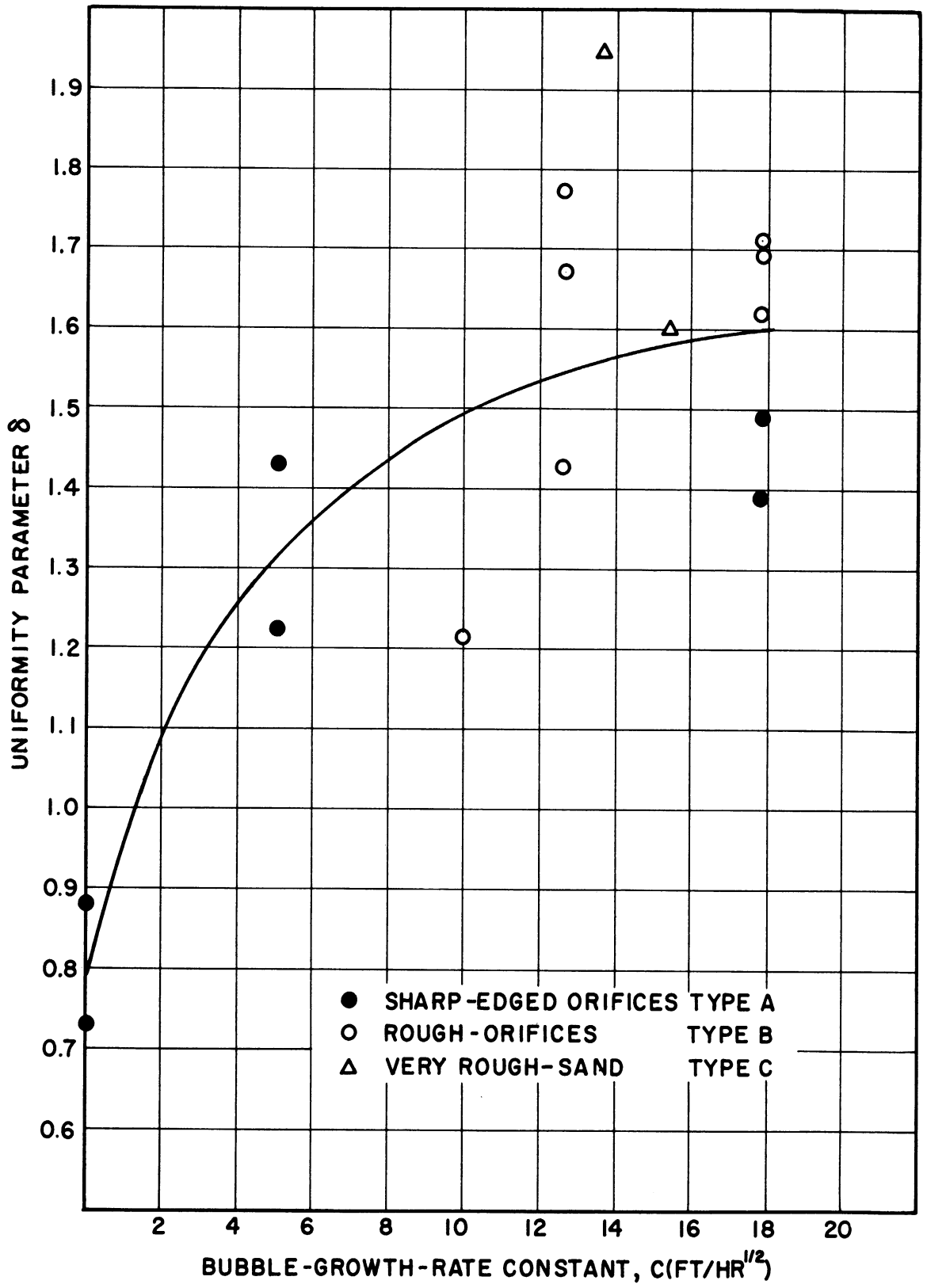

Figure 29. Uniformity of Sprays from Water Jets.

The size uniformity for the sprays from the flashing jets compares quite favorably with the uniformity of the sprays from these other atomizers.

It is impossible to quote typical mean drop-sizes for various methods of spray formation as this parameter is very dependent on the injection conditions. One can qualitatively say, however, that the mean drop-sizes for sprays from flashing jets are somewhat larger than drop-sizes from gas atomizers, but somewhat smaller than drop-sizes from disk sprayers. The mean drop-sizes for the sprays from flashing jets are similar to those often observed in sprays from swirl nozzles.

The mean drop-sizes correlated here are the linear mean diameters, which are simply the arithmetic averages of the drop diameters in one location or in a whole spray. The choice of this particular mean to correlate the data is somewhat arbritrary, as any one of the various means might have been employed. The choice of a particular mean depends upon the application of the spray. For example, if the process being considered is controlled by the magnitude of the surface area, the surface-mean diameter would be the most desirable to correlate. The various mean diameters reported in Table IV are sufficient to cover the means required for the analysis of most processes where sprays are employed.

Characteristics of the Sprays

It was pointed out earlier that the drop-size is not necessarily the most important spray characteristic for a particular application. This section will present some of the other characteristics of the sprays from the flashing jets. One characteristic that is available from these analyses is the variation in drop-size across a plane perpendicular to the spray axis. This particular characteristic is mainly of interest in the manner in which it relates to the break-up mechanism.

Figure 30 shows the variation in drop-diameter across the sprays from the flashing water jets for the three types of nozzles. In most cases, the largest drops are the furthest away from the spray axes. The drop-size decreases approaching the axis, and then usually increases again at the spray axis. This can be explained by the manner in which vapor bubbles disintegrate the jet. Consider a portion of a flashing jet in which one or more bubbles have expanded and shattered the jet. The drops from the shattered jet have two components of velocity, one parallel to the spray axis given by the original momentum of the jet, and one perpendicular to the spray axis and away from it caused by the rapid expansion of vapor bubbles inside the jet. At a given distance from the orifice, the larger drops will have moved the furthest away from the spray axis because the drag has a greater effect on the smaller drops and reduces the distance they travel from the axis before coming to their terminal velocities[29].

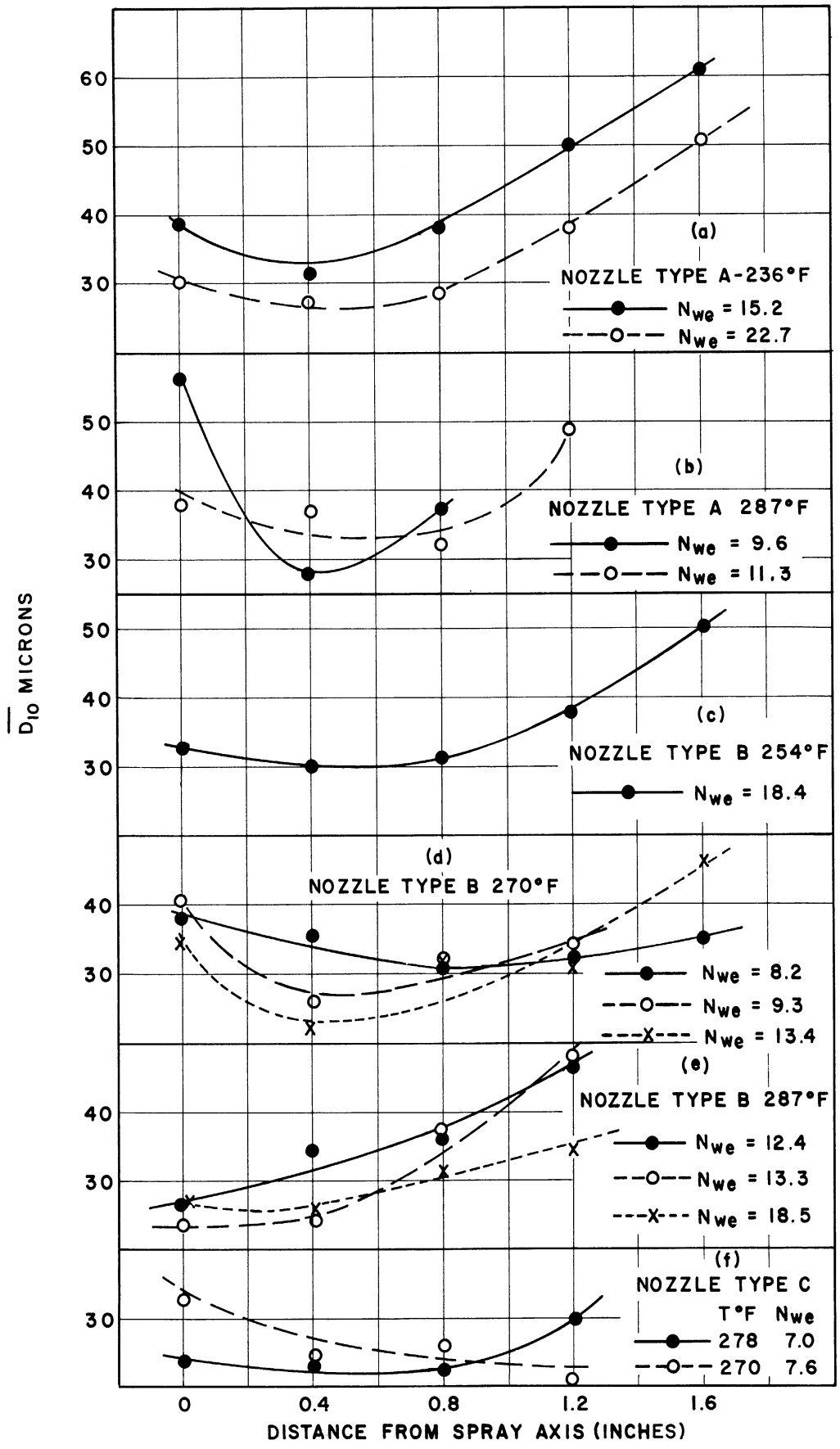

Figure 30. Variation in Drop-Diameters across Sprays from Flashing Water Jets.

The reason that the drop-size does increase at the spray axis is that portions of the jet are not exploded by the vapor evolution, and only have an initial velocity component in the direction of the spray axis. This tendency for large drops to exist at the spray axis should decrease as the intensity of the break-up is greater, for fewer portions of the jet could escape the expansion effect of the growing vapor bubbles. For example, in Figure 30c, 30d, and 30e, the tendency for the existence of larger drops at the axis almost disappears when the temperature is up to 287°F. Weber number also affects this as can be seen by comparing Figure 30b and 30e. Although both are at the same temperature, the drop-sizes increase at the axis in Figure 30b, where the Weber numbers are lower.

The sprays from the nozzles with sand on the surfaces have smaller drop-sizes because the sand particles tear ligaments off the outside of the jet. This is demonstrated in Figure 30f by the fact that the tendency for larger drops to be farther from the spray axis is less than with the other nozzles. The smaller drops are formed from the liquid ligaments which are torn off at the outside surface of the jet, and so downstream of the orifice, tend to be further from the axis. This is the same reason that the variation in drop-size across the sprays is very different when sprays are made merely by pressure injection of cold liquid. The liquid jets are disintegrated by the action of stresses at the jet surface. This break-up action at the surface produces smaller drops from the liquid at the

surface. The result is that, downstream of the break-up point, the smallest drops are the furthest away from the spray axis, and the largest in the center.

The velocities of the drops in a spray are also available from a spray analysis. The velocity of the drops in a plane perpendicular to the spray axis vary with the position with respect to the spray axis and with the size of the drops. Figure 31 shows the velocities for a spray from one of the flashing jets. The velocities given are averages for the velocities found in a given location and lying within a given size range. The plot shows that the drops have the highest velocities at the spray axis and decrease with distance from the axis. The drop-size has a strong effect, the larger ones going the fastest. The smaller drops for each location appear to approach a constant velocity. This same general pattern of velocities was observed in all thespray analyses from the flashing jets. The fact that the larger drops are traveling the fastest is to be expected, because it takes longer for them to decelerate to a terminal velocity and their velocities during the deceleration and at the terminal values are higher. This situation is considerably more complicated than a single drop in a large expanse of vapor, however, as in this case, the vapor starts to move. There is a net transfer of momentum from the drops to the vapor in the spray zone. The vapor will obtain more momentum at the more dense parts of the spray, accounting for the higher velocities at the spray axis. The fact that the smaller drops approach

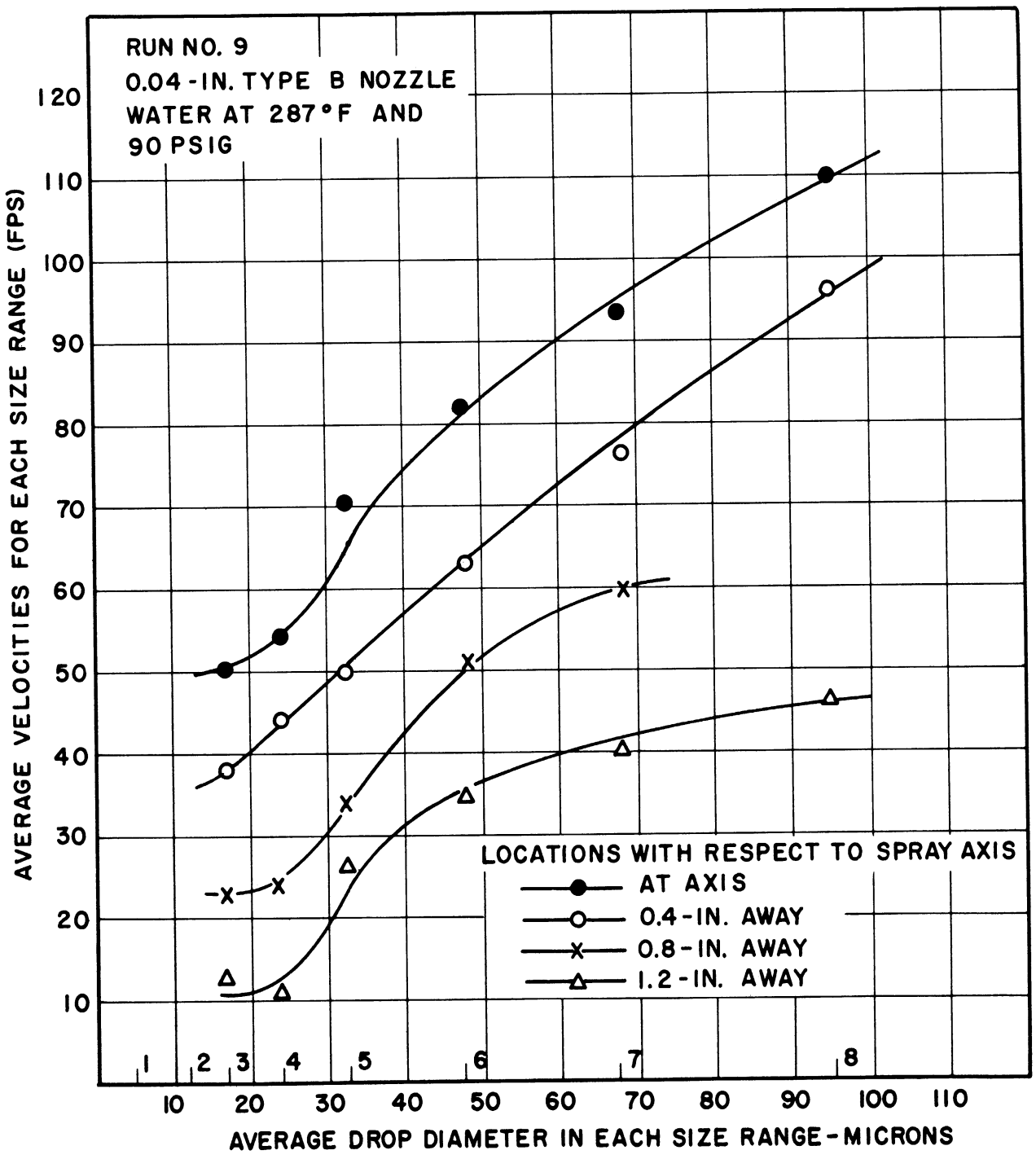

Figure 31. Velocity of Drops in a Spray from Flashing Water Jet 6 Inches from the Orifice.

a constant value at any location is probably because they are the only ones that have decelerated to their terminal velocities at that location. Their terminal velocities are so small relative to the vapor velocity, that they appear to be traveling at the same velocity of the vapor.

The primary value of the velocity data in this study is to obtain temporal drop-size distributions. The velocity data are available as a by-product of the analyses if one would like to make a study of the velocity distributions in a spray zone.

From the fact that it was only necessary to take spray samples at locations that extended to radii of 1.8 in. for the sprays from the largest diameter jets, we can see that the spray zones are fairly small. The greatest diameter of the spray zones six inches from the orifice was about four inches. The spray zones did not continue to expand at distances greater than six inches from the orifice. This may or may not be desirable depending on a particular application. The spray zones are much smaller than the zones of sprays from swirl nozzles, air atomizers, or disc atomizers at a given flow rate. For example, York (32) had to take samples of an air atomizer spray at radii up to nine inches to obtain an analysis when 50 lb./hr. of water were injected. Samples at radii up to 1.4 inches would suffice for a spray from a flashing jet at this flow rate.

The orifices were usually positioned about four feet above the ground in the spray analyses. The sprays appeared to have been almost completely vaporized by the time they reached the floor except

in the cases of the sprays from the largest diameter orifices. These high vaporization rates result from the spray being at the liquid saturation temperature when it is formed. We can see how the conditions affect the vaporization rate. The mass transfer rate for vaporization from a spherical drop is given by

$$-\frac{dm}{dt} = k_g (y_i - y) \pi D^2 \tag{7}$$

where

$\frac{dm}{dt}$ = instantaneous molar rate of vaporization of the liquid,
D = the diameter of the drop,
y_i, y = the mole fraction of the vaporizing liquid in the gas at the interface and at great distance, respectively, and
k_g = the mass transfer coefficient.

The mass transfer coefficient for the vaporization of a liquid on a spherical surface into a moving vapor is given by Frössling[8] by a correlation that has been confirmed by several investigators

$$\frac{k_g RTD}{D_m P} = 2\left[1 + 0.276\left(\frac{DV\rho_g}{\mu}\right)^{1/2}\left(\frac{\mu}{\rho_g D_m}\right)^{1/3}\right] \tag{8}$$

where

R = the gas constant,
T = the absolute temperature of the gas,
D_m = molecular diffusivity of the vaporized liquid through the surrounding gas,
P = the absolute pressure,
V = relative velocity between the drop and gas,
μ = viscosity of the gas, and
ρ_g = density of the gas.

Substituting Frössling's relation into the mass transfer rate expression,

the vaporization rate is given by

$$-\frac{dm}{dt} = \frac{2\pi D_m\, p_v D}{RT}\left[1 + 0.276\left(\frac{DV\rho_g}{\mu}\right)^{1/2}\left(\frac{\mu}{\rho_g D_m}\right)^{1/3}\right] \qquad (9)$$

where

p_v = the vapor pressure of the vaporizing liquid at the drop surface temperature.

Equation (9) is written assuming the drop is a pure liquid and the mole fraction of the vaporizing liquid at great distances from the drop is negligible compared to the value at the interface.

From Equation (9) it can be seen that the vaporization rate is proportional to the vapor pressure of the liquid which is an increasing function of the drop temperature. The molecular diffusivity of the vaporizing liquid in the gas also increases with temperature. The vaporization rate increases with drop velocity.

The high vaporization rates for the sprays from the flashing jets are a distinct advantage in many applications. This is obvious for those applications where the purpose of spraying is to increase the liquid surface and therefore promote rapid vaporization.

CHAPTER VI

CONCLUSIONS

The Break-Up

The break-up of a cylindrical superheated liquid jet is similar to that of a cold liquid jet up to a certain critical temperature range having a magnitude of about 5°F. Below this temperature range, the only difference between the break-up of a superheated jet and a cold jet is that there may be light spray around the jet. This spray is caused by the growth and bursting of bubbles on the surface of the jet. The spray is only evident for jets formed from rough-surface orifices, where the micro-roughnesses provide turbulent eddies to initiate the nuclei for the formation of surface bubbles. The diameters of these bubbles grow in direct proportion to time, and their presence has a negligible effect on jet break-up. Above the critical temperature range, the superheated liquid jet is completely shattered into a fine spray. The shattering of the jet is mainly a result of the growth of vapor bubbles inside the body of the jet. If the jet is formed by an orifice with a rough surface, these bubbles are nucleated on the surface of the orifice and their subsequent growth inside the jet a short distance from the orifice shatters the jet. If the jet is formed by a sharp-edged orifice, the bubbles which shatter the jet are not necessarily nucleated at the orifice, but often slightly downstream of the orifice by a random disturbance.

The mean temperature of the critical temperature range at which a jet of a given low viscosity liquid shatters is a function of the Weber number of the jet. The shattering temperature decreases with increasing Weber number. There appears to be a discontinuity in the shattering temperature-Weber number relation at a Weber number of 12.5, the shattering temperatures above this Weber number being much lower than those below it. This break in the shattering temperature-Weber number curve corresponds approximately to the critical Weber number for the change in the mechanism of cold liquid jet break-up from that caused by sinuous deformation to that referred to as atomization.

The shattering temperatures for water and Freon-11 jets indicate that a general function relating the shattering temperatures of jets of all low-viscosity liquids to their Weber numbers may be found by plotting the bubble-growth-rate constant at the shattering temperature versus the Weber number. This relation, found from the data of water and Freon-11 jets, is

$$\begin{aligned} C &= 19.7 - 0.581\ N_{we} \text{ for } N_{we} < 12.5 \\ C &= 11.5 - 0.491\ N_{we} \text{ for } N_{we} > 12.5 \end{aligned} \qquad (1)$$

where

C is given in ft./hr.$^{1/2}$

This equation is limited to temperatures above the saturation temperature of the liquid at the receiving pressure, as below this temperature, there would obviously be no vapor evolution from flashing. The bubble-growth-rate constant employed in this correlation

is that which relates the proportionality of the difference in bubble radius and initial bubble radius to the square root of time for a vapor bubble growing in a superheated or super-saturated liquid. This constant provides a measure of comparison of the growth rates of vapor bubbles in various superheated and supersaturated systems. It is a function of the superheat or degree of supersaturation and the liquid physical properties. It may be calculated from

$$C = \left(\frac{\Delta\tau C_2}{L}\right)\left(\frac{\rho_2}{\rho_1}\right) \left(\pi D_{th}\right)^{1/2} \qquad (2)$$

for superheated systems, and from

$$C' = \left(\frac{C_i - C_f}{1 - C_f}\right) \left(\frac{\rho_2}{\rho_1}\right) \left(\pi D_m\right)^{1/2} \qquad (3)$$

for supersaturated systems.

The values of the calculated bubble-growth-rate constants for supersaturated systems indicate that the bubble-growth rates are so low, that flashing will have no effect on the jet break-up at low injection pressures (below 300 psig). This fact has been confirmed experimentally for carbon dioxide dissolved in water.

The shattering temperatures for low viscosity jets have been found to be independent of the viscosity or the Reynold's number. This may not necessarily be the case for high viscosity jets. The information from these experiments is applicable to the break-up of superheated jets all pure liquids injected into atmospheric pressure. This is true because the viscosities of all pure

liquids at their saturation temperature at one atmosphere are low and lie in a small range.

The Sprays

The mean drop-sizes of the sprays from flashing water jets that have been shattered by vapor evolution can be given by the relation

$$\overline{D_{10}} = \frac{1840 - 5.18\ T\ (°F)}{N_{we}}\ (\text{microns}) \qquad (4)$$

This equation is correlated from the drop-size data for jets injected at temperatures between 236°F and 287°F and Weber numbers ranging from 9.3 to 22.7. The equation correlating the drop-sizes for both the water and Freon-11 sprays can be given by

$$\overline{D_{10}} = (246 - 8.30\ C)\ (\sigma)^{0.31}\ (N_{we})^{-1} \qquad (5)$$

when the interfacial tension is given in dynes/cm. and the bubble-growth-rate constant at the injection temperature is given in ft./hr.$^{\frac{1}{2}}$. Since Equation (5) is based upon only one point for Freon-11 and assumes only surface tension affects the drop-size at a given Weber number and bubble-growth rate, it should be considered as an extrapolation of the Freon-11 data point rather than as a true correlation. The range of the linear mean drop-sizes for the sprays from the flashing jets in these experiments was small, between 24 and 43 microns. This indicates that more intense conditions than those required to shatter the liquid jet do not have a great effect on the

drop-size. These drop-sizes may be compared to the drop-size of a spray from a cold water jet injected with a Weber number of 14.9 whose linear mean was 142 microns. There is no difference in the drop-sizes of the sprays from the sharp-edged and rough-surface nozzles, but the drop-size from the nozzle with sand on the surface is smaller. This is because the sand particles tear liquid ligaments off the surface of the jets. Flashing is definitely a means by which fine sprays may be obtained from the break-up of cylindrical liquid jets at low Weber numbers and the corresponding low injection pressures.

The drop-size distributions can be correlated to the logarithmic-normal-probability distribution function. The uniformity parameters for the distributions do not correlate well with any of the experimental parameters. The average value of the uniformity parameter, δ, for the sprays from the shattered water jets from the sharp-edged and rough-surface orifices is 1.55 ± 0.12. This indicates that the uniformity of the drops from the flashing jets is as good or better than typical sprays from cold liquid jets, gas atomizers, swirl nozzles, or vaned-disc atomizers.

In a plane perpendicular to the axis of the sprays from the flashing jets, the mean drop-size is usually the highest for the drops the farthest from the spray axis. The drop-size decreases approaching the axis, and often increases again slightly at the axis. This pattern is caused by the manner in which the

expanding bubbles inside the jet explode the jet and push the largest drops the furthest away from the axis. The larger drops in the center of the spray result from portions of the jet that are not exploded by the expanding bubbles. The velocities of the drops are the highest at the spray axis, and decrease with distance from the axis. At any location with respect to the axis, the larger drops have the highest velocity. The drops in any location smaller than about 20 microns appear to approach a constant celocity.

The sprays are contained in relatively small zones, the greatest diameter in this study being six-inches. The vaporization rates of the sprays are high because the liquid drops are formed at their saturation temperatures.

CHAPTER VII

RECOMMENDATIONS

High Viscosity

The results of this study are applicable to low viscosity liquids. This includes all superheated jets of pure liquids injected into a region of atmospheric pressure, as the viscosities of most pure liquids at their saturation temperatures at one atmosphere are low, usually below 0.5 cp. This does not include, however, mixtures such as high concentration sucrose solutions and wide-boiling-range hydrocarbon mixtures.

The minimum temperature for the shattering of a high viscosity jet would probably be higher than for jets of low viscosity, because the investigations of Rayleigh[26], Weber[30], and Hinze[11], have indicated the jet stability is increased with high viscosities. Hinze[11] found that the critical Weber number for the transition of the region of break-up of a cold liquid jet from sinuous break-up to atomization was increased with liquid viscosity. Since there appears to be a "critical" Weber number for the shattering temperature -- Weber number relation for a flashing jet, it seems reasonable that this critical Weber number would also be affected by liquid viscosity. The effect of high visocisty on the bubble-growth rate in a superheated liquid is unknown, as the assumptions included in the theoretical treatment of the problem included one of the inviscid liquid. The solution of the bubble-growth-rate problem is also for pure liquids, not liquid mixtures or solution.

The break-up of flashing high-viscosity jets is mainly of interest as applied to spray drying, where viscous mixtures or sludges are generally injected. The small spray zones and high vaporization rates of the sprays from flashing jets are particularly attractive as regards this application. An experimental study of the break-up of high-viscosity flashing jets is therefore recommended. The approach may have to be entirely empirical as a result of the complicating effects of high viscosity on the bubble-growth-rate relation and the jet stability.

Orifice Design

Vapor evolution inside the orifice throats was avoided in this study because of its deleterious effect on the flow-metering. The reduction in flow rate is not too serious if its magnitude can be predicted accurately and reproducibly from theoretical or experimental studies. Vapor evolution inside of a small long orifice may be employed to advantage as a fine spray may be attained at a low superheat in this manner. Extreme care would probably have to be employed in design of the nozzles so that the bubble nucleation would occur at the same point in the orifice throat and cause mixing of the evolved vapor and liquid inside the orifice. For example, a sharp obstruction at the upstream end of the orifice might promote continuous bubble nucleation at that point.

A long orifice nozzle made of a transparent material could be employed to make a photographic study of the growth of vapor bubbles in the superheated liquids. This would provide experimental evidence for the theoretically predicted hypothesis that the bubble-growth rate is independent of turbulence for the degrees of turbulence in this study.

APPENDICES

A. SUPPLEMENTARY EXPERIMENTAL DETAILS

B. SUMMARY OF DATA AND CALCULATED VALUES

C. SAMPLE CALCULATIONS

D. LITERATURE CITATIONS

APPENDIX A. SUPPLEMENTARY EXPERIMENTAL DETAILS

1. Determination of the maximum orifice length.

When injecting a flashing jet, vapor evolution can occur inside the orifice throat if the orifice is long enough. If this takes place, the evolved vapor and liquid mix inside the orifice throat and the specific volume of the mixture is considerably greater than that of the pure liquid phase. This can reduce the volumetric flow rate through the orifice at a given pressure to well below that when vapor is evolved outside of the orifice. Therefore, all of the nozzles employed in this study had to be tested to insure that vapor evolution did not occur inside the orifices throughout the range of experimental conditions.

One way in which the location of vapor evolution, inside or outside the orifice, can be determined is by visual observation. Liquid is injected at a constant pressure and the temperature increased. When the jet is shattered, a short section of the jet is observed near the orifice exit if vapor evolution occurs outside the orifice. If vapor evolution has been initiated inside the orifice, no jet is visible and a mixture of liquid and vapor issues from the orifice. However, complete mixing of the liquid and vapor inside the orifice does not always occur when vapor is evolved inside the orifice. Occasionally, roughness conditions will be such that the phases separate inside the orifice. In these cases, a short section of jet may be visible although vapor has been evolved inside the orifice. Therefore, a more reliable method of checking the nozzles had to be employed.

There should be no decrease in volumetric flow rate at a given injection pressure as injection temperature is raised if vapor evolution occurs exclusively outside the orifice. The flow rates were measured for all the experimental nozzles at 80 psig and 120 psig at temperatures varying from about 100°F to about 300°F. The temperature of the liquid that is passing through the flowmeter is constant throughout a run, the temperature adjustments of the liquid taking place downstream of this location. The flowmeter therefore measures flow at constant density, or mass flow rates. The flow meter readings therefore were reduced somewhat as temperature was raised because the liquid density through the orifice was reduced and thus the mass flow rate. The readings could easily be corrected for volumetric flow rate by multiplying them by the ratio of the liquid density through the orifice at the highest flowmeter reading to the liquid density at the injection temperature. The volumetric flow rates for all the experimental nozzles employed here remained constant at both injection pressures and throughout the temperature ranges. A reductionin volumetric flow rate was experienced in several nozzles that had L/D ratios of four to six.

2. Calibration of Pressure Gauge, Thermocouple, Flowmeter, and Time-Delay Unit.

The pressure gauge was calibrated with an Amthor dead weight gauge tester. The indicator on the pressure gauge could be adjusted so that all the pressure readings, from 10 psig to 140 psig, agreed with the weights on the gauge tester to within 0.5 lb. Flow conditions during operation of the apparatus were

such that a constant pressure only to the nearest 1 psig could be maintained. The accuracy of the pressure gauge was therefore entirely satisfactory for these experiments.

The iron-constantan thermocouple was calibrated in a mineral oil bath by a -5° -250°C mercury thermometer. The calibration is shown in Figure 32. The potentiometer circuit was a Leeds & Northrup # 72010 with an externally connected standard cell #PL-127-130000. The accuracy of the calibration is such that temperature readings may be made to the nearest 0.5°F. The thermocouple wire was attached to the outside of the pipe just upstream of the place the nozzles were connected. The pipe and wire were heavily insulated. There was a thermowell just upstream of the flexible tubing that led to the pipe to which the nozzles were connected. There was a reduction in temperature between the thermowell and the thermocouple location. At a given flow rate, however, this temperature reduction should be constant at any given injection temperature. This provided a means to check how accurately the thermocouple measurement of the pipe temperature corresponded to the actual liquid temperature in the pipe. The thermocouple was attached to the pipe and insulated, and then the thermowell and thermocouple readings were recorded through a range of temperature when water was injected through a given nozzle at constant pressure. The thermocouple wire was removed, and then attached to the pipe again with heavier insulation than the first time. The thermowell and thermocouple readings were taken again with the same nozzle and injection pressure. The

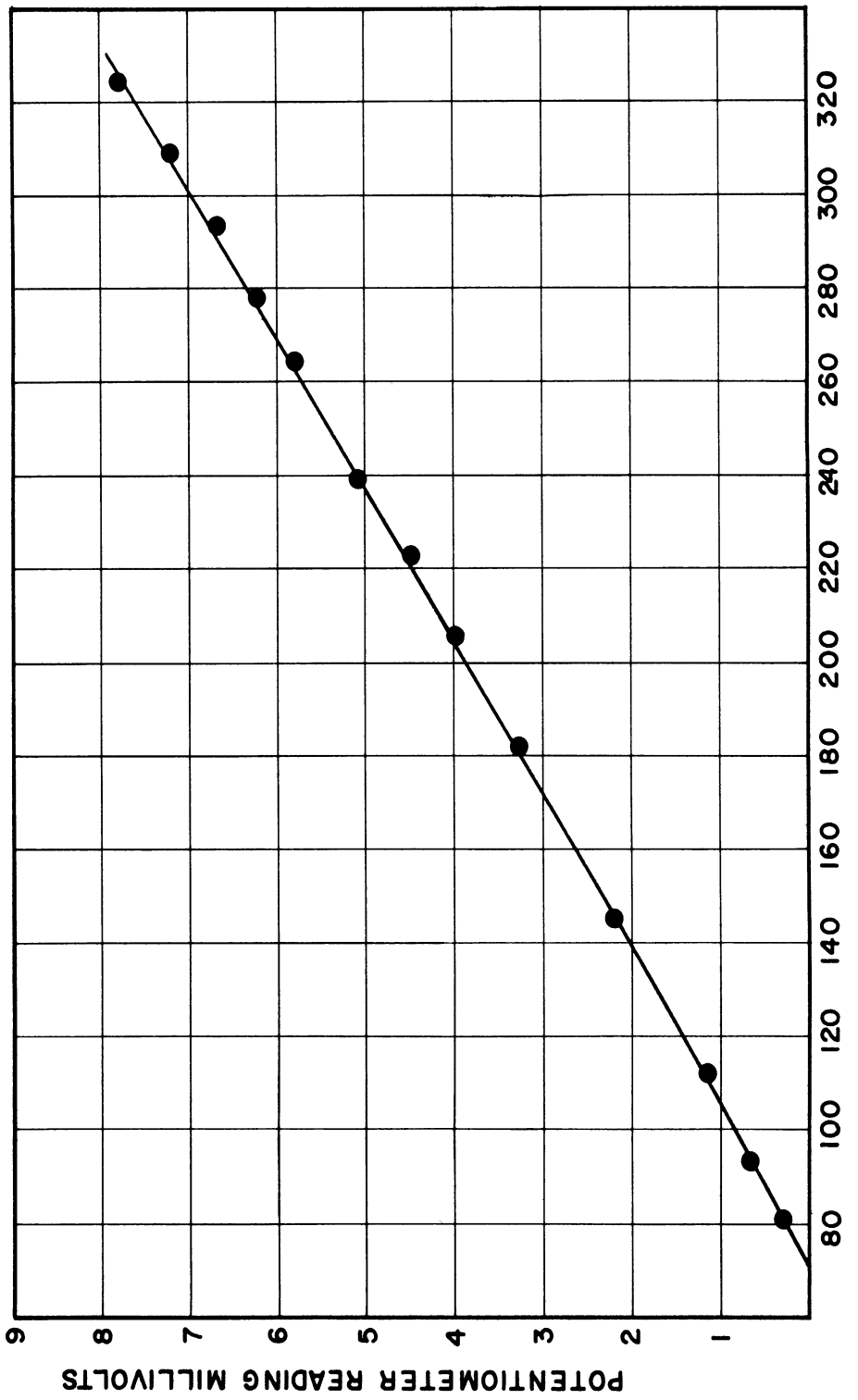

Figure 32. Thermocouple Calibration.

readings maintained the same correspondence as in the preceding trial. It was concluded from this that the insulation was sufficient so that there was negligible temperature reduction between the liquid and outside of the pipe.

The water in the storage tank was saturated with steam at 120 psig during the flowmeter calibration and all flow rate measurements, the injection temperature and pressure adjustments taking place downstrean of the storage tank and flowmeter. This provided that the water passing through the flowmeter was always at the same temperature and pressure. The liquid injected through a nozzle was collected in a graduate cylinder for 30 to 60 seconds while the injection pressure remained constant. The volume and temperature of the collected liquid was recorded and the volume corrected to 80°F. The calibration curve is presented in Figure 33.

The time-delay unit was designed so that when one of the photolights was triggered, an impulse would be sent to the other photolight after a definite time-delay that could be set from about 10 to 25 microseconds. The actual time-delay could not be measured electronically so the unit had to be calibrated photographically. This can be done by taking double-flash photographs of an object moving at a known velocity and measuring the distance between the exposures of the object on the photograph. The calibration was made by taking double-flash silhouette photographs of a moving band saw blade. The blade velocity was determined by measuring the

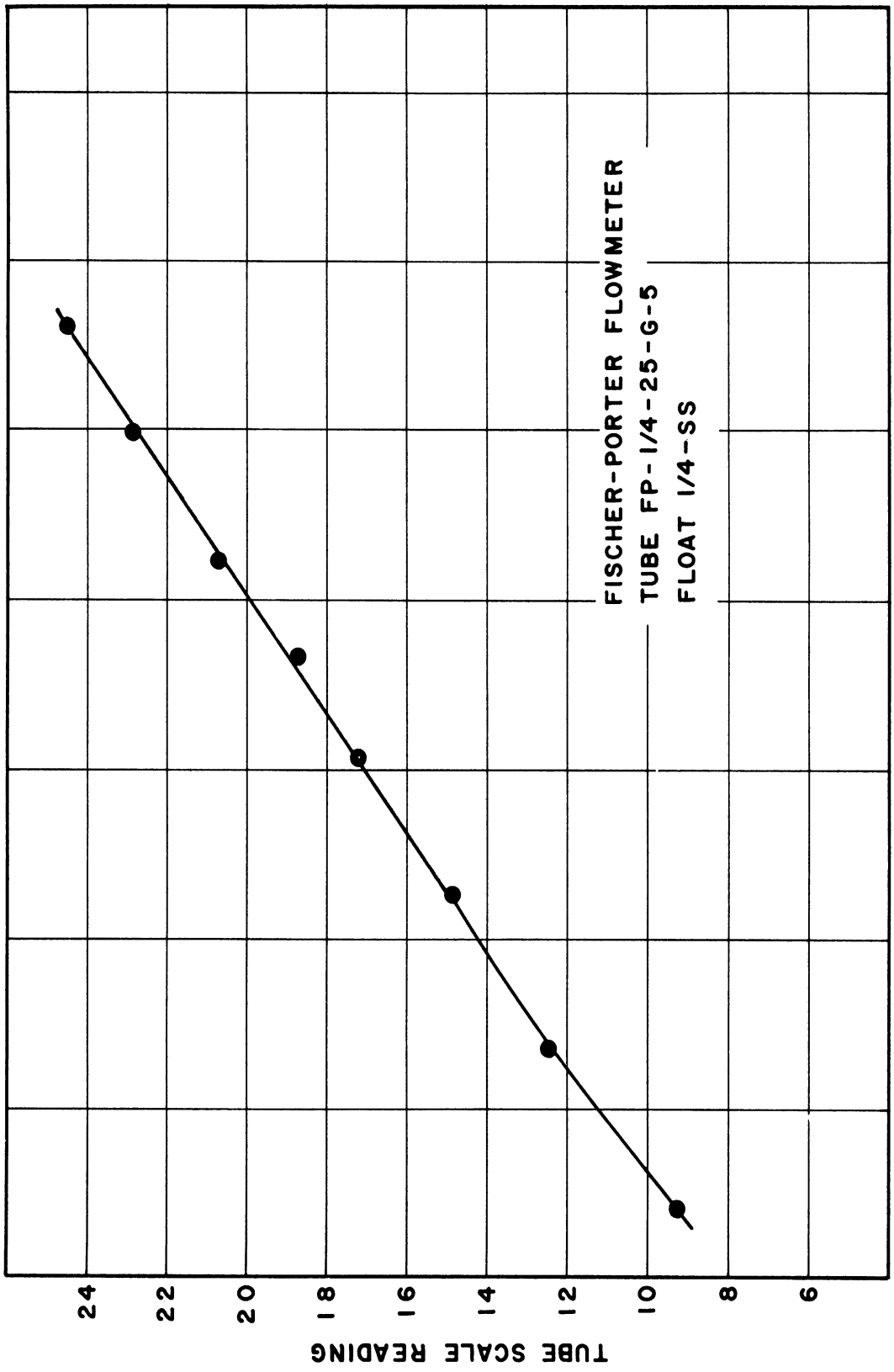

Figure 33. Flowmeter Calibration for Saturated Water at 120 psig.

rotational frequency of the driving wheel with a Strobotac, which is a variable frequency flash unit. After the band saw blade was run for about five minutes, the driving wheel motion could be "stopped" by the flashes from the Strobotac and the rotational frequency recorded. Several photographs were taken of the saw blade at a few delay unit settings. The distance between the two exposures of a saw tooth was found from the photographs. It was easy to distinguish a saw tooth in each exposure as each one had a unique profile from chips and dirt particles. The time delay from seven photographs at the setting for the spray analyses in these experiments was 22.4 ± 0.4 microseconds.

3. Control of the Exposure.

It has been pointed out that the aperture opening on the camera lens must remain constant for all spray analyses to maintain a constant depth of field. The light intensity must therefore be controlled by filters in front of the photolights. The optical density of a photograph from a certain type of film and developed by a standard technique will be a function of the light intensity and the exposure time. The optical density is a measure of the degree by which the exposed negative can transmit light. Hanson[10] has photographed circular ink spots on a miscroscope slide with Kodak Contrast Process Ortho film and under various exposure conditions to obtain negatives over a range of optical density. The actual sizes of the spots were measured with a microscope and compared to the size of the drops on the negatives. Hanson found that

the size of a 16.5 micron spot on a negative was within ten percent of its true size if the optical density of the negative could be maintained between 1.6 and 2.0. The accuracy improves as the drop size increases, the measured size being within five percent of the true size for a 37.8 micron spot. The exposure conditions for these experiments are controlled to maintain the optical density within the aformentioned limits.

The effect of the filters on the light intensity was determined by taking several photographs with 1 to 7 0.002-inch thick Mylar film filters in front of the photolight when the aperture setting was f-3.5, all the way open. The optical densities of the negatives were measured with a Kodak Color Densitometer Model No. 1. The effect of the filters on the optical density is shown in Figure 34. Note that the density is not always constant for a given number of filters because the light intensity from the photolight can vary from flash to flash. The density of the negatives were essentially independent of the location on the negative. If a photograph is taken with no filters, an approximately four inch diameter region of the 4 x 5 negative is exposed, leaving unexposed corners. In addition to the filters, the lights were enclosed in 3/8 inch thick plexiglass cases, which apparently were sufficient to diffuse the light beam so that the whole field of the lens was exposed to the same degree.

During a spray analysis, a dense spray can reduce the light intensity considerably. A photo floodlight was therefore directed to the lens through a plexiglass sheet and six filters and

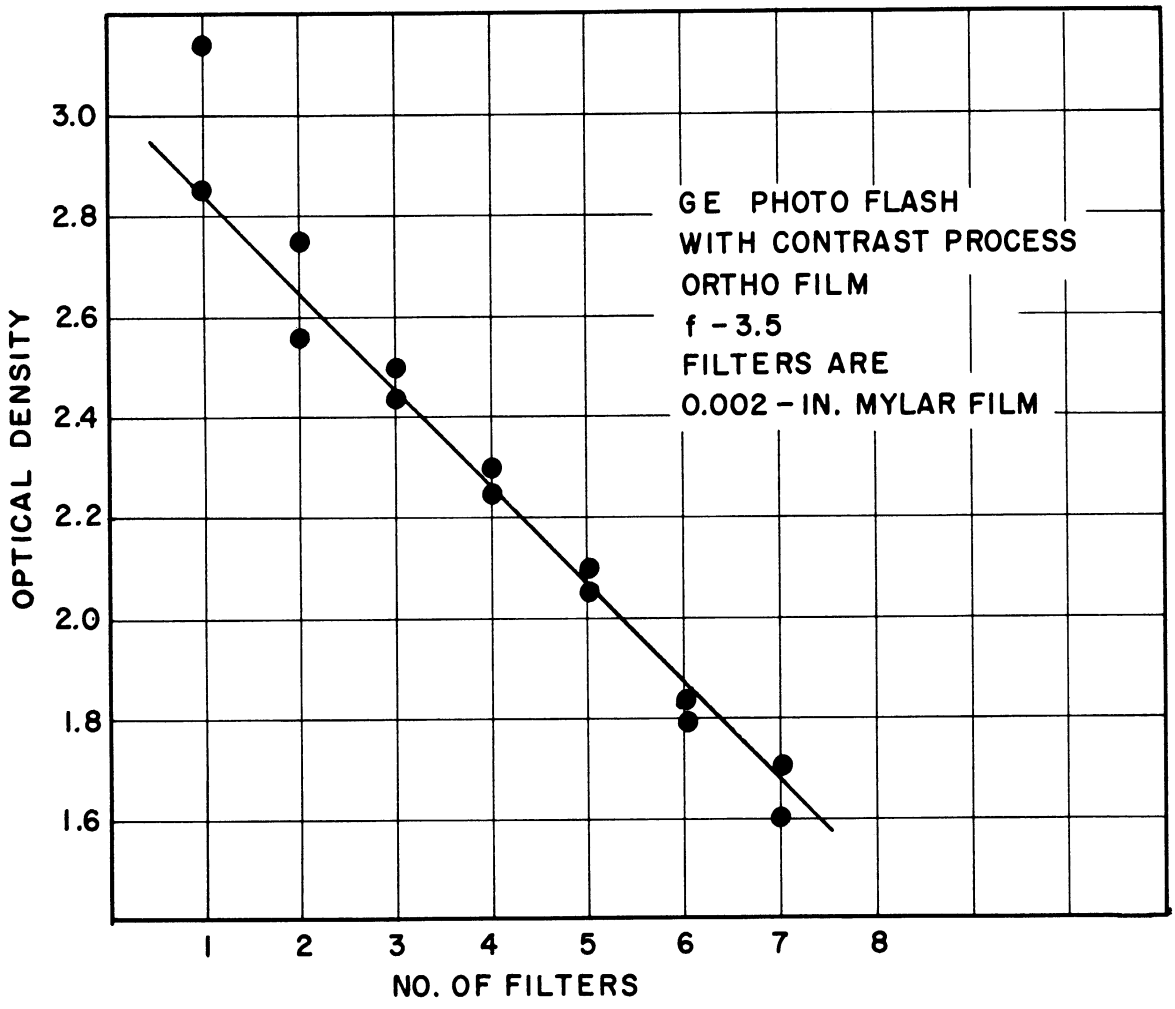

Figure 34. Effect of Filters on Optical Density.

the light intensity at the lens measured with a Weston Master II universal exposure meter model 735 No. 6583722. For any location in a spray formed under certain conditions, the photo floodlight could be directed at the lens through the spray. The number of filters to be employed during the analysis could then be determined by the number required to obtain the same exposure meter reading as with the plexiglass and six filters with no spray. Employing this technique, it was fairly easy to maintain the optical density of the negatives within 1.6 and 2.0.

In the early phases of the study, photographs of the sprays were often underexposed and showed no drops although the lighting conditions seemed to be all right. It was found that this was caused by condensation of vapor on the lens. A shutter was placed over the lens and opened just before taking each photograph. The camera had to be backed away and the lens wiped dry before taking the next photograph as the lens became fogged before the shutter could be closed again. This was a serious problem when photographing the high-flow-rate sprays because if the picture was not taken immediately after the shutter was opened, the lens would fog. The shutter was employed in all the analyses, although it made the analyses more tedious. It is recommended that a mechanical shutter that could be triggered with the photolights be employed to provide a more convenient solution to this problem.

4. Developing Technique.

The optical density of the negatives can vary considerably with variations in the developing technique. A standard procedure which

was carefully adhered to for the developing of all spray photographs was therefore employed. The developing tanks were immersed in a bath of running water at 68°F. The films were developed in Kodak D-11 developer for five minutes, with agitation the full first minute, and intermittently every minute thereafter. The films were then rinsed, and fixed in Kodak acid fixer for ten minutes with agitation every minute. The films were taken from the fixer, rinsed in water for 30 seconds with agitation, and then immersed in Hypo clearing agent for two minutes. The films were then washed in water from five to ten minutes and dried. A Wratten Series two red safelight filter was employed for lighting during the developing process.

5. Minimum Drop Sample.

Each photograph at a spray location has a certain number of drops within the limits of focus that are classified into size ranges to obtain the experimental distribution. The more drops in a sample, the closer will the measured size distribution approach the actual size distribution for that location in the spray. The accuracy of the sample distribution is not only dependent on the number of drops, however, but also on whether the distribution remains constant at that location, as the spray may pulse and fluctuate. The number of photographs at a given sample location must therefore satisfy two conditions: (1) provide the minimum number of drops for an accurate distribution, and (2) provide the average spray condition at that location.

The drops from photograph No. 131, taken of Location 2 in Run No. 5, were counted 50 at a time and the cumulative distribution obtained after counting each successvie group of 50 drops. The cumulative distribution curves for the samples are given in Figure 35. The curves for 50 and 150 drops are omitted to eliminate confusion between the curves. Note that the curve for 100 drops is much lower than the curve for 300 drops for the small drops and much higher for the large drops. The curves for 200 and 250 drops, however, lie fairly close to the curve for 300 drops on either side. This shows that as the sample includes between 200 and 300 drops, the distribution curve is approaching a constant function. About 85 percent of the samples from each location for each run contained over 200 drops, and often considerably more, sometimes up to 1000. In those cases where less than 200 drops were counted, the drop density in that location was small enough so that the drops did not contribute greatly to the anlaysis for the entire spray.

In the preliminary tests for the minimum sample, two photographs of the same sample location of a spray injected under given conditions gave almost the same distribution if there were at least about 200 drops on a photograph. For example, the cumulative distributions for two photographs at location 2 of Run No. 5 are shown in Figure 36. The curves are fairly close. Two photographs of each sample were therefore taken in all analyses. In view of the difficulty in taking the photographs of the flashing jets resulting from the lens fogging problem, it was desirable to keep the number of photographs down to a minimum. The distributions obtained from

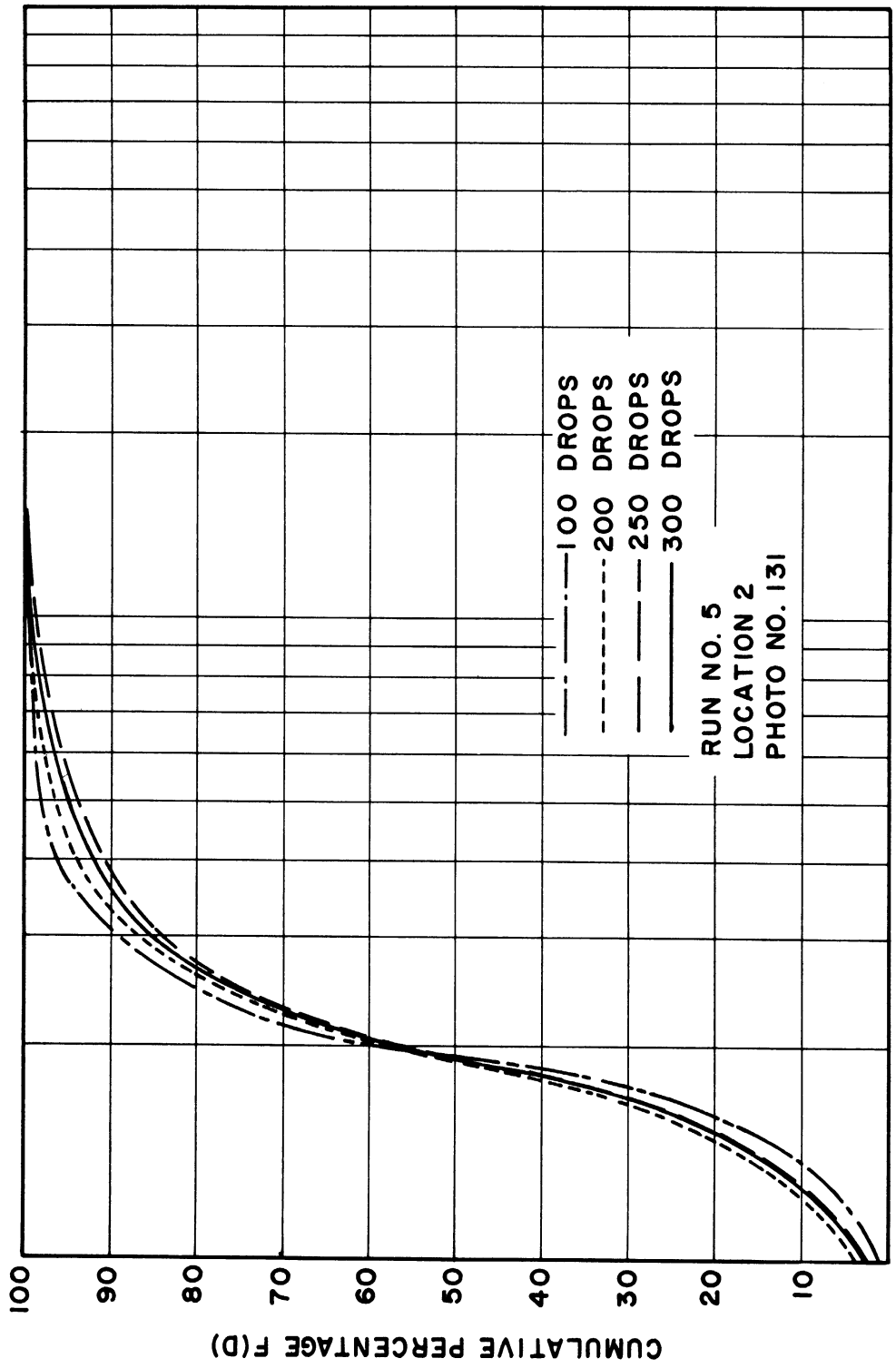

Figure 35. Determination of Minimum Sample.

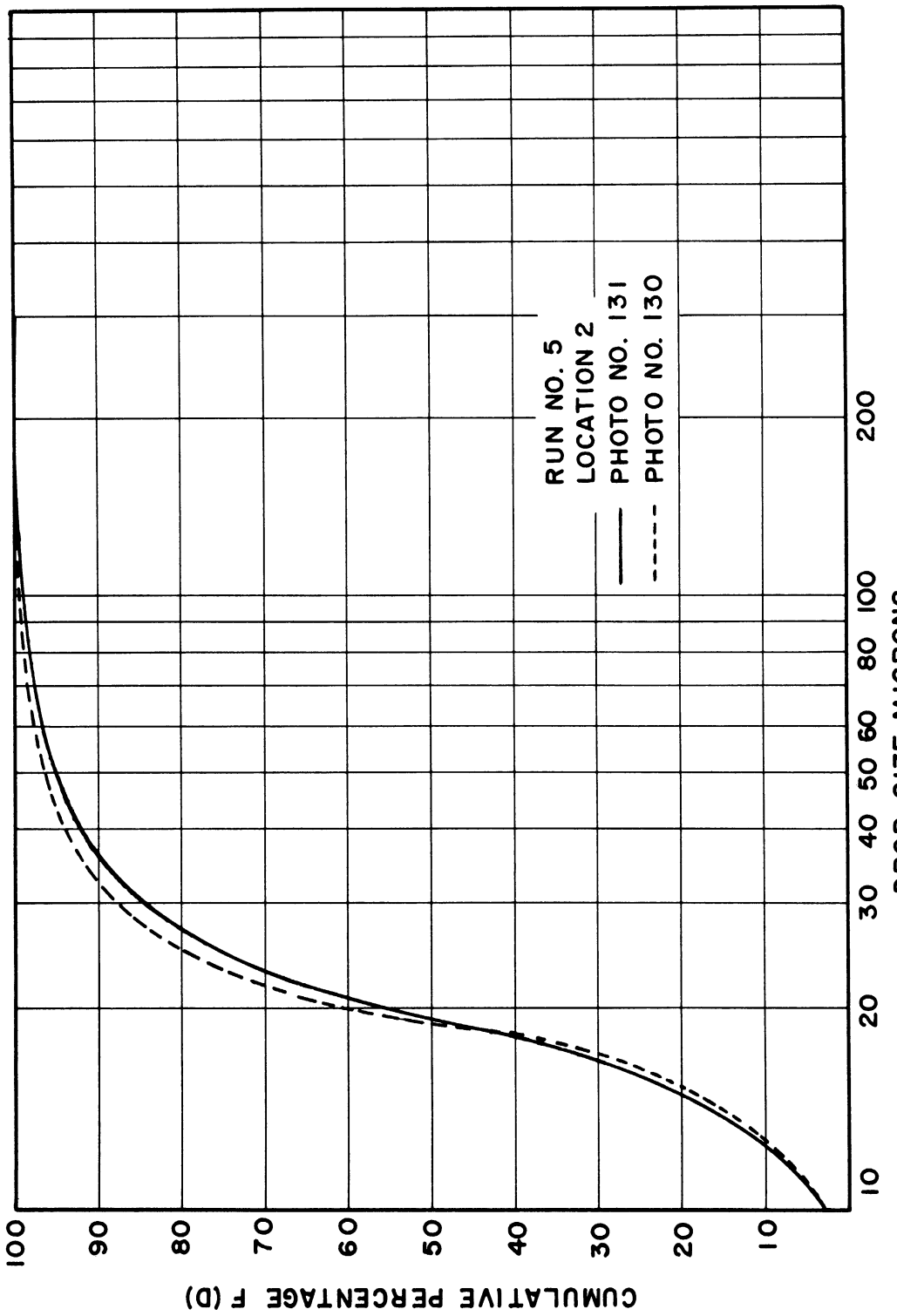

Figure 36. Comparison of Distributions from Two Photographs at a Sample Location.

TABLE VI. DETERMINATION OF MINIMUM SAMPLE

(for conditions of Run No. 5, Location 2)

A. Drops counted 50 at a time - photo No. 131.

No. of Drops Counted		No. of Drops and Cumulative Percentage in Each Size Range								
		1	2	3	4	5	6	7	8	9
50	No.	1	7	23	12	5	1		1	
	%	2.0	16.0	62.0	86.0	96.0	98.0	98.0	100.0	
100	No.	2	11	46	27	10	3		1	
	%	2.0	13.0	59.0	86.0	96.0	99.0	99.0	100.0	
150	No.	7	21	60	38	17	4	2	1	
	%	4.7	18.7	58.7	83.9	95.3	98.0	99.3	100.0	
200	No.	12	26	75	49	26	6	4	2	
	%	6.0	19.0	56.5	81.0	94.0	97.0	99.0	100.0	
250	No.	12	35	95	59	30	8	5	5	1
	%	4.8	18.8	56.8	80.4	92.4	95.6	97.6	99.6	100.0
300	No.	15	42	117	71	34	9	6	5	1
	%	5.0	19.0	58.0	81.7	93.0	96.0	98.0	99.7	100.0

B. Comparison of Photo No. 130 and 131

No. of Drops Counted		No. of Drops and Cumulative Percentage in Each Size Range								
		1	2	3	4	5	6	7	8	9
#130	No.	14	38	123	72	25	6	5	2	1
286	%	4.89	18.17	61.18	86.35	95.10	97.20	98.95	99.65	100
#131	No.	17	46	128	77	37	10	6	6	1
328	%	5.18	19.20	58.22	81.70	92.98	96.03	97.86	99.69	100

two photographs are usually accurate because of the large number of drops per photograph for these relatively dense sprays.

6. Flow Rate Check

There are two major sources of error in the photographic analysis of sprays. One is in the determination of which drops should be accepted as part of the photographic sample. Although standard drops are referred to in order to define the limit of focus, the decision as to whether to accept or reject many drops is often arbitrary. Another source of error is in the velocity measurements. The velocities are measured assuming that all drops remain in the plane of the sample locations that is parallel to and intersects the spray axis. In reality, many drops cross this plane. In a double-flash photograph of the sprays, most of the drops are traveling in the same direction, but there are often several that seem to be going in other directions. Only drops that are going in the same direction as the majority are sampled in these analyses for the velocity measurements. Employing this technique, the drops in a given size range for a certain sample location did not differ in velocity by more than 25 percent. The average velocities in each size range at each location were plotted versus the average drop diameter, and the velocities for the calculations obtained for the best curves through these points.

One way in which the overall accuracy of the spray analyses may be measured is by comparing the computed flow rate of the spray from the drop-size analyses and their velocities, and the flow rate of the injected liquid jet. This computed flow rate from the analyses

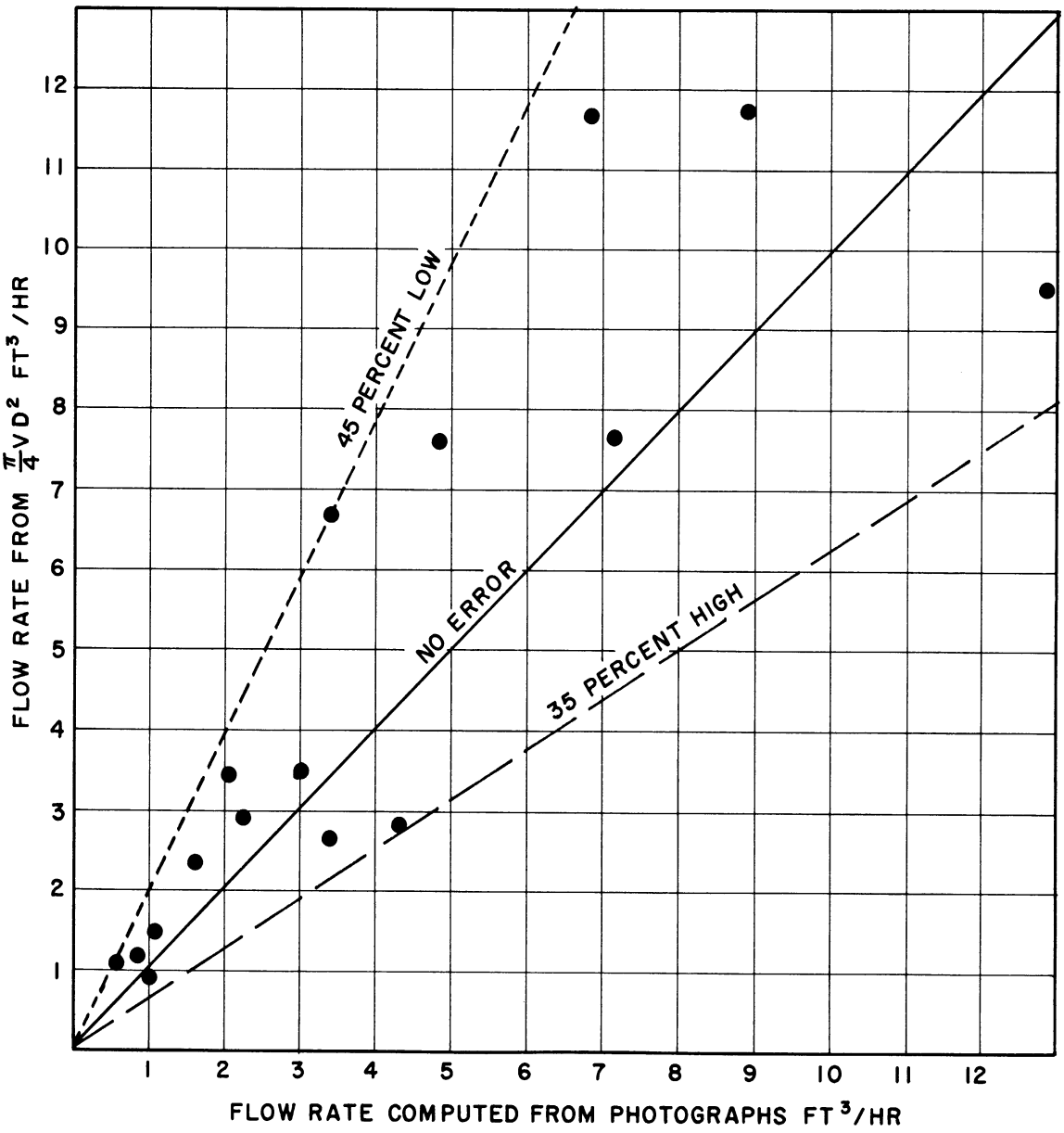

Figure 37. Comparison of Spray Flow Rates and Injection Flow Rates.

is dependent on both the accuracy of the depth of focus and the accuracy of the velocity measurements. The standard drops that were chosen for these analyses were 0.91 mm from the point of focus so that the depth of focus was 1.82 mm. The sample volume is known from this figure and the total number of drops passing a 0.5 inch thick plane perpendicular to the spray axis can then be computed by multiplying the number of drops in each size range for each location by the ratio of the volume of the annulus of which the sample is a portion to the volume of the sample. The flow rate of the spray is then determined by computing the volume of the drops in each size range in each annulus and multiplying by their velocities. These computed spray flow rates are compared to the flow rates calculated from the jet diameters and the jet velocities in Figure 37 for the sprays from the water jets. The computed values from the sprays are within 45 percent on the low side and 36 percent on the high side of the values computed from the jet diameter and velocity. The standard deviation is 27 percent. The flow rates computed from the sprays are usually low. This is to be expected from the rapid vaporization rate of the spray and the fact that drops less then five microns are not resolved on the photographs.

7. The Time-Delay Unit.

A circuit diagram of the time-delay unit is shown in Figure 38.

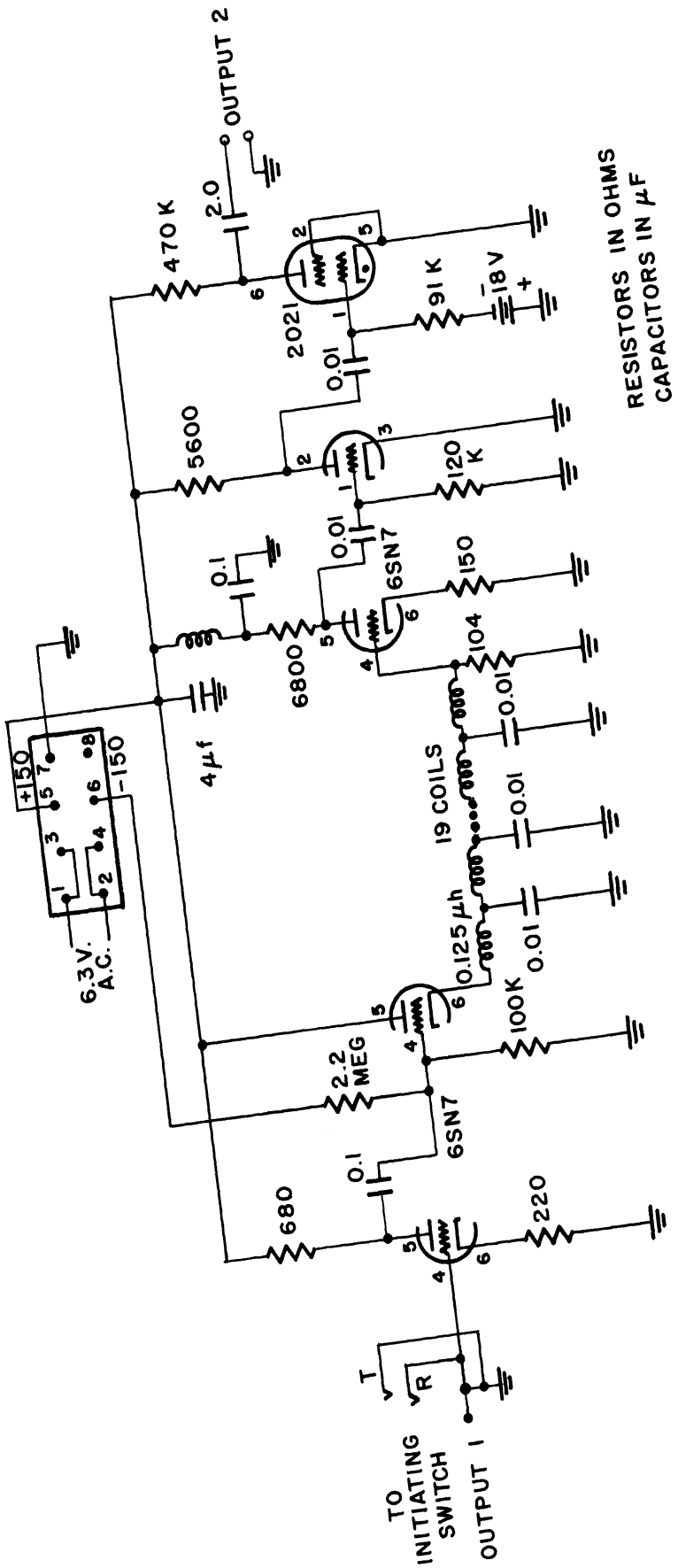

Figure 38. Time-Delay Unit Circuit.

APPENDIX B. SUMMARY OF DATA AND CALCULATED VALUES

LIST OF TABLES

APPENDIX B. SUMMARY OF DATA AND CALCULATED VALUES

The original data are in two data books under the author's name and dated December 29, 1958 and February 17, 1960. These data books, and the photographs are located in the Multi-Phase Fluids Laboratory in the Fluids Building at the North Campus of the University of Michigan, Ann Arbor, Michigan.

1. Break-Up Data.

TABLE AI.

BREAK-UP TEMPERATURES FOR WATER AND FREON-11

Run No.	Nozzle Type	Injection Pressure (psig)	Jet Diameter (inches)	Shattering Temperature (°F)	Re	N_{we}	C (ft./hr.$^{\frac{1}{2}}$)
				Water			
1B	A	120	0.025	282	125,000	8.81	16.3
2B	A	131	0.025	280	131,000	9.60	15.9
3B	A	100	0.032	272	143,000	9.34	14.0
4B	A	120	0.032	268	152,000	11.20	13.1
5B	A	130	0.032	266	157,000	12.12	12.6
6B	A	80	0.066	237	220,000	15.16	5.8
7B	A	120	0.066	215	239,000	22.53	0.7
8B	B*	120	0.031	273	150,000	10.83	14.3
9B	B	93	0.031	272	132,000	8.42	14.0
10B	B	134	0.031	270	157,000	12.12	13.6
11B	B	84	0.035	268	139,000	8.56	13.1
12B	B	128	0.035	237	148,000	12.87	5.8
13B	B	60	0.053	270	170,000	9.24	13.6
14B	B	80	0.053	258	197,000	12.28	10.8
15B	B	96	0.053	235	192,000	14.60	5.4
16B	B	120	0.053	223	200,000	18.15	2.5
				Freon-11			
17B	A	94	0.025	152	86,600	18.10	5.0
18B	A	95	0.032	118	99,200	23.60	2.8

* With Sharp Downstream Edge

2. Bubble Size Data.

TABLE AII.

BUBBLES ON SURFACE OF 0.031 INCH DIAMETER.
268°F WATER JET INJECTED AT 120 PSIG

Photograph Number	Bubble Diameter* (Inches)	Distance from Orifice* (Inches)	Time (μ sec.)	Predicted Growth for Submerged Bubble, $2Ct^{\frac{1}{2}}$ (Inches)
27	0.020	0.280	168	0.066
64	0.022	0.235	141	0.060
64	0.018	0.200	120	0.055
64	0.017	0.175	105	0.052
64	0.010	0.140	84	0.046
97	0.023	0.345	207	0.073
97	0.027	0.377	226	0.076
93	0.029	0.394	236	0.078
93	0.031	0.425	255	0.081
99	0.019	0.183	110	0.053
99	0.021	0.239	143	0.061
100	0.018	0.173	104	0.052
101	0.015	0.145	87	0.047
101	0.019	0.162	97	0.050
103	0.017	0.155	93	0.049
104	0.028	0.363	218	0.075
107	0.014	0.136	82	0.046
107	0.018	0.214	128	0.057

* These are the measured values on the photographs divided by 10, representing the actual values.

3. Drop-Size Data

The number of drops and their average velocities are given for the drops found to lie in each size range at each sample location. The sample locations referred to are shown in Figure 4. The size ranges referred to are given in the following table:

Size Range No.	Size Range (Microns)
1	0 - 10
2	10 - 14.1
3	14.1 - 20
4	20 - 28.2
5	28.2 - 40
6	40 - 56.4
7	56.4 - 80
8	80 - 113
9	113 - 160
10	160 - 226
11	226 - 320
12	320 - 453
13	453 - 640

TABLE AIII.

RUN NO. 1. 0.040 INCH DIAMETER TYPE A ORIFICE
WATER JET AT 287°F AND 120 PSIG

Location	Photos	Total Drops	Number of Drops in Each Size Range									
			1	2	3	4	5	6	7	8	9	10
1	2	593	14	67	145	130	107	61	41	18	9	1
2	2	596	6	36	124	136	154	84	35	18	2	1
3	2	406	5	25	56	116	129	60	15			
4	2	351	3	6	25	56	95	101	54	10	1	
			Average Velocities in Each Size Range (fps)									
1	2					66	85	97	104	121	129	
2	2				60	61	63	89	89	108	115	
3	2					47	51	65	76			
4	1				17	16	24	31	48	77		

TABLE AIV.

RUN NO. 2. 0.031 INCH DIAMETER TYPE B ORIFICE WITH SHARP DOWNSTREAM EDGE
WATER JET AT 287°F AND 120 PSIG

Location	Photos	Total Drops	Number of Drops in Each Size Range									
			1	2	3	4	5	6	7	8	9	10
1	2	634	7	42	111	165	164	109	32	2	1	1
2	2	397		8	28	61	112	109	73	6		
3	2	128			3	14	44	65	66	25	1	
4	2	93					5	26	38	24		
			Average Velocities in Each Size Range (fps)									
1	1					36	40	42	46		74	
2	1					35	37	43	49			
3	1				30	30	32	34	36	62	74	
4	1				14	15	24	23	27	52	53	

TABLE AV.

RUN NO. 3. 0.080 INCH DIAMETER TYPE A ORIFICE
WATER JET AT 204°F AND 80 PSIG

Location	Photos	Total Drops	Number of Drops in Each Size Range												
			1	2	3	4	5	6	7	8	9	10	11	12	13
1	4	192		1	3	14	23	36	26	31	15	14	15	12	2
2	4	109		1	4	7	13	20	16	17	11	8	4	6	2
			Average Velocities in Each Size Range (fps)												
1	2						34		61	68	85	86	88	99	
2	2						33	34	50		82			95	

TABLE A VI

RUN NO. 4. 0.080-INCH DIAMETER TYPE A ORIFICE WATER JET AT 236°F AND 80 PSIG

Location	Photos	Total Drops	Number of Drops in Each Size Range											
			1	2	3	4	5	6	7	8	9	10	11	12
1	4	648	21	93	183	145	88	53	28	17	10	7	2	1
2	2	685	1	45	145	228	181	60	18	4	1	2		
3	2	539	5	31	96	118	136	115	26	8	2	2		
4	2	384		7	30	43	80	154	51	17	2			
5	2	212		1	14	26	27	60	62	18	4			
			average velocities in each size range (fps)											
1	1				42	44	52	62	68	74		126		127
2	1				34	35	38	45	60	80	92			
3	1				32	35	37	40	48	78	95	103		
4	1					21	22	24	40	62	85			
5	1						10	17	20	32	61			

TABLE A VII

RUN NO. 5. 0.080-INCH DIAMETER TYPE A ORIFICE WATER JET AT 236°F AND 120 PSIG

Location	Photos	Total Drops	Number of Drops in Each Size Range									
			1	2	3	4	5	6	7	8	9	10
1	2	373	11	74	137	68	42	20	8	10	2	1
2	2	614	31	84	251	149	62	16	11	8	2	
3	2	596	11	35	116	201	168	51	9	5		
4	2	366	6	29	72	66	81	68	31	13		
5	2	273		8	23	43	54	81	61	3		
			average velocities in each size range (fps)									
1	1				50	54	61	69	80	95	110	135
2	1				41	46	48	50	72	90		
3	1				35	42	44	52	60		92	
4	1				20	22	24	25	40	62	90	93
5	1					10	14	25	37	68	72	

TABLE A VIII

RUN NO. 6. 0.030-INCH DIAMETER TYPE A ORIFICE
WATER JET AT 287°F AND 130 PSIG

Location	Photos	Total Drops	Number of Drops in Each Size Range											
			1	2	3	4	5	6	7	8	9	10	11	12
1	4	386	5	16	64	81	86	54	34	17	13	11	4	1
2	4	748	12	82	187	205	207	49	5	1				
3	4	501	6	20	94	119	135	108	18	1				
4														
			average velocities in each size range (fps)											
1	2						75	95	105	135		142	-	
2	1				11	16		28	31					
3	2				4	5	8	10	21					

TABLE A IX

RUN NO. 7. 0.031-INCH DIAMETER TYPE B ORIFICE
WATER JET AT 287°F AND 90 PSIG

Location	Photos	Total Drops	Number of Drops in Each Size Range									
			1	2	3	4	5	6	7	8	9	10
1	2	469	6	60	132	142	86	32	6	3	2	
2	2	178		9	36	55	53	16	3	4	1	1
3	2	209	1	1	34	53	76	41	2	1		
4	2	34			1	1	14	17	1			
			average velocities in each size range (fps)									
1	1				56	54	65	73	82			125
2	1			35	37	43	56	63	72	81		113
3	1				11	10	10	21	37	61		
4	1						6	12	16			

TABLE AX

RUN NO. 8. 0.040-IN. DIAMETER TYPE B ORIFICE
WATER JET AT 270°F AND 130 psig

Location	Photos	Total Drops	Number of Drops in Each Size Range										
			1	2	3	4	5	6	7	8	9	10	11
1	2	294	2	9	56	84	85	28	16	10	2	1	1
2	2	610	6	56	142	181	174	43	6	1	1		
3	2	760	1	20	128	223	260	110	16	2			
4	2	198		4	25	51	81	33	3	1			
			Average Velocities in Each Size Range (fps)										
1	1		50	52	60	67	76	100	140				
2	1		28	30	39	42	52	80	94				
3	1			30	33	34	48	61	90				
4	1			16	17	24	28	38					

TABLE AXI

RUN NO. 9. 0.040-IN. DIAMETER TYPE B ORIFICE
WATER JET AT 287°F AND 90 psig

Location	Photos	Total Drops	Number of Drops in Each Size Range								
			1	2	3	4	5	6	7	8	9
1	2	657	8	72	223	221	123	4	3	2	1
2	2	583	9	54	167	203	131	17	1	1	
3	2	395	1	7	51	73	156	90	14	3	
4	2	337		2	26	53	115	104	34	3	
			Average Velocities in Each Size Range (fps)								
1	1				50	54	71	81	91	120	134
2	1				38	44	50	63	77	98	
3	1				22	24	34	51	60		
4	1				12	12	27	36	41	48	

TABLE AXII

RUN NO. 10. 0.040-IN. DIAMETER TYPE B ORIFICE
WATER JET AT 287°F AND 130 psig

Location	Photos	Total Drops	Number of Drops in Each Size Range								
			1	2	3	4	5	6	7	8	9
1	2	409	8	56	118	121	76	24	3	3	
2	2	1095	29	117	331	316	243	51	8		
3	2	611	4	48	123	158	169	99	9	2	
4	2	271	3	11	40	57	100	47	11	2	
			Average Velocities in Each Size Range (fps)								
1	1			34	35	46	52	73	104	97	
2	1			21	22	27	32	34			
3	1			20	20	26	33	35	42		
4	1				14	17	27	29	28		

TABLE AXIII

RUN NO. 11. 0.060-IN. DIAMETER TYPE B ORIFICE
WATER JET AT 254°F AND 120 psig

Location	Photos	Total Drops	Number of Drops in Each Size Range									
			1	2	3	4	5	6	7	8	9	10
1	2	378	1	30	111	108	87	25	9	4	2	1
2	2	680	14	77	213	178	123	52	17	5	1	
3	2	831	24	105	259	192	159	66	17	7	1	1
4	2	658	5	33	112	153	204	112	28	7	3	1
5	2	199		5	22	26	42	66	29	8		1
			Average Velocities in Each Size Range (fps)									
1	1			42	43	64	83	98	134	138		145
2	1			38	39	57	72	87	118	135	145	
3	1			18	18	20	24	38	46	83		
4	1				17	19	23	28	44	62		
5	1				13	13	17	20	29		50	

TABLE AXIV

RUN NO. 12. 0.060-IN. DIAMETER TYPE B ORIFICE
WATER JET AT 270°F AND 80 psig

Location	Photo	Total Drops	Number of Drops in Each Size Range									
			1	2	3	4	5	6	7	8	9	10
1	2	139		3	29	47	33	15	8	3	1	
2	2	362		21	111	107	77	27	12	3	2	2
3	2	736	1	30	155	233	249	54	9	2	3	
4	2	686	2	34	137	200	223	70	18	2		
5	2	497		8	65	152	180	78	12	2		
			Average Velocities in Each Size Range (fps)									
1	1			35	35	54	68	107	114			
2	1			30	32	44	54	100	106	115		
3	1				20	18	24	31	48	62		
4	1				13	14	19	24	35			
5	1				9	9	11	20	26	30		

TABLE AXV

RUN NO. 13. 0.060-IN. DIAMETER TYPE B ORIFICE
WATER JET AT 270°F AND 120 psig

Location	Photos	Total Drops	Number of Drops in Each Size Range								
			1	2	3	4	5	6	7	8	9
1	2	229		6	48	64	79	21	6	4	1
2	2	1264	54	170	442	371	195	27	4	1	
3	2	686	7	64	164	199	152	77	19	4	
4	2	681	7	51	145	183	192	87	13	3	
5	2	166		3	18	29	30	61	21	4	
			Average Velocities in Each Size Range (fps)								
1	1			42	43	64	83	98	134	138	145
2	1			38	39	57	72	87	118	135	145
3	1			18	18	20	24	38	46	83	
4	1				17	19	23	28	44	62	
5	1				13	13	17	20	29		50

TABLE AXVI

RUN NO. 14. 0.020-IN. DIAMETER TYPE C ORIFICE
WATER JET AT 80°F AND 94 psig

Location	Photos	Total Drops	Number of Drops in Each Size Range												
			1	2	3	4	5	6	7	8	9	10	11	12	13
1	4	253			12	24	40	33	32	35	14	22	20	13	8
2	4	351		5	33	78	116	50	30	21	10	6	1	1	
			Average Velocities in Each Size Range (fps)												
1	3				54	54	53	72	80	88	104	115	114	115	
2	1				21	20	22		58	65	90	99			

TABLE AXVII

RUN NO. 15. 0.020-IN. DIAMETER TYPE C ORIFICE
WATER JET AT 270°F AND 130 psig

Location	Photos	Total Drops	Number of Drops in Each Size Range									
			1	2	3	4	5	6	7	8	9	10
1	2	584	14	32	130	183	155	47	11	6	4	2
2	2	949	26	98	272	289	227	35	2			
3	2	746	12	49	170	287	210	16	2			
4	2	403	17	64	152	116	51	3				
			Average Velocities in Each Size Range (fps)									
1	1				48	57	76	94	115	140		145
2	1			30	32	42	47	48	58	78		
3	1			12	13	16	20	29	30			
4	1			6	6	8	10	14				

TABLE AXVIII

RUN NO. 16. 0.020-IN. DIAMETER TYPE C ORIFICE
WATER JET AT 278°F and 120 psig

Location	Photos	Total Drops	Number of Drops in Each Size Range								
			1	2	3	4	5	6	7	8	9
1	2	949	23	87	301	326	184	21	5	2	
2	2	810	43	117	289	193	135	28	5		
3	2	508	37	101	187	91	65	23	4		
4	2	404	2	34	98	109	117	40	4		
			Average Velocities in Each Size Range (fps)								
1	1				44	44	59	72	92	98	130
2	1				28	31	50	59	79	88	
3	1				18	20	24	31	41	50	
4	1				8	8	12	20	26		

TABLE AXVIX

RUN NO. 17. 0.030-IN. DIAMETER TYPE A ORIFICE
FREON-11 JET AT 152°F AND 94 psig

Location	Photos	Total Drops	Number of Drops in Each Size Range							
			1	2	3	4	5	6	7	8
1	4	840	3	30	166	289	238	72	32	10
2	4	165	1	16	56	57	24	11		
			Average Velocities in Each Size Range (fps)							
1	2			30	30	32	40	52	71	92
2	2			21	23	29	35	40		

TABLE AXX

RUN NO. 18. 0.020-IN. DIAMETER TYPE C ORIFICE
FREON-11 JET AT 125°F AND 95 psig

Location	Photos	Total Drops	Number of Drops in Each Size Range										
			1	2	3	4	5	6	7	8	9	10	11
1	3	1042	10	53	86	219	286	228	94	50	12	3	1
2	3	133	5	26	43	42	13	4					
3	3	35	1	5	15	8	5	1					
			Average Velocities in Each Size Range (fps)										
1	2				35	37	42	55	71	79		90	
2	2			20	21	25	30	39					
3	2			12	13	15	19	22					

APPENDIX C

SAMPLE CALCULATIONS

1. 1. Calculation of Jet Velocity.

$$V = (2g_c \Delta P v_2)^{\frac{1}{2}} \qquad (1)$$

For Run No. 4B

conversion factor $g_c = 32.2$ ft./sec.^{2}

injection pressure $\Delta P = 120 \pm 1$ psig (x 144 in.^{2}/ft.^{2})

liquid specific volume at liquid temperature[21] (268°F.) $v_2 = 0.01715$ ft.^{3}/lb.

$$V = (2 \times 32.2 \times 120 \times 144 \times 0.01715)^{\frac{1}{2}}$$

$$V = 138.2 \text{ ft./sec.}$$

2. Calculation of Weber number.

$$N_{we} = \frac{\rho_g V^2 d}{2g_c \sigma} \qquad (2)$$

For Run No. 4B

surrounding gas density $\rho_g = 0.0591$ lb/ft.^{3} at 212°F. (air)[12]

jet velocity (Calc. 1) $V = 138.2$ ft./sec.

jet diameter $d = 0.032$ in. (x 1/12 ft./in.)

conversion factor $g_c = 32.2$ ft./sec.^{2}

interfacial tension at 212°F.[21] $\sigma = 58.9$ dyne/cm. (x 6.85×10^{-5} $\frac{\text{lb./ft.}}{\text{dyne/cm.}}$

$$N_{we} = \frac{0.0591 \times (138.2)^2 \times 0.032}{12 \times 2 \times 32.2 \times 58.9 \times 6.85 \times 10^{-5}}$$

$$N_{we} = 11.2$$

3. Calculation of Reynold's Number.

$$R = \frac{Vd}{v_2 \mu} \tag{3}$$

For Run No. 4B

jet velocity (calc. 1) $V = 138.2$ ft./sec.

jet diameter $d = 0.032$ in. (x 1/12 ft./in.)

liquid specific volume at liquid temperature (268°F.)[21] $v_2 = 0.01715$ ft.^{3}/lb.

liquid viscosity at liquid temperature[21] $\mu = 0.21$ cp. (x 0.000672 $\frac{\text{lb./ft.-sec.}}{\text{cp.}}$)

$$R = \frac{138.2 \times 0.032}{12 \times 0.01715 \times 0.21 \times 0.000671}$$

$R = 152{,}000$

4. Calculation of Bubble-Growth-Rate Constant.

$$C = \left(\frac{\Delta T c_2}{L}\right)\left(\frac{\rho_2}{\rho_1}\right)\left(\pi \frac{k}{\rho_2 c_2}\right)^{\frac{1}{2}} \tag{4}$$

For Run No. 4B, or water at 268°F. under 1 atmosphere

superheat $\Delta T = 56$°F.

average liquid heat capacity (212°F.-268°F.) $c_2 = 1.014$ b.t.u./lb.-°F.

latent heat of vaporization at 212°F. $L = 970.3$ b.t.u./lb.

note that:

$$X = \frac{\Delta T c_2}{L} = \frac{h_{2i} - h_{2f}}{h_{1f} - h_{2f}} \tag{5}$$

liquid enthalpy at initial temperature (268°F.) h_{2i} = 236.80 b.t.u./lb.

liquid enthalpy at final temperature (212°F.) h_{2f} = 180.07 b.t.u./lb.

vapor enthalpy at final temperature (212°F.) h_{1f} = 1150.4 b.t.u./lb.

$$X = \frac{236.80 - 180.07}{1150.40 - 180.07} = 0.0585 \text{ wt. fraction flashing}$$

liquid density at 268°F. ρ_2 = 58.3 lb./ft.^{3}

vapor density at 212°F. ρ_1 = 0.0373 lb./ft.^{3}

liquid conductivity(212-268°F) k = 0.394 b.t.u./hr.-ft.-°F.

$$C = (0.0585)\left(\frac{58.3}{0.0373}\right)\left(3.14 \times \frac{0.394}{58.3 \times 1.014}\right)^{\frac{1}{2}}$$

$$C = 13.2 \text{ ft./hr.}^{\frac{1}{2}}$$

5. Calculation of Bubble-Growth-Rate Constant for Dissolved Gas.

$$C' = \left(\frac{C_i - C_f}{1 - C_f}\right)\left(\frac{\rho_2}{\rho_1}\right)(\pi D_m)^{\frac{1}{2}} \qquad (6)$$

For hexane saturated with methane at 300 psig when pressure is reduced to 1 atmosphere at 86°F.

initial gas concentration from bubble point calculation[14] C_i = 0.1076 mole fraction = 0.224 wt. fraction

final gas concentration from bubble point[14] C_f = 0.0035 mole fraction = 0.0007 wt. fraction

density of gas dissolved in liquid (calculated from expansion data[14] ρ_2 = 21.33 lb./ft.^{3}

density of gas coming out of solution[12] $\rho_l = 0.0402$ lb./ft.^{3}

molecular diffusivity of gas in liquid[14] $D_m = 0.000395$ ft.^{2}/hr.

$$C' = \left(\frac{0.0224 - 0.0007}{1 - 0.0007}\right)\left(\frac{21.33}{0.0402}\right)(3.14 \times 0.000395)^{\frac{1}{2}}$$

$$C' = (0.0214)(531)(0.0353)$$

$$C' = 0.398 \text{ ft./hr.}^{\frac{1}{2}}$$

6. Calculation for One Location in Spray.*

Run No. 11. 0.060-in. diameter type B orifice water jet at 254°F. and 120 psig location No. 2

1	2	3	4	5	6	7	8	9	10
size range	size interval (micron)	no. of drops	drop velocity (Ft/sec)	drops x velocity (3x4)	% in each range (% of 5)	cumulative %	% per unit size (6/2)	geom. av. diam.	av. diam. x % (6x9)
1	10	14	37	518	1.39	1.39	0.14	5	6.9
2	4.1	77	37	2849	7.61	9.00	1.86	11.9	90.6
3	5.9	213	39	8307	22.20	31.20	3.76	16.8	373.0
4	8.2	178	54	9612	25.69	56.89	3.13	23.7	608.9
5	11.8	123	72	8856	23.67	80.56	2.01	32.4	766.9
6	16.4	52	86	4472	11.95	92.51	0.73	47.4	566.4
7	23.6	17	117	1989	5.32	97.83	0.23	67.2	357.5
8	33	5	134	670	1.79	99.62	0.05	95.1	170.2
9	47	1	144	144	0.38	100	0.01	134	50.9
totals		680		37417	100.00			total	2991.8
								$\overline{D_{10}}$	29.9

* Column 7 is experimental cumulative distribution, F(D), for this location.

Column 8 is experimental probability distribution f(D), for this location.

7. Calculation for the Whole Spray.

RUN NO. 11. 0.060-INCH DIAMETER TYPE B ORIFICE
WATER JET AT 254°F. AND 120 PSIG

	location	sample annulus volume ratio	no. drops x velocity x volume ration for each size range										
			1	2	3	4	5	6	7	8	9	10	totals
	1	1	43	1290	4773	6912	7221	2675	1179	556	288	145	25082
	2	8	4144	22792	66456	76896	70848	35776	15912	5360	1152		299336
	3	16	6912	30240	74592	58368	61056	35904	14144	9296	1600	1760	293872
	4	24	2040	13464	45696	66096	107712	77952	28224	10416	5040	1920	358560
	5	32		2560	11264	13312	24192	52800	32480	13568		2240	152416
	totals		13139	70346	202781	221584	271029	205107	91939	39169	8080	6065	1129266
1	percent		1.16	6.23	17.96	19.62	24.00	18.16	8.14	3.47	0.72	0.54	100.00
2	cumulative percent, F(D)		1.16	7.39	25.35	44.97	8.97	87.13	95.27	98.74	99.46	100	
3	size range (microns)		10	4.1	5.9	8.2	11.8	16.4	23.6	33.0	47.0	66.0	
4	percent per size range, f(D)		0.12	1.52	3.04	2.39	2.03	1.11	0.34	0.11	0.02	0.01	
5	geom. av. diameter		5	11.9	16.8	23.7	32.4	47.4	67.2	95.1	134	190	
6	geom. av. diameter^2		25	142	282	562	1050	2247	4516	9044	17956	36100	
7	geom. av. diameter^3		125	1690	4738	13319	34020	106508	303475	860084	2406104	6859000	
8	percent x D_{av}		6	74	302	465	778	861	547	330	96	103	3561
9	percent x D_{av}^2		29	885	5065	11026	25200	40806	36760	31383	12928	19494	183576
10	percent x D_{av}^3		145	10528	85094	261319	816480	1934185	2407286	2987115	1732395	3703860	14001408

NOTES: Row 2 is experimental cumulative distribution, F(D), for the whole spray.

Row 4 is experimental probability distribution f(D), for the whole spray.

The sum of row 8 is $\sum D_{av} \Delta N$, so that:

$$\overline{D_{10}} = \left(\frac{\sum D_{av} \Delta N}{\sum \Delta N} \right)$$

$$\overline{D_{10}} = \frac{3561}{100} = 35.6 \text{ microns.}$$

The sum of row 9 is $\sum D_{av}^2 \Delta N$, so that:

$$\overline{D_{20}} = \left(\frac{\sum D_{av}^2 \Delta N}{\sum \Delta N} \right)^{1/2}$$

$$\overline{D_{20}} = \left(\frac{183,576}{100} \right)^{1/2} = 42.9 \text{ microns.}$$

The sum of row 10 is $\sum D_{av}^3 \Delta N$, so that:

$$\overline{D_{30}} = \left(\frac{\sum D_{av}^3 \Delta N}{\sum \Delta N}\right)^{1/3}$$

$$\overline{D_{30}} = \left(\frac{14,001,408}{100}\right)^{1/3} = 52.0 \text{ microns.}$$

Also,

$$\overline{D_{32}} = \overline{D_{30}}^3 \; / \; \overline{D_{20}}^2$$

$$\overline{D_{32}} = \left(\frac{14,014.08}{1,835.76}\right) = 76.3 \text{ microns.}$$

APPENDIX D

LITERATURE CITATIONS

1. Bankoff, S. G. and Mikesell, R. D. Growth of Bubbles in a Liquid of Initially Nonuniform Temperature, Paper No. 58-A-105, Annual Meeting ASME, New York, N.Y., Nov. 30-Dec. 5, 1958.

2. Baron, T. Atomization of Liquid Jets and Droplets, University of Illinois Technical Report No. 4, Feb. 15, 1949.

3. Carslaw, H. S. and Jaeger, J. C. Conduction of Heat in Solids, London, England: Oxford University Press, 1947, 219.

4. Castleman, R. A., Jr. The Mechanism of Atomization Accompanying Solid Injection, NACA Report No. 440, 1932.

5. Castleman, R. A., Jr. "The Mechanism of the Atomization of Liquids," Bur. Std. Jour. of Research, 6, No. 3, (1931), 369.

6. Deragabedian, P. Paper No. 53-SA-10, Heat Transfer and Fluid Mechanics Institute, Los Angeles, Calif., June, 1953.

7. Forster, H. K. and Zuber, N. "The Growth of a Vapor Bubble in a Superheated Liquid," Journal of Applied Physics, 25, No. 4, (1954) 474-478.

8. Frössling, N. "Uber die Verdunstung fallender Tropfen," Gerlands Beitre Geophys., 52, (1938), 170.

9. Hanlein, A. "Uber den Zerfall eines Flussigkeitsstrahles," Forschung auf Gebeite des Ingenieurewesens, 2, No. 4, (1931), 139.

10. Hanson, A. R. The Effect of Relative Velocity on the Evaporation of a Liquid Fuel Spray, Ph. D. Thesis, University of Michigan, 1951.

11. Hinze, J. O. AIChE Journal, 1, (1959), 189.

12. Hodgman, C. D., Weast, R. C. and Wallace, C. W. (ed.). Handbook of Chemistry and Physics, 35th Edition, Cleveland, Ohio: Chemical Rubber Publishing Company, 1953.

13. Holroyd, H. B. "On the Atomization of Liquid Jets," J. Franklin Inst., 215, (1933), 93.

14. Katz, D. L. et al. Handbook of Natural Gas Engineering, New York: McGraw-Hill Book Company, Inc., (1959), Chapter 4.

15. Lamb, G. Hydrodynamics, New York: Dover Publications, 1945, p. 131.

16. Lane, W. R. "Shatter of Drops in Streams of Air," Ind. Eng. Chem., 43, (1951), 1312.

17. Lee, D. W. and Spencer, R. C. Photomicrographic Studies of Fuel Sprays, NACA Report No. 454, 1933.

18. Littaye, G. "Influence de la Vitesse de l'Air sur le Diametre des Petites Gouttes Obtenues par Atomisation," Comptes Rendus, 218, (1944), 440.

19. Miesse, C. C. "Correlation of Experimental Data on the Disintegration of Liquid Jets," Ind. Eng. Chem., 47, (1955), 1690.

20. Mugele, R. A. and Evans, H. D. Ind. Eng. Chem., 43, (1951), 1317.

21. Perry, J. H. (ed.). Chemical Engineer's Handbook, 3rd Edition, New York: McGraw-Hill Book Company, Inc., 1950.

22. Plesset, M. S. and Zwick, S. A. "A Nonsteady Heat Diffusion Problem with Spherical Symmetry," J. Appl. Phys., 23, No. 1, (1954), 95-98.

23. Plesset, M. S. and Zwick, S. A. "The Growth of Vapor Bubbles in Super-Heated Liquids," J. Appl. Phys., 25, No. 4, (1954), 492-500.

24. Putnam, A. A. et al. Injection and Combustion of Liquid Fuels, WADC Technical Report 56-344, March, 1957.

25. Ranz, W. E. On Sprays and Spraying, Dept. of Engineering Research Bulletin No. 65, The Pennsylvania State University, 1956.

26. Rayleigh, Lord. Proc. Lond. Math. Soc., 34, (1892), 153.

27. Rayleigh, Lord. "On the Instability of Jet," Proc. Lond. Math. Soc. 10, (1878), 4.

28. Tyler, E. "Instability of Liquid Jets," Phil. Mag. (London), 16, (1933), 501.

29. Walker, W. H., Lewis, W. K., McAdams, W. H. and Gilliland, E. R. Principles of Chemical Engineering, 3rd Edition, New York: McGraw-Hill Book Company, Inc., 1937, 296-300.

30. Weber, C. "Zum Zerfall eines Fluessigkeitsstrahles," Zeit. fur Angewandte Mathematic, 11, (1931), 106.

31. York, J. L. Photographic Analysis of Sprays, Ph. D. Thesis, University of Michigan, 1949.

32. York, J. L. and Stubbs, H. E. "Photographic Analysis of Sprays," Trans. ASME, 74, (1952), 1157.